Title

Exploring the Versatility of Noble Metal Catalysts in Organic Transformations: From Ligand Exchange to Electrochemical Reduction of CO2

Author

Brar, Aneelman

Publication Date

2023

Peer reviewed|Thesis/dissertation

UNIVERSITY OF CALIFORNIA, MERCED

Exploring the Versatility of Noble Metal Catalysts in Organic Transformations: From Ligand Exchange to Electrochemical Reduction of captured CO_2

By

Aneelman Brar

A dissertation submitted in partial satisfaction of the requirements for the degree of

Doctor Of Philosophy

In

Chemistry

Graduate Division

Of the

University Of California, Merced

Committee in charge:
Prof. Hrant P. Hratchian (Chair)
Prof. Michael Findlater
Prof. Anthony F. Cozzolino
Prof. Rebeca Arevalo

May 2023

The Dissertation of Aneelman Brar is approved, and it is acceptable in quality and form for publication on microfilm and electronically:

_____

Dr. Hrant P. Hratchian (Chair)

_____

Dr. Michael Findlater

_____

Dr. Rebeca Arevalo

_____

Dr. Anthony F. Cozzolino

Dedication

In the loving memory of Gurudev Shri Shri Hari Giri Ji

To my lovely parents and brother for their love and inspiring words, without whom it was impossible to finish this work!!

Table of Contents

List of Figures

List of Schemes

List Of Tables

List of Abbreviations

^{o} C - Degree Celsius
THF – Tetrahydrofuran
DFT – Density Functional Theory
$CDCl_3$ – Chloroform – d
SM – Suzuki Miyaura Coupling
MeCN – Acetonitrile
CPE – Controlled Potential Electrolysis
AC- Ammonium Carbamate
DMADMC – Dimethyl Ammonium Dimethyl carbamate
GC – Gas Chromatography
equiv – equivalent(s)
SAO – Secondary arsine oxides
NR – No Reaction
RT – Room Temperature
MHz – Mega Hertz
s – singlet (NMR)
d – doublet (NMR)
t – triplet (NMR)
m- Multiplet (NMR)
dd – doublet of doublets (NMR)

Acknowledgements

Firstly, I thank the almighty god for all the blessings throughout my Ph.D. journey. I want to acknowledge Gurudev for believing in me and motivating me to pursue a Ph.D., always encouraging me and showing me the right path during difficult times.

I would like to express my deep and sincere gratitude to my research advisor Dr. Michael Findlater. With his remarkable mentorship, constant guidance, and never-ending enthusiasm, everything is possible, and a beginner researcher like me could also fulfill my research dream. He creates an inspiring and highly supportive environment where your ideas can bloom into exciting discoveries. Michael is a passionate, kind, patient, and extraordinary teacher who is always ready to share his knowledge, wisdom, and advice. A person like me could not ask for a better advisor. I am proud that he gave me a chance to be part of his lab and that I could learn and work with him.

I am grateful to several faculty members, including my research exam and dissertation committee members at UC Merced and Texas Tech University. I want to give a special shoutout to Dr. Anthony F. Cozzolino, who taught me computational chemistry and UV-Vis technique and shared his expertise. He very easily breaks down the most complex problem. It was indeed my pleasure and an honor to work with him and learn science from him. I would like to thank Dr. Rebecca Arevalo, Dr. Hrant P. Hratchian, Dr. Guigen Li, and Dr. Kristin Hutchins for serving on my committee and providing valuable feedback on my research.

My sincere thanks to the facility managers of Chemistry and Biochemistry both at Texas Tech and UC Merced: Dr. Kaz Surowiec, Dr. Piotr Dobrowolski, Dr. Daniel Unruh, Scott Hiemstra, Jerry Franco, Quentin Vaughn, Jeanne Bertonazzi, Dr. David Rice, Kennedy Nguyen

I would like to thank my previous group members, Dr. Sem Tamang, Dr. Zheng, Dr. Sara, Dr. Deepika, Dr. Arpita, and Dr. Aida. It was great working with them, and I appreciate the time they took to provide suggestions about my chemistry. I am also grateful to my lab members, Dr. Miguel, Dr. Andrew, Dr. Della, and Koto for their immense support and encouragement. I am thankful to everyone for their love and friendship.

Also, I would like to thank my friends Mathew, Akaljot, Mohit, Jagdeep, Harleen, Arpit and Avro for always having my back and listening to my nonstop chattering. Words won't do justice to all their support and encouragement!! I am happy to have them in my life.

How can I leave my pillars of strength, my mom, dad, and brother. This would not have been possible without them. My dad shared this dream with me. I am forever indebted to them for giving me endless love and opportunities so that I can excel in my life. Whatever I am today and will be in the future, I owe my success to them. Life is not pain with them on my side.

Curriculum Vita

Education

University of California (Transferred)	Merced, California
Ph.D. in organic and organometallic chemistry	May 2023
Texas Tech University (Moved to UC, Merced)	Lubbock, Texas
Ph.D. Chemistry (Organic & Organometallic chemistry)	July 2021
Panjab University,	Chandigarh, India
Master's in chemistry (H.S.)	May 2018
Panjab University	Chandigarh, India
Bachelor's in chemistry (H.S)	May 2016

Research Experience

Graduate Researcher at the University *of California, Merced* *July 2021- Present*

- Designing an electrocatalytic system employing pincer-based metal ligand complexes to directly convert the captured carbon dioxide into renewable fuels and valuable chemicals. (Collaboration with cross-functional teams) (Summer Internship at UC Irvine)
- Developed tertiary phosphine oxide ligand based recyclable system for Suzuki Miyaura and Negishi reaction yielding biphenyls; precursors for drug molecule, provided evidence for pseudo homogeneous catalysis using techniques such as ICP-MS, NMR, TEM.
- As a safety captain of the lab, maintained laboratories as per UC Merced EHS rules, maintaining chemical inventory, writing reports.
- Theoretical and experimental study of Arsenic Tautomerization in comparison to phosphorus analogs.

Graduate Student at Texas Tech University *2018- July 2021*

- Synthesized several ligands (pincer, amidinates, guanidinates) and metal complexes of transition metals (iron, nickel, iridium, palladium); characterized with NMR, IR, and X-Ray Crystallography.
- Conducted experimental and computational studies of ligand exchange in iridium-based pincer complexes; deduced mechanism using techniques like UV-Vis, NMR and DFT.
- Multistep Synthesis of Alkyne substituted terpyridine ligands, and purification was done by column chromatography.
- Room temperature double hydroboration of nitriles under solvent and metal-free system.

Master's Student at the Panjab University *2016-2018*

- Developed a greener catalytic system for Suzuki coupling employing Pd- Ni Nanoparticles; Nanomaterial synthesized, characterized, and optimized the reactivity for organic transformation such as Suzuki Coupling.

Mentorship Experience

Graduate Teaching Assistant, Texas Tech University *Aug 2018 - May 2021*

- Taught chemistry majors students about experiments involving multi-step synthesis, organometallic complexes, purification, and isolation and analyses using FT-IR, NMR, GC-MS, TLC, and column chromatography techniques.
- Monitored Student performances and conducted weekly office hours for a class of 50 students to deepen understanding of the subject matter.
- Mentored 4 undergraduate and 2 fellow graduate students in the research lab about handling hazardous chemicals, working with gloveboxes, running columns, data documentation, and complex synthesis and reaction optimizations.

Publications

1. The Role of Non-innocent Ammonium Counterions in Electrocatalytic Reduction of Carbon Dioxide and its Implications for Reactive Carbon Capture (*Manuscript in progress*)
2. A computational chemistry approach to the study of tautomerization of $As^{V}(O)(H)$ to $As^{III}(OH)$ (*Manuscript in progress*)
3. Homogeneous and Recyclable Palladium Catalyst: Application in Suzuki Miyaura Cross-Coupling Reactions. A. K. King, **A. Brar**, G. Li, and M. Findlater. (*Under revisions*)
4. A New Iron Age: Replacing precious metal catalysts for hydroboration of carbonyls, **A. Brar**, M. Findlater. (*Under revisions*)
5. A tertiary phosphine oxide ligand-based recyclable system for Suzuki-Miyaura and Negishi reaction: Evidence for pseudo homogeneous catalysis, **A. Brar**, A.K. King, M. Findlater, Catal. Sci. Technol., 2023, https://doi.org/10.1039/D2CY01734B
6. Experimental and Computational Studies of Phosphine Ligand Displacement in Iridium-Pincer Complexes Employing Pyridine and Acetonitrile. **A. Brar**, S. Shafiei-Haghighi, D. K. Unruh, QA. F. Cozzolino, and M. Findlater, Organometallics 2020, 39, 3461-3468
7. Transition metal – and solvent-free Double Hydroboration of Nitriles. D. Bedi, **A. Brar** and M. Findlater, Green Chemistry 2020, 22, 1125-1128
8. Amphiphilic metallosrufactants as potential Scaffolds for Facile Fabrication of Pd-NiO Nanocomposites for the Environmentally Benign Synthesis of Xanthene Derivatives. N. Kaur, P. Dhariwal, **A. Brar**, G. Kaur, A. Bhalla, C. Prakash and G. R. Chaudhary, Materials Today Chemistry 2019, 14, 10019

Awards and Fellowship

- Grad Slam Campus Champion — April 2023
- Grad Excel Peer Mentorship Award — Jan 2023
- Chemistry Graduate Student Organization Endowed Scholarship — May 2021
- Study Abroad Competitive Scholarship — Mar 2021
- Outstanding Teaching Assistant in Organic Chemistry — August 2020
- Helen DeVitt Jones Graduate Fellowship — March 2020

Poster (PP) and Oral Presentation (OP)

- A tertiary phosphine oxide ligand-based recyclable system for Suzuki-Miyaura and Negishi reaction: Evidence for pseudo homogeneous catalysis (*OP* at *ACS National Meeting in San Diego, March 2022)*
- Experimental and Computational Studies of Phosphine Ligand Displacement in Iridium-Pincer Complexes Employing Pyridine and Acetonitrile (*OP at ACS Southwest Regional meeting in El paso, Nov 2019)*
- A tertiary phosphine oxide ligand-based recyclable pseudo homogeneous system for Suzuki-Miyaura and Negishi reaction (*PP at RSC Twitter Conference , Feb 2023)*
- A tertiary phosphine oxide ligand-based recyclable system for Suzuki-Miyaura and Negishi reaction: Evidence for pseudo homogeneous catalysis (*PP at University of California, Merced Research Week showcase)*
- Captured CO_2 as a source of renewable fuels and chemicals using electrocatalyst (*PP at Annual Meeting, Center for Direct Conversion of Captured CO_2, February 2023)*

Organization

1. Graduate Student Association, UC, Merced
2. Chemistry Graduate Student Association, Texas Tech
3. American Chemical Society

Leadership & Community

- Treasurer - Graduate Student Association, UCM
- Student Fee Advisory Committee Member, UCM
- Delegate Assembly Chair, Graduate Student Association,
- UCM Volunteer - USDA Food Distribution
- Volunteer - Judge for 19th and 20th and Annual Graduate Student Research Poster Competition

Abstract

Chemical targets produced by transformations of organic molecules are valuable, serving as building blocks for the agrochemical, pharmaceutical and polymer industries. These transformations may be carried out catalytically or stoichiometrically, but catalysts are used in the synthesis of 80-90 percent of all industrially manufactured products, demonstrating the indispensable role catalysts play in industry. Several organic transformations ranging from cross-coupling to hydrofunctionalization to oxidation or reduction reactions are typically catalyzed by precious metals like iridium (Ir), palladium (Pd), platinum (Pt), rhodium (Rh) etc. These 'noble' metals have revolutionized synthetic organic chemistry, allowing chemists to build novel molecules and functional materials with high selectivity, atom economy, and versatility by using mild reaction conditions facilitated by these catalysts.

Density Functional Theory (DFT) is a computational method used to study the electronic structures of molecules and materials. These methods can inform and guide catalysis research by providing valuable insights into the molecular-level mechanisms of catalytic reactions. DFT can predict the electronic and structural properties of molecules, which can help to identify the key steps and intermediates involved in catalytic reactions. DFT can also be used to design and optimize catalysts for specific reactions, comprehend the role of solvents and other environmental factors in catalytic reactions, and predict the behavior of catalytic systems under different conditions. Overall, DFT has proven itself to be a critical tool in catalysis research, assisting in the optimization of reaction conditions and improvement of reaction efficiency.

The first chapter of this dissertation describes a recyclable catalytic system which has applications in both Suzuki-Miyaura (SM) and Negishi coupling reactions. We investigated the nature of active species catalyzing the reaction – a controversial topic in light of recent research which has suggested 'metal–free' coupling chemistry and in the fundamental nature of the catalyst, whether the system is heterogeneous or homogeneous. We utilized the commercially available cyclohexyldiphenyl phosphine oxide ligand and $Pd(OAc)_2$ (palladium acetate) to catalyze coupling reactions and concluded the catalytic system to be 'pseudo homogeneous'. All the substrates studied afforded good to excellent reaction yields and the catalyst system could be reused in up to ten cycles.

In the second chapter of this dissertation, the synthesis, characterization, and ligand exchange studies of iridium-based pincer complexes is reported. The iridium complex (^{tBu}POCOP)Ir(PPh_3) (^{tBu}POCOP = 2,6-bis(di-*tert*-butylphosphonito)benzene) acts as a convenient source of latent Ir(I), a $14e^-$ species [(^{tBu}POCOP)Ir]; which is susceptible to ligand exchange chemistry. The reactions with acetonitrile and pyridine afford the corresponding (^{tBu}POCOP)Ir(NCMe) and (^{tBu}POCOP)Ir(Py) complexes, respectively. NMR, UV-vis spectroscopy, and density functional theory (DFT) calculations were used to evaluate the key equilibria and determine the kinetic and thermodynamic parameters of the ligand exchange process between (tBuPOCOP)Ir(PPh_3) and L (L = MeCN or pyridine). These studies provided experimental and computational support of the proposed pathway of phosphine displacement, i.e., it occurs either via an associative or a dissociative pathway.

In the third chapter of this dissertation, the electrochemical reduction of captured carbon dioxide using an iridium pincer complex was studied. Recently, the reactive capture of

carbon dioxide, (i.e., capturing CO_2 and reducing it directly) has garnered a lot of interest. Amines have been used most extensively for carbon dioxide capture. Amines react with dilute CO_2 in a 2:1 ratio to form the corresponding ammonium carbamate. We utilized commercially available ammonium carbamate with the highly selective and robust CO_2 to formate reduction catalyst **10** [Ir(POCOP)]. When ammonium carbamate was used as the substrate instead of CO_2, only hydrogen was produced. An equivalent electrolysis with ammonium hexafluorophosphate also resulted in only hydrogen. These results indicate that the use of amine-captured CO_2, which generates an equivalent of ammonium, modifies the H^+ activity in solution, which can lead to hydrogen production for catalysts that have high selectivity when CO_2 is the substrate. The fourth chapter of this dissertation discusses the utilization of DFT calculations to study the chemistry of elements from the pnictogen family, i.e., arsenic tautomerization chemistry and supramolecular assembly of antimony and bismuth. Unlike arsenic's analog phosphorus, arsenic doesn't have an extensive synthetic literature to rely upon. To study arsenic in depth and help biologists by providing them with CRM's we decided to synthesize As-HCs/ As-sugars using a proposed synthetic strategy with a SAO key intermediate. Because of the scarce literature precedent, we decided to probe the route computationally, deducing the stability of the As^{III} or As^{V} states.

1. Recyclable Palladium Catalysts – Application in Suzuki Miyaura and Negishi Coupling reactions.

Modified with permission from RSC.
Aneelman Brar, Andrew K King, Michael Findlater
https://pubs.rsc.org/en/Content/ArticleLanding/2023/CY/D2CY01734B

1.1. Introduction

Palladium-catalyzed cross coupling reactions between an aryl halide electrophile and an organoboron nucleophile are a clean and efficient strategy for the formation of biaryls; which facilitates a myriad of applications in the synthesis of pharmaceutical precursors, agrochemicals, and high-tech materials.[1-4] The cross-coupling reaction using boronic acid/esters, known as the Suzuki-Miyaura coupling reaction[5] (SM) has been investigated extensively because of the broad availability and relative air and moisture stability of boronic acids and their derivatives. [6] In parallel, the development of other cross coupling methodology has resulted in several different strategies. For example, the Negishi coupling is a valuable alternative due to fast transmetalation of organozinc reagents to palladium in comparison with boronic acid. [7]

Catalysis plays a crucial role in cross-coupling reactions by enhancing the reaction rate and selectivity. The palladium complex catalyst facilitates the formation of reactive intermediate and stabilizes them, promoting the formation of the new carbon -carbon bond. It could be homogeneous or heterogeneous catalysis depending upon the phase of the catalyst with respect to reactants and products.

Most coupling reactions employ palladium catalysts which are highly reactive but expensive due to their scarcity.[3, 8, 9] Palladium is a non-abundant platinum group metal, as such palladium salts are expensive and natural deposits will eventually be depleted.[10, 11] In an effort to improve the sustainability of palladium-catalyzed cross coupling reactions and make the reactions more environmental friendly, ideally the palladium content should be recovered at the end of the reaction.[12] Henceforth making recyclability, a crucial part of cross coupling reactions. Also, it significantly reduces the cost of the reaction, minimizes waste production, and improves efficiency. Reduction in waste generated also makes the reaction/catalytic system more environmentally friendly and sustainable.

1.2. Phosphine oxide catalyzed Suzuki miyaura reaction

Generally, the Suzuki–Miyaura coupling reaction is performed using palladium catalysts in the presence of ancillary ligands, most often N-heterocyclic carbenes or tertiary phosphines.[13] Phosphine oxides have also seen widespread application as ligands for cross-coupling reactions arising from their pentavalent nature, which provides air and moisture stability.[14-16] Denmark and co-workers employed triphenyl phosphine oxide as a ligand in the cross-coupling of arylsilanolates with aryl bromides; where they described phosphine oxide as a 'buffering ligand' that stabilizes the highly active palladium nanoparticles formed *in situ* which govern catalysis.[17] Later, Ackermann reported the first use of secondary phosphine oxides in the arylation of α C–H acidic compounds.[18]

The dominant role palladium plays in cross-coupling reactions presents a sustainability issue as palladium is a non-abundant metal. In developing more sustainable approaches to

chemical synthesis, it would be desirable to either replace or, at least, recycle palladium catalysts over multiple catalytic runs.[10, 11] Different approaches to catalyst reuse have previously been reported, including work by Fan and co-workers where a palladium/phosphine dendrimer system was successfully re-used up to 9 times in SM cross-coupling reactions.[19] Impressively, only 0.2 mol% of Pd catalyst is required to reach full conversion, however reaction conditions are rather forcing – heating at reflux in dioxane. A report by Afewerki *et al.* described the use of a Pd heterogeneous catalyst derived from rice husk waste which could be reused in up to 6 cycles in SM chemistry.[20] Ye and co-workers reported the recyclability of a Pd-based electride material Y_3Pd_2; which was recycled 20 times. The catalyst recyclability is excellent but 40 mol% of catalyst was required.[21] In any attempt to make a more cost-effective and sustainable catalytic system the importance of palladium recovery and reuse is integral to newly developed methods.[22, 23]

Recent work by Ananikov and co-workers introduced the concept of "cocktail" catalysis.[24-29] The Ananikov group demonstrated that rather than being homogenous or heterogenous the nature of the metal catalyst can be mixed, with a "cocktail" of metal species responsible for driving reactions. Hence a dynamic metal catalyst system can contain multiple species which are key to catalytic activity with nanoparticle and molecular catalysts both present. Leaching of heterogenous species can occur giving the same phenomena observed with pseudo-homogenous catalysis. These systems then comprise potentially reusable and recyclable catalysts.

Thus, we sought a simple approach to palladium recycling which employs inexpensive and readily available ligands under ambient conditions; we investigated the use of tertiary phosphine oxides as ligands in palladium-catalyzed SM and Negishi coupling reactions.

The coupling reaction between iodotoluene and phenylboronic acid (**Scheme 1.1**) was chosen as a model reaction with which to study the effectiveness of our catalytic system.

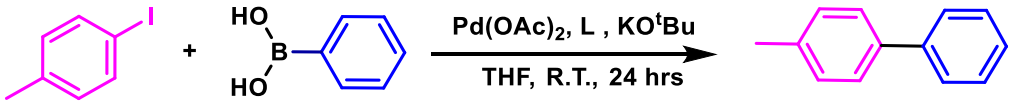

Scheme 1.1. Model Reaction for tertiary phosphine oxide (**L**) palladium catalyzed SM Reaction

Different commercially available phosphine oxide ligands were screened (**Table 1.1**) and the use of cyclohexyl diphenylphosphine oxide (**L1)** as ligand and THF as solvent were found to provide optimal reaction conditions. Although the goal of our work was to investigate recyclable palladium catalysts, we considered it important to demonstrate that a robust SM catalyst had been achieved. Thus, we explored a limited scope of substrates.

Table 1.1. Optimization of reaction parameters with various phosphine oxide ligands

Entry	Ligand (L)	Spectroscopic Conversion (%)
1	Without Ligand	35
2	Tricyclohexyl phopshine oxide	92
3	Tri-octyl phosphine oxide	96
4	Cyclohexyl diphenylphosphine oxide	>99
5	Triphenyl phosphine oxide	91
6	Triphenyl phosphine oxide[b]	97
7	Diphenyl (2,4,6-trimethyl benzoyl) phosphine oxide	89
8	3-methyl-2-phenyl-2-phospholene oxide	86
9	1,2-bis diphenylphosphinoethane monoxide	7

Reaction Conditions: a) 4-Iodotoluene (0.3 mmol), KO^{t}Bu (0.6 mmol), Phenyl boronic acid (0.6 mmol), Pd $(OAc)_2$ (5 mol%), Phosphine Oxide (10 mol%), THF (3ml), R.T., 24 h. b) $PdCl_2$ (5 mol%). The spectroscopic conversion was calculated using ^{1}H NMR spectroscopy using tetramethyl silane as an internal standard

To demonstrate the further utility of this system we ran a series of coupling reactions between aryl halides or aryl triflates and phenyl boronic acid. As summarized in **Table 1.2**, our catalytic system demonstrated a respectable reactivity profile and good functional group tolerance under mild reaction conditions. Most functional groups investigated were well tolerated, and isolated biphenyls were obtained in good to excellent yields. An unsuccessful attempt was made to effect sp^2 - sp^3 couplings with cyclic alkyl bromides. Additional experiments were carried out with 4-iodopyridine and 2-iodopyridine, spectroscopic conversion of the starting materials proved to be poor (26% and 13% respectively). We hypothesize that this is due to the coordination of the pyridine moiety to the Pd nanoparticles thus hindering catalytic turnover. When the solvent system is changed to a mixture of ethanol and water the reaction exhibits full conversion and 2-phenylpyridine (**1s**) was isolated in good yield.

Table 1.2. Substrate Scope in SM Coupling Reaction

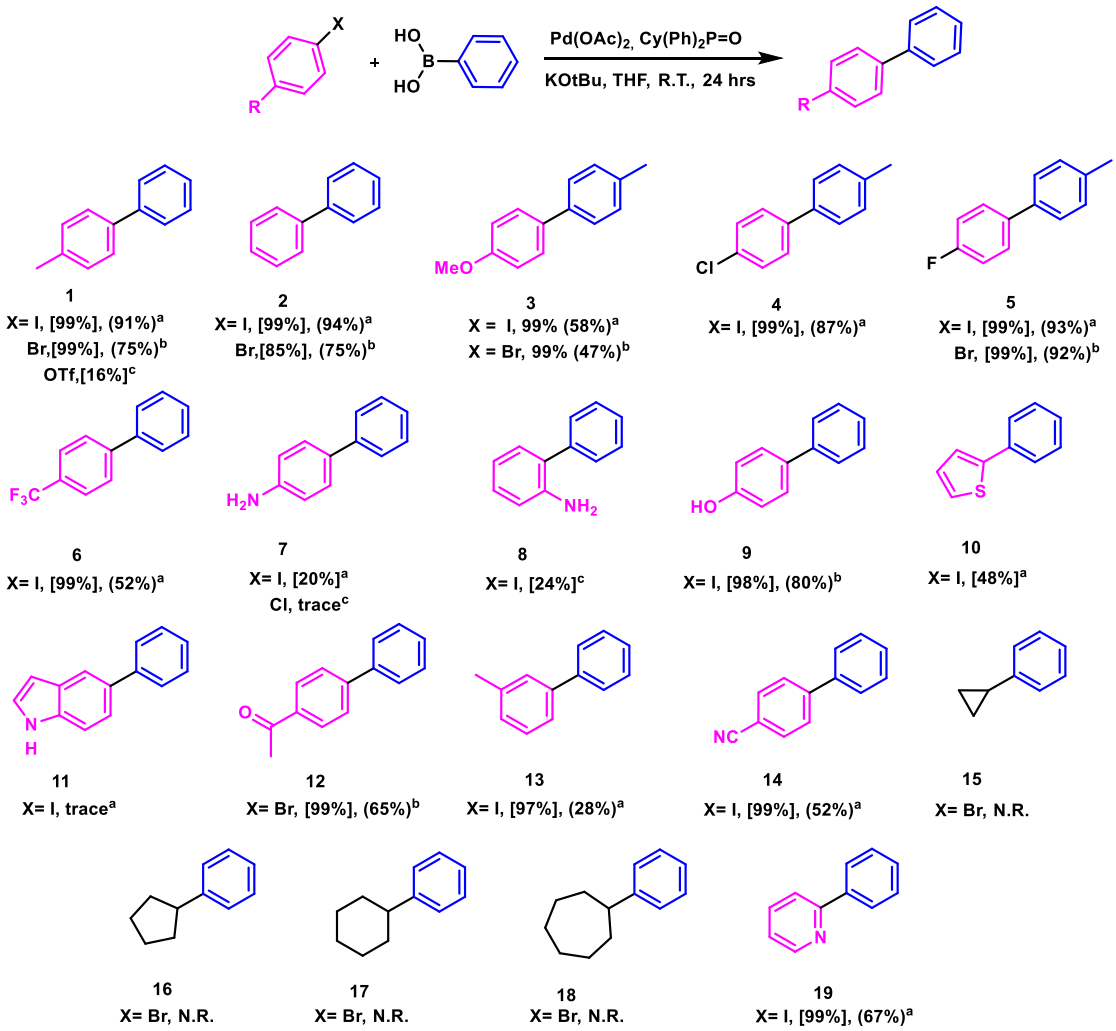

Reaction Condition a) Halide substrate (0.3 mmol), KO^{t}Bu (0.6 mmol), Phenyl boronic acid (0.6 mmol), $Pd(OAc)_2$ (5 mol%), Phosphine Oxide (10 mol%), THF (3ml), R.T., 24 h. b) temperature = 70 ^oC, c) Solvent Toluene, temperature = 100 ^oC. [] denotes the conversions reported by Gas chromatography and (Isolated Yields).

1.2.1. Recycling Studies

We investigated the recyclability of $Pd(OAc)_2$ with cyclohexyl diphenylphosphine oxide for Suzuki-Miyaura coupling. As illustrated in **Table 1.3**, the catalyst system could be recycled through 10 consecutive coupling reactions without any loss of activity and good yields of the coupled product in each run were obtained. Catalyst and product were readily separable in hexane, and the recovered (precipitated) catalyst was re-used directly in

subsequent catalytic cycles. Separation was achieved via a simple filtration operation akin to a heterogeneous process.

Table 1.3. Recyclability Study of Suzuki-Miyaura Catalyst

Cycle	Temperature	Spectroscopic Yield (%)	Selectivity (1a:1a')
1	R.T.	>99	7:1
2	R.T.	>99	55:1
3	R.T.	>99	105:1
4	R.T.	>99	400:1
5	R.T.	>99	>400:1
6	R.T.	>99	150:1
7	R.T.	>99	280:1
8	R.T.	>99	400:1
9	R.T.	>99	400:1
10	R.T.	>99	400:1

Reaction conditions- Recyclability studies with $PCyPh_2$, $Pd(OAc)_2$. [a] $Pd(OAc)_2$ (0.015 mmol), Ligand (0.03 mmol), Iodotoluene (0.3 mmol), Phenylboronic acid (0.6 mmol), Potassium tert-butoxide (0.6 mmol), Solvent = 2 mL, Reaction time = 24 h. Spectroscopic yield calculated with tetramethylsilane as an internal standard. Ratio of heterocoupled product 4-methyl-1,1-biphenyl (1a) to homocoupled product 4,4-dimethyl-1,1-biphenyl (1a′).

1.3. Negishi Coupling

To further explore potential applications of our catalytic system, we decided to investigate the Negishi coupling. The coupling reaction between iodotoluene and tolylzinc iodide (**Scheme 1.2**) was performed and was found to proceed cleanly and in good to excellent yield.

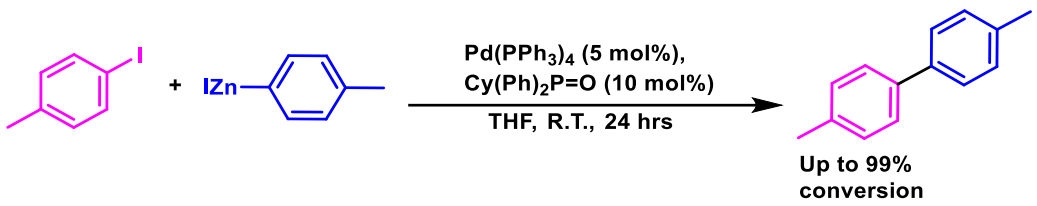

Scheme 1.2. Model Reaction for tertiary phosphine oxide palladium-catalyzed Negishi coupling cross coupling.

Substrate scope and recyclability were subsequently explored in a manner consistent with earlier Suzuki-Miyaura studies**.** (**Table 1.4**) Once more, the catalyst and product were readily separable via hexane addition to spent reaction mixture; simple filtration allowing reclamation of catalyst. The recovered catalyst was re-used in subsequent catalytic cycles after recharging with reagents. The palladium catalyst could be re-used up to ten times without significant loss of yields (**Table 1.5**). The scope of our Negishi coupling chemistry was explored using phenyl zinc bromide and a total of eight substrates and isolated yields of up to 85 % were obtained.

Table 1.4. Substrate scope in Negishi Coupling Reaction

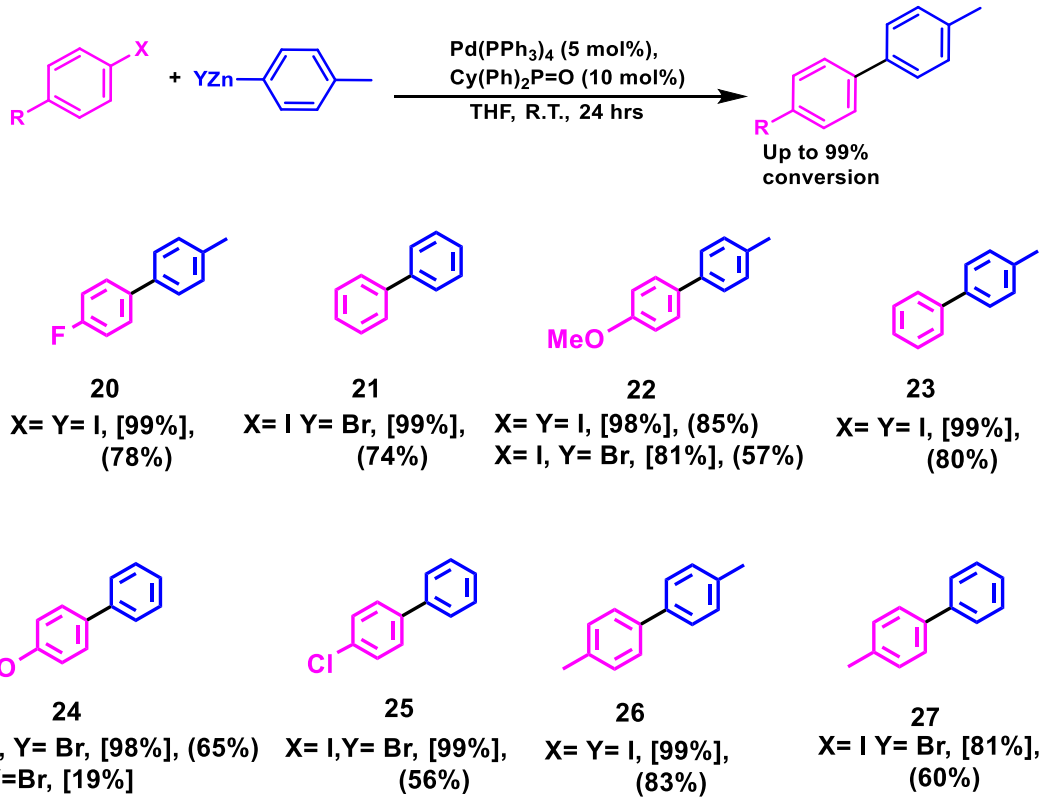

Table 1.5. Recyclability of Negishi Catalyst

Cycle	Temperature	Spectroscopic Yield (%)	Selectivity (2c:2c')
1	R.T.	>99	10:1
2	R.T.	>99	11:1
3	R.T.	>99	10:1
4	R.T.	>99	16:1
5	R.T.	>99	25:1
6	R.T.	>99	16:1
7	R.T.	>99	25:1
8	R.T.	>99	25:1
9	R.T.	>99	25:1
10	R.T.	>99	25:1

Reaction conditions: Recyclability studies w/ O=PcyPh$_2$, Pd(PPh$_3$)$_4$. [a] Pd(PPh$_3$)$_4$ (0.015mmol),Ligand (0.03mmol), 4-Iodoanisole (0.3 mmol), Tolylzinc iodide (0.6mmol), Solvent=2ml, reaction time = 24 hrs. Spectroscopic yield calculated with tetramethylsilane as an internal standard. Ratio of heterocoupled product 4-methoxy-4'-methyl-1,1'-biphenyl (2c) to homocoupled product 4,4'- dimethoxy-1,1'-biphenyl (2c'). [b] Reaction time = 36 hrs. [c] Reaction time = 48 hrs.

1.4. Homogenous, Heterogenous and pseudo-Homogenous catalysis

To determine the nature of the active catalytic species, present in solution, several test reactions were carried out. In testing catalyst homogeneity, a mercury drop test is typically employed, however this can often lead to inconclusive results due to the fact that mercury only forms amalgams with certain metals.[30] A Suzuki-Miyaura reaction between 4-iodotoluene and phenylboronic acid was conducted under standard conditions and allowed to stir for three hours, the reaction was then filtered and allowed to stir for a further 21 hours (24 hours total).[31] From the precipitate, black palladium species were observable suggesting the formation of nanocomposites, surprisingly the reaction still proceeded to completion suggesting that even after filtration catalytically active Pd species remain present in solution (i.e. homogenous reactivity).[19, 32]

Recent reports suggest that many supposed heterogenous systems actually operate in a pseudo-homogenous regime in which the heterogeneous species acts as a "well" of active Pd species which can 'break off' and be catalytically active in solution.[33, 34] To probe for

such behavior, further tests were then performed in an effort to "trap" nanocomposite palladium structures. Thus, poly(vinylpyridine) was added to a standard Suzuki-Miyaura reaction (7.5 mol% polymer); the polymer acts to suppress heterogeneous catalysis by nanocomposites. The reaction mixture was allowed to stir at room temperature for 24 hours. The reaction proceeded to completion, further suggesting that the catalytically active Pd species are homogeneous in nature. Analogous tests were carried out for Negishi coupling reactions. Previous reports have demonstrated the use of heterogenous catalysts in palladium-catalyzed Negishi couplings.[35, 36]

To further characterize the palladium nanostructures formed during the reaction, transmission electron microscope (TEM) imaging was used to explore heterogeneous structural details. As evidenced by TEM imaging the recovered Pd catalyst is nanoparticulate in nature (**Figure 1.1**).

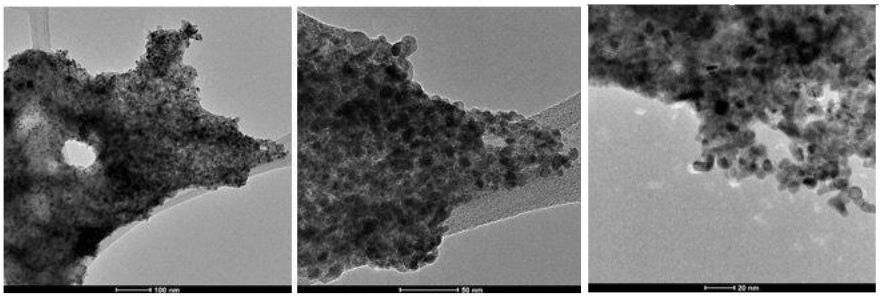

Figure 1.1. TEM images of Pd nanocomposites generated in catalytic SM reactions at 100, 50 and 20 nm magnification.

Given the evidence, we propose that the active palladium species responsible for SM coupling are homogenous in nature but are sourced from a heterogeneous palladium nanocomposite; our catalyst is pseudo-homogenous. To further interrogate the nature of the catalytically relevant species, ^{31}P NMR was carried out in both the solid-state (SSNMR) (**Figure 1.2**) and in the solution state. Analysis of the catalyst both before and after precipitation from solution affords a signal in the ^{31}P NMR at 35.9 ppm consistent with the phosphine oxide being present in both solution and the solid-state.

1.5. Pd-GAP catalyzed Suzuki Miyaura Cross coupling reaction

Homogenous catalysis is widely used due to the abundance of compounds and complexes that are soluble in organic solvents.[37] A key drawback for this approach is separability, with catalysts typically being lost to waste at the end of a reaction as the recovery process is simply not cost effective.[38]As an alternative, heterogeneous catalysts can be employed, as the catalyst and products are in different phases and are easily separated; this allows reclamation of the catalyst to be reused in subsequent reactions, increasing the overall efficiency of the catalytic system.[39] In contrast to homogeneous systems, heterogeneous catalysts typically operate under more extreme reaction conditions (elevated temperature, pressure etc.) and are often less selective as a result.[40] By making homogenous catalysts

recyclable or by designing systems that facilitate better separability this key advantage of heterogeneous catalysis can be incorporated into homogenous systems. Inspired by group-assisted purification (GAP)[41] chemistry and the recently reported metalla-GAP (m-GAP)[42, 43] chemistry we sought to expand the use of ligands which contain a phosphoramide motif in homogenous catalysis and to further explore their potential as recyclable catalytic systems. This represents an alternative and, perhaps, complementary approach to the phosphine oxide chemistry described above.

Extensive work has focused on methods recovering palladium content from spent catalysts to reduce the excessive costs.[12] Catalyst recycling methodologies have the potential to improve the sustainability of palladium-catalyzed reactions and make the processes "greener".[22] Recycling of palladium catalysts is highly desirable as "active" Pd species can be recovered and re-used and previous reports have described separable heterogeneous and immobilized SM catalysts.[44] Recent work in our group has focused on the use of GAP, initially reported by Li and co-workers as ligand architectures for metal catalysts[42] We hypothesized that this could provide an alternative to fully heterogeneous or immobilized catalysts as the transformation occurs in a homogeneous manner with all the advantages associated with homogeneous catalysis. In our efforts to further extend the use of m-GAP ligands we applied the approach to palladium-catalyzed SM cross couplings. We also sought to determine if the presence of the GAP group would have any deleterious impact on catalytic behaviour i.e., would this be an effective homogeneous catalyst regardless of any catalyst recycling?

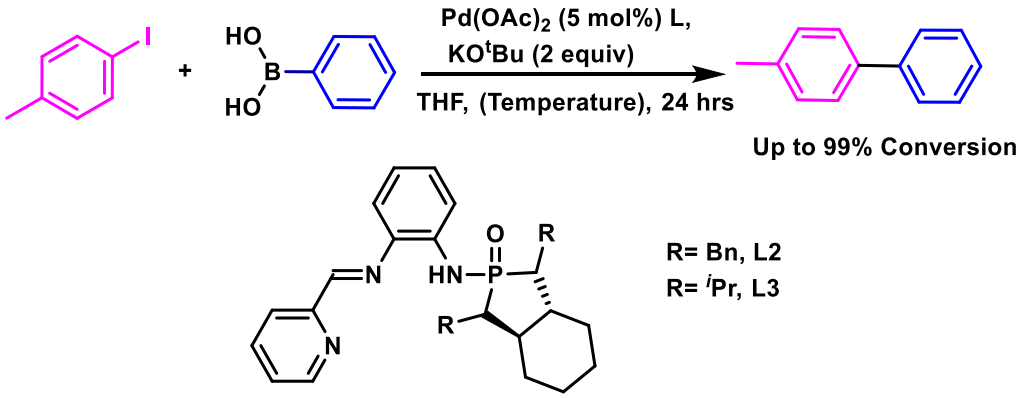

Scheme 1.3. Pd GAP catalyzed SM coupling reaction.

In our initial experiments 4-Iodotoluene and phenylboronic acid were used for substrate screening with m-GAP ligands and palladium acetate, to determine the optimal reaction conditions (**Scheme 1.3** and **Table 1.6**).

Table 1.6. Optimization of Suzuki-Miyaura cross-coupling with m-GAP complexes.

Entry[a]	Ligand	Solvent	Temperature	Yield (%)[d]	Selectivity (1a:1a')
1	L2[b]	THF	R.T.	53	7:1
2	L3	THF	R.T.	48	6:1
3	L2	THF	60	26	30:1
4	L2	1,4-Dioxane	100	92	105:1
5	L3	1,4-Dioxane	R.T.	45	7:1
6	L3[b,c]	THF	R.T.	>99	8:1
7	N/A	THF	R.T.	32	12:1

Reaction Conditions – [a] $Pd(OAc)_2$ (0.015 mmol), Ligand (0.015 mmol), Iodotoluene (0.3 mmol), Phenylboronic acid (0.6 mmol), Potassium tert-butoxide (0.6 mmol), Solvent = 2 ml, Reaction time = 24 hours. [b]Catalyst prepared via overnight stirring. [c]48 hours [d]Spectroscopic yield calculated with tetramethylsilane as an internal standard. [e]Ratio of heterocoupled product (4-methyl-1,1-biphenyl (1a)) to homocoupled product (4,4-dimethyl-1,1-biphenyl (1a')).

GAP ligands **L2** and **L3** were screened under various conditions in the presence of palladium acetate and potassium tert-butoxide as base in an effort to optimize reaction conditions[42, 43] Under ambient temperature and using THF as a solvent, the catalyst system derived from **L2** was found to afford both slightly higher conversion and higher selectivity for cross- vs. homo-coupling products than the catalyst system derived from **L3** (**Table 1.6**, Entries 1 and 2). Raising the temperature to 60 °C resulted in lower overall conversion albeit with an improved product selectivity (**Table 1.6**, Entry 3). Improved results could be obtained using **L3** if the reaction time was extended to 48 h and the catalyst mixture was allowed to stir overnight prior to use in the coupling chemistry (**Table 1.6**, entry 6). Reactions without the use of exogenous ligands were also found to effectively catalyze the reaction, albeit with diminished conversion. After consideration of the reaction time, solvent employed and temperature, we selected **L2**, THF and room temperature as perfectly cromulent reaction conditions. Our catalytic conditions are comparable in performance to

other well-established SM protocols employing $PdCl_2$(dppf), although much lower loadings are possible employing current state of the art methodology.[45-50]

Table 1.7. Substrate Scope for Pd GAP catalyzed SM.

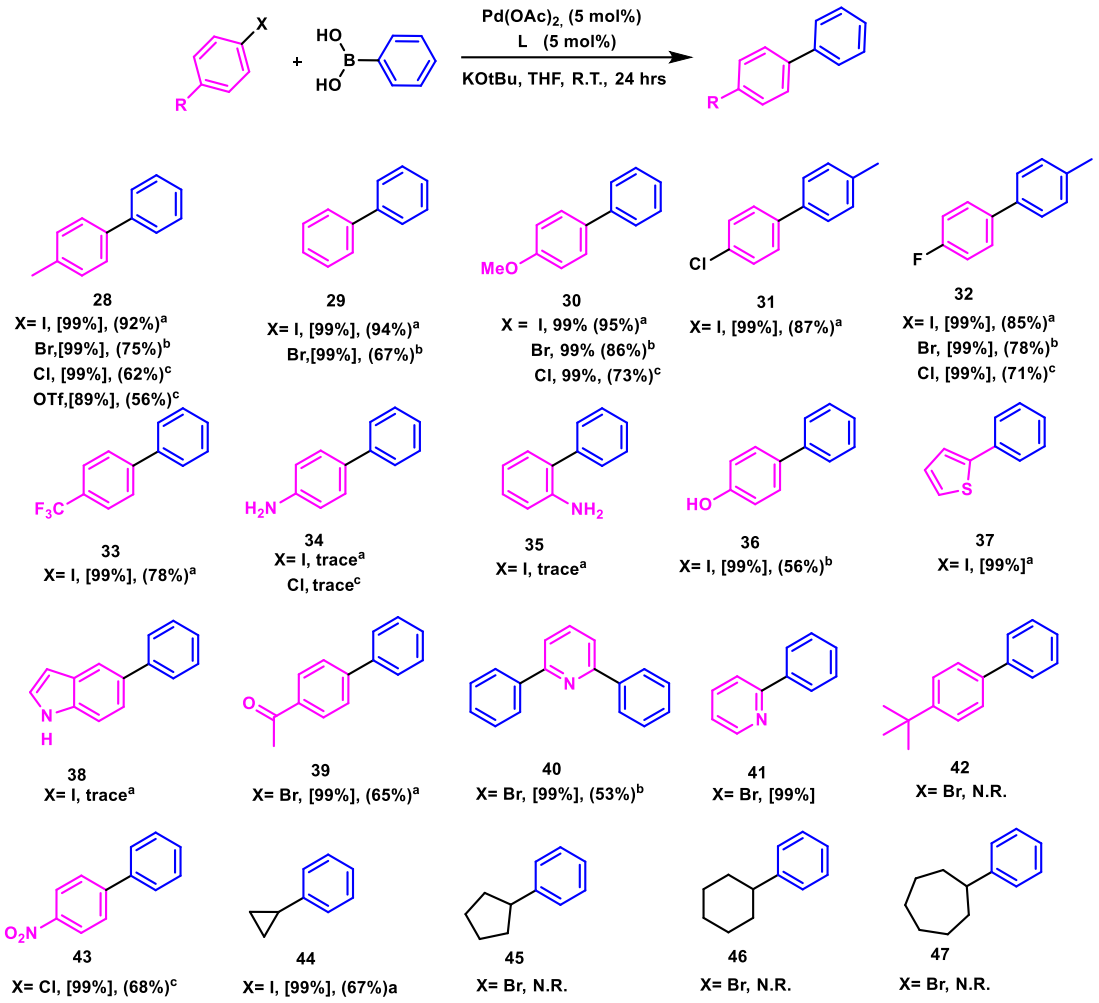

Reaction Conditions- [a]$Pd(OAc)_2$ (0.015 mmol), Ligand **L2** (0.015 mmol), Aryl halide/triflate (0.3 mmol), Phenylboronic acid (0.6 mmol), Potassium *tert*-butoxide (0.6 mmol), Solvent = 2 ml, Reaction time = 24 hours, Temperature = 50 °C. [Spectroscopic yield] (Isolated yield). Catalyst prepared via overnight stirring. Spectroscopic yield calculated with tetramethylsilane as an internal standard. [b]Temperature = 70 °C. [c]Temperature = 90 °C.

The substrate scope was explored to ensure that our m-GAP palladium complex would exhibit comparable performance to other SM catalyst. Thus, **L2**/Pd system was deployed as a catalyst for several SM couplings with a broad range of aryl halide and pseudo-

halide substrates (**Table 1.7**). As expected, aryl iodide substrates (**28-33**) tended to afford good to excellent yields in coupling reactions with phenylboronic acid; the use of substrates with a second halogen atom (not iodine) (**31-33**) delivered excellent chemo selectivity as C-C bond formation occurs exclusively at the C-I bond of the substrate, with no evidence for "double coupling" observed.[51, 52] To probe the limits of our system, we challenged the catalyst with substrates with functional groups often found to be incompatible with Suzuki conditions. Substrates containing alcohol, primary amine and indole groups (**34**, **35**, **38**) were poor coupling partners. This is likely a result of amino group coordination and N-H oxidative addition at palladium.[53-55]Poor reactivity is also observed with iodophenols under the previously optimized reactions conditions, however increasing the reaction temperature to 70 °C gave full conversion. To our delight the Pd-GAP catalyst afforded excellent conversion of the heterocycle 2-iodothiophene (**36**) to coupled product under our optimized conditions. Having investigated the scope of SM coupling reactions with aryl iodides we then turned our attention to aryl bromides (**28-30, 31, 39-42**). To facilitate catalytic turnover the reaction temperature was increased to 70 °C. Functional group tolerance of the aryl bromides was consistent with the results obtained for aryl iodides (**28-30**) and good to excellent yields were obtained. 4-bromoacetophenone (**39**) proved to be a competent substrate, efficient and highly selective C-C bond formation occurred with no undesired reaction of the ketone group observed.[56] No reaction was observed with 2-bromoacetophenone which is nominally an sp^3-sp^2 coupling reaction.[57]2-bromopyridine, 2,6-dibromopyridine and 4-^{t}butylbromobenzene (**40-42**) gave good conversion with modest yields. The suitability of aryl chloride substrates was examined, which required more forcing conditions to promote catalytic activity (90 °C) (**28, 30, 32, 34, 43**). Functional group tolerance remained consistent with the observed reactivity of aryl iodides and bromides. Full conversion was observed with a variety of substrates with the products obtained in good yields (**28, 30, 32, 43**). Coupling reactions between sp^3 and sp^2 centres (**44-47**) were unsuccessful. After exploring the substrate scope the recyclability of catalytic system was studied. The catalyst was reused nine times (ten catalytic cycles in total) which is excellent for a homogenous catalyst and activity remains consistent and comparable to previously reported heterogeneous SM catalysts.[56] It is possible that the first catalytic cycle serves to attenuate the precatalyst or convert the system into a more active form of the catalyst (see discussion below) which results in both higher conversion and increased selectivity for cross-coupled (versus homo-coupled) product. The importance of the GAP ligand to recyclability was probed by attempting a "ligand free" recycling experiment. Surprisingly, a catalytic system simply employing palladium acetate and potassium *tert*-butoxide did exhibit limited recyclability. However, elevated temperatures were required, and the system exhibited limited recyclability before becoming inactive (5 catalytic cycles were observed at 70 ^{o}C). This demonstrated the superiority of the m-GAP system for recyclability applications. Moreover, the nature of the catalyst system was not entirely clear, though strong evidence suggests it is homogeneous in nature. On the homogeneity of the species present in the reaction it can be remarked that recent literature studies suggest that the active

catalytic species present in SM coupling reactions are homogenous in nature, even if nanocomposite structures form *in situ*.[31, 33, 34] Palladium and other platinum group metals are route-dependent human toxicants and limits for these metals are as low as 10mg g^{-1} (10 ppm). Inductively coupled plasma-mass spectroscopy (ICP-MS) analyses were carried out to assess residual Pd in the organic compounds using an aqua regia digest protocol. Levels of residual Pd were found to be in the range of ~0.21 ppm which demonstrates that our Pd-GAP complexes are robust and may be applied in active pharmaceutical ingredient synthesis. Further mechanistic investigations into these reactions are currently underway and will be reported in due course.

Despite repeated attempts, we were unable to obtain crystals of suitable quality to study using X-ray diffraction experiments. Thus, we chose to study the Pd-GAP complexes computationally via Density Functional Theory (DFT) to determine their optimized structures and hence the coordination chemistry of the complexes.[58] Geometries and free enthalpy for the complexes were calculated using exchange correlation functional PBE with zeroth-order regular approximation (ZORA).[59] The geometric parameters of the optimized structure were compared to the structures of analogous palladium complex **1**.

All the calculated distances matched the crystallographic distances within three significant figures (**Table 1.8**). Spin restricted Kohn-Sham determinants were chosen to describe the closed shell wavefunctions, employing the RI approximation and the tight SCF convergence criteria provided by the ORCA.[60]Atom-pairwise dispersion correction with Becke-Johnson damping scheme (D3) were utilized for the calculation, and the def2-TZVP, def2-TZVPP basis set and SARC/J auxiliary basis set were used for all the atoms.[61-64] Frequency calculations confirmed that the structures are energetic minima and allowed for the calculation of free energies. The predicted structures of **2** and **3** are four coordinate square planar structure with the coordination shell composed of a tridentate GAP ligand and an acetate ligand. The structures were optimized as Pd (II) with a singlet ground state.

1.6. Conclusion

In conclusion, we have developed a highly recyclable catalyst system for both Suzuki-Miyaura and Negishi couplings. The robust nature of both catalytic systems, (one developed from commercial sources) is demonstrated via recycling experiments which deliver high yields in up to 10 catalysis cycles. The GAP and phosphine oxide ligand-based palladium catalysts are excellent for coupling different aryl halides with boronic acids. Finally, investigation of the nature of the active catalyst species of phosphine oxide based catalytic system was done via TEM, poisoning experiments and both solution and solid-state NMR analysis; strongly supporting a pseudo-homogenous catalytic system.

1.7. Experimental Section

1.7.1. General Considerations

Reagents were purchased from Sigma Aldrich or Alfa Aesar and used without further purification. Laboratory grade Tetrahydrofuran (THF) was purchased from Fisher Scientific and dried over sodium/benzophenone and distilled prior to use. NMR data was collected at 400 or 500 MHz on Jeol or Varian instruments in $CDCl_3$ at 298 K and referenced to tetramethylsilane. Gas Chromatography-Mass Spectrometry (GC-MS) data was collected using Thermo Scientific ISQ Single Quadrupole system. All the phosphine and phosphine oxide ligands were purchased from Sigma Aldrich or Alfa Aesar and used without further purification. Ligands **L2** and **L3** were prepared according to the literature procedures.[42] Heated and anhydrous reactions were performed in screw cap vials or Teflon-sealed reaction tubes. All manipulations were carried out under an inert atmosphere using standard Schlenk and glovebox techniques, unless otherwise stated.

1.7.2. General procedure for palladium-catalyzed Suzuki Miyaura coupling:

Using phosphine oxide as ligand-

Inside an argon-atmosphere glovebox, a borosilicate glass vial was charged with $Pd(OAc)_2$ (3.2 mg, 0.015 mmol), cyclohexyldiphenyl phosphine oxide **L1**(8.5 mg, 0.03 mmol) with anhydrous THF (3 mL) as solvent. Subsequently, 4-Iodotoluene (65 mg, 0.3 mmol) was added followed by potassium tert-butoxide (67.6 mg, 0.6 mmol) and phenylboronic acid (73.16 mg, 0.6 mmol). The reaction mixture was removed from the glovebox and stirred at RT under an argon atmosphere for 24 hours. The reaction solvent was removed under reduced pressure and the resulting residue was extracted with hexane and dried in vacuo to afford the product (**1**) as a white powder.

Using-1,3-Dibenzyl-2-((2-(I-(14yridine-2-ylmethylene) amino) phenyl) amino)octahydro-1H-ben zo[d][1,3,2]diazaphosphole 2-oxide as ligand-

Inside an argon-atmosphere glovebox, a borosilicate glass vial was charged with $Pd(OAc)_2$ (3.2 mg, 0.015 mmol) and **L2** (8.1 mg, 0.015 mmol) with anhydrous THF (3 mL) as solvent. Subsequently, 4-Iodotoluene (65 mg, 0.3 mmol) was added followed by potassium tert-butoxide (67.6 mg, 0.6 mmol) and phenylboronic acid (73.16 mg, 0.6 mmol). The reaction mixture was removed from the glovebox and stirred at 50 ºC under an argon atmosphere for 24 hours. The reaction solvent was removed under reduced pressure and the resulting residue was extracted with hexane and dried in vacuo to afford the product (**28**) as a white powder.

1.7.3. General procedure for palladium-catalyzed Negishi coupling*:*

Inside an argon-atmosphere glovebox, a borosilicate glass vial was charged with $Pd(PPh_3)_4$ (17.3 mg, 0.015 mmol) and cyclohexyldiphenyl phosphine oxide (**L1**) (8.5 mg, 0.03 mmol) with anhydrous THF (3 mL) as solvent. Subsequently, 4-Iodotoluene (65 mg, 0.3 mmol) was added followed by Tolylzinc iodide (1.2 ml, 0.6 mmol, 0.5 M in THF). The reaction mixture was removed from the glovebox and stirred at RT under an argon atmosphere for 24 hours. The reaction solvent was removed under reduced pressure and the resulting residue was extracted with hexane and dried in vacuo to afford the product (**20**) as a white powder (83 % yield).

1.7.4. General procedure for Pd catalyst recycling:

Following the end point of the reaction, the solvent was evaporated in a vacuum and the resulting residue was extracted with hexane. The precipitate was re-dissolved in THF, and the reagents were added. This methodology was repeated for each subsequent catalytic cycle. Procedure for Pd catalyst recycling with aqueous work-up: Following the end point of the reaction the solvent was evaporated in vacuum and the resulting residue was extracted with hexane. The precipitate was then washed with de-ionized water, filtered, and subsequently dried in a vacuum oven overnight (30 mmHg, 120 °C). The precipitate was re-dissolved in THF, and the reagents were added. This methodology was repeated for subsequent catalytic cycles.

1.7.5. Active catalyst studies:

Homogenous catalysis test: $Pd(OAc)_2$ (5 mol%) and cyclohexyldiphenyl phosphine oxide (**L1**) (10 mol%) were stirred under the reaction conditions with K*o*tBu (5 mol%) and 4-Iodotoluene (5 mol%) for 3 hours, filtered, and the filtrate was used as catalyst in the test reaction. High reactivity was observed providing completion of the reaction under the standard conditions (24 hrs). Pd black was observed as a precipitate, however the reaction proceeded to completion suggesting a homogenous Pd active species.

1.8. Appendix

Figure 1.2. Solid state ^{31}P NMR to confirm the presence of **L1**.

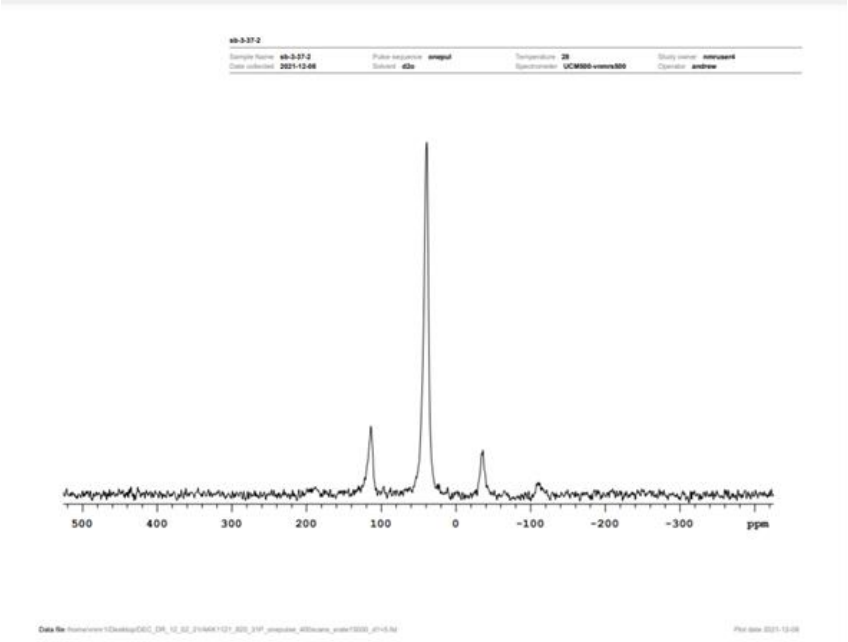

Table 1.8. Comparison between optimized and crystallographic bond parameters of analogous complex Pd 1 as shown below the table.

Bond Parameters	Crystal structure	Optimized geometry (PBE)	Optimized geometry (B3LYP)
Pd(1) - N(1)	2.035(5)	2.080	2.115
Pd(1) - N(2)	1.933(5)	1.973	1.977
Pd(1) - N(3)	1.990(5)	2.015	2.034
Pd(1) - O(3)	2.005(4)	2.063	2.061
O(1) - C(10)	1.213(7)	1.236	1.226
O(2) - C(21)	1.202(7)	1.231	1.222
N(2)-Pd(1)-N(1)	81.06(2)	81.14	80.73
O(3)-Pd(1)-N(1)	104.25(17)	104.65	106.06
O(3)-Pd(1)-N(2)	174.001(17)	174.07	173.04

Pd Complex 1

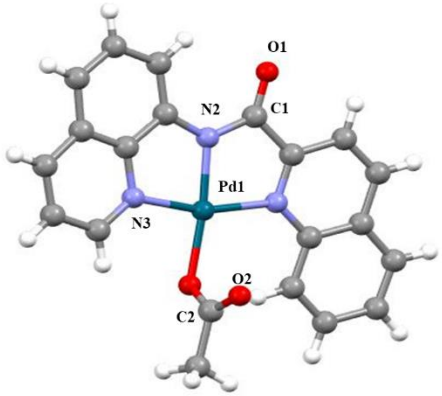

Table 1.9. The energies associated with the Pd complexes 2 and 3.

Entry	Basis Set	Gibb's free Energy(G)	Enthalpy (H)	Dispersion	Energy (E)
Pd complex 2	TZVP	-7262.166	-7262.057	-0.13211	-7262.726
	TZVPP	-7262.181	-7262.072	-0.13222	-7262.482
Pd complex 3	TZVP	- 6957.407	-6957.307	-0.11596	-6957.663
	TZVPP	-6957.422	-6957.322	-0.11608	-6957.68

Palladium Complex 2

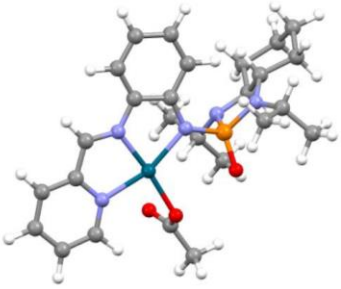

Palladium Complex 3

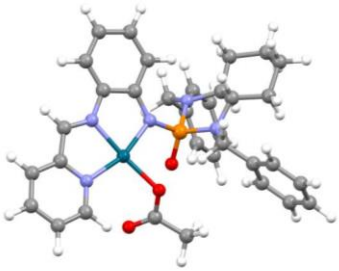

1.9. References

1. Diederich, F.; Stang, P. J., *Metal-catalyzed cross-coupling reactions*. John Wiley & Sons: 2008.
2. Shen, D.; Xu, Y.; Shi, S.-L., A Bulky Chiral N-Heterocyclic Carbene Palladium Catalyst Enables Highly Enantioselective Suzuki–Miyaura Cross-Coupling Reactions for the Synthesis of Biaryl Atropisomers. *Journal of the American Chemical Society* **2019,** *141* (37), 14938-14945.
3. Miyaura, N.; Suzuki, A., Palladium-Catalyzed Cross-Coupling Reactions of Organoboron Compounds. *Chemical Reviews* **1995,** *95* (7), 2457-2483.
4. Negishi, E.-i.; De Meijere, A., *Handbook of organopalladium chemistry for organic synthesis*. John Wiley & Sons: 2003.
5. Miyaura, N.; Suzuki, A., Stereoselective synthesis of arylated (E)-alkenes by the reaction of alk-1-enylboranes with aryl halides in the presence of palladium catalyst. *Journal of the Chemical Society, Chemical Communications* **1979,** (19), 866-867.
6. Hall, D. G., Structure, Properties, and Preparation of Boronic Acid Derivatives. Overview of Their Reactions and Applications. In *Boronic Acids*, 2005; pp 1-99.
7. Negishi, E.; King, A. O.; Okukado, N., Selective carbon-carbon bond formation via transition metal catalysis. 3. A highly selective synthesis of unsymmetrical biaryls and diarylmethanes by the nickel- or palladium-catalyzed reaction of aryl- and benzylzinc derivatives with aryl halides. *The Journal of Organic Chemistry* **1977,** *42* (10), 1821-1823.
8. Martin, R.; Buchwald, S. L., Palladium-Catalyzed Suzuki−Miyaura Cross-Coupling Reactions Employing Dialkylbiaryl Phosphine Ligands. *Accounts of Chemical Research* **2008,** *41* (11), 1461-1473.
9. Palladium Prices Monthly average. http://www.lppm.com/statistics.aspx.
10. Renner, H.; Schlamp, G.; Kleinwächter, I.; Drost, E.; Lüschow, H. M.; Tews, P.; Panster, P.; Diehl, M.; Lang, J.; Kreuzer, T.; Knödler, A.; Starz, K. A.; Dermann, K.; Rothaut, J.; Drieselmann, R.; Peter, C.; Schiele, R.; Coombes, J.; Hosford, M.; Lupton, D. F., Platinum Group Metals and Compounds. In *Ullmann's Encyclopedia of Industrial Chemistry*, pp 1-73.
11. Genkin, A. D.; Evstigneeva, T. L., Associations of platinum-group minerals of the Noril'sk copper-nickel sulfide ores. *Economic Geology* **1986,** *81* (5), 1203-1212.
12. Sanderson, K., Chemistry: It's not easy being green. *Nature* **2011,** *469* (7328), 18-20.
13. Kotha, S.; Lahiri, K.; Kashinath, D., Recent applications of the Suzuki–Miyaura cross-coupling reaction in organic synthesis. *Tetrahedron* **2002,** *58* (48), 9633-9695.
14. Grushin, V. V., Mixed Phosphine−Phosphine Oxide Ligands. *Chemical Reviews* **2004,** *104* (3), 1629-1662.

15. Billingsley, K. L.; Buchwald, S. L., A General and Efficient Method for the Suzuki–Miyaura Coupling of 2-Pyridyl Nucleophiles. *Angewandte Chemie International Edition* **2008,** *47* (25), 4695-4698.
16. Das, P.; Bora, U.; Tairai, A.; Sharma, C., Triphenylphosphine chalcogenides as efficient ligands for room temperature palladium(II)-catalyzed Suzuki–Miyaura reaction. *Tetrahedron Letters* **2010,** *51* (11), 1479-1482.
17. Denmark, S. E.; Smith, R. C.; Tymonko, S. A., Phosphine oxides as stabilizing ligands for the palladium-catalyzed cross-coupling of potassium aryldimethylsilanolates. *Tetrahedron* **2007,** *63* (26), 5730-5738.
18. Ackermann, L.; Vicente, R.; Hofmann, N., Air-Stable Secondary Phosphine Oxide as Preligand for Palladium-Catalyzed Intramolecular α-Arylations with Chloroarenes. *Organic Letters* **2009,** *11* (19), 4274-4276.
19. Wu, L.; Li, B.-L.; Huang, Y.-Y.; Zhou, H.-F.; He, Y.-M.; Fan, Q.-H., Phosphine Dendrimer-Stabilized Palladium Nanoparticles, a Highly Active and Recyclable Catalyst for the Suzuki−Miyaura Reaction and Hydrogenation. *Organic Letters* **2006,** *8* (16), 3605-3608.
20. Afewerki, S.; Franco, A.; Balu, A. M.; Tai, C.-W.; Luque, R.; Córdova, A., Sustainable and recyclable heterogenous palladium catalysts from rice husk-derived biosilicates for Suzuki-Miyaura cross-couplings, aerobic oxidations and stereoselective cascade carbocyclizations. *Scientific Reports* **2020,** *10* (1).
21. Ye, T.-N.; Lu, Y.; Xiao, Z.; Li, J.; Nakao, T.; Abe, H.; Niwa, Y.; Kitano, M.; Tada, T.; Hosono, H., Palladium-bearing intermetallic electride as an efficient and stable catalyst for Suzuki cross-coupling reactions. *Nature Communications* **2019,** *10* (1).
22. Anastas, P. T.; Warner, J. C., *Green Chemistry: Theory and Practice*. Oxford University Press: New York,, 1998.
23. Molnár, Á., Efficient, Selective, and Recyclable Palladium Catalysts in Carbon−Carbon Coupling Reactions. *Chemical Reviews* **2011,** *111* (3), 2251-2320.
24. Ananikov, V. P.; Beletskaya, I. P., Toward the Ideal Catalyst: From Atomic Centers to a "Cocktail" of Catalysts. *Organometallics* **2012,** *31* (5), 1595-1604.
25. Kashin, A. S.; Ananikov, V. P., Catalytic C–C and C–Heteroatom Bond Formation Reactions: In Situ Generated or Preformed Catalysts? Complicated Mechanistic Picture Behind Well-Known Experimental Procedures. *The Journal of Organic Chemistry* **2013,** *78* (22), 11117-11125.
26. Eremin, D. B.; Ananikov, V. P., Understanding active species in catalytic transformations: From molecular catalysis to nanoparticles, leaching, "Cocktails" of catalysts and dynamic systems. *Coordination Chemistry Reviews* **2017,** *346*, 2-19.
27. Polynski, M. V.; Ananikov, V. P., Modeling Key Pathways Proposed for the Formation and Evolution of "Cocktail"-Type Systems in Pd-Catalyzed Reactions Involving ArX Reagents. *ACS Catalysis* **2019,** *9* (5), 3991-4005.
28. Prima, D. O.; Kulikovskaya, N. S.; Galushko, A. S.; Mironenko, R. M.; Ananikov, V. P., Transition metal 'cocktail'-type catalysis. *Current Opinion in Green and Sustainable Chemistry* **2021,** *31*, 100502.
29. Chernyshev, V. M.; Ananikov, V. P., Nickel and Palladium Catalysis: Stronger Demand than Ever. *ACS Catalysis* **2022,** *12* (2), 1180-1200.
30. Gorunova, O. N.; Novitskiy, I. M.; Grishin, Y. K.; Gloriozov, I. P.; Roznyatovsky, V. A.; Khrustalev, V. N.; Kochetkov, K. A.; Dunina, V. V., When Applying the Mercury Poisoning Test to Palladacycle-Catalyzed Reactions, One Should Not Consider the Common Misconception of Mercury(0) Selectivity. *Organometallics* **2018,** *37* (17), 2842-2858.

31. Bulatov, E.; Lahtinen, E.; Kivijärvi, L.; Hey-Hawkins, E.; Haukka, M., 3D Printed Palladium Catalyst for Suzuki-Miyaura Cross-coupling Reactions. *ChemCatChem* **2020,** *12* (19), 4831-4838.
32. Wu, L.; Li, Z.-W.; Zhang, F.; He, Y.-M.; Fan, Q.-H., Air-Stable and Highly Active Dendritic Phosphine Oxide- Stabilized Palladium Nanoparticles: Preparation, Characterization and Applications in the Carbon-Carbon Bond Formation and Hydrogenation Reactions. *Advanced Synthesis & Catalysis* **2008,** *350* (6), 846-862.
33. Phan, N. T. S.; Van Der Sluys, M.; Jones, C. W., On the Nature of the Active Species in Palladium Catalyzed Mizoroki–Heck and Suzuki–Miyaura Couplings – Homogeneous or Heterogeneous Catalysis, A Critical Review. *Advanced Synthesis & Catalysis* **2006,** *348* (6), 609-679.
34. Sun, B.; Ning, L.; Zeng, H. C., Confirmation of Suzuki–Miyaura Cross-Coupling Reaction Mechanism through Synthetic Architecture of Nanocatalysts. *Journal of the American Chemical Society* **2020,** *142* (32), 13823-13832.
35. Wu, W.-Y.; Lin, T.-C.; Takahashi, T.; Tsai, F.-Y.; Mou, C.-Y., A Palladium Bipyridyl Complex Grafted onto Nanosized MCM-41 as a Heterogeneous Catalyst for Negishi Coupling. *ChemCatChem* **2013,** *5* (4), 1011-1019.
36. Moore, L. R.; Vicic, D. A., A Heterogeneous-Catalyst-Based, Microwave-Assisted Protocol for the Synthesis of 2,2′-Bipyridines. *Chemistry – An Asian Journal* **2008,** *3* (6), 1046-1049.
37. Parshall, G. W., Industrial applications of homogeneous catalysis. A review. *Journal of Molecular Catalysis* **1978,** *4* (4), 243-270.
38. van Leeuwen, P. W. N. M., Catalysis, Homogeneous. In *Encyclopedia of Physical Science and Technology (Third Edition)*, Meyers, R. A., Ed. Academic Press: New York, 2003; pp 457-490.
39. Schlögl, R., Heterogeneous Catalysis. *Angewandte Chemie International Edition* **2015,** *54* (11), 3465-3520.
40. Clark, J. H.; Macquarrie, D. J., Heterogeneous Catalysis in Liquid Phase Transformations of Importance in the Industrial Preparation of Fine Chemicals. *Organic Process Research & Development* **1997,** *1* (2), 149-162.
41. Kaur, P.; Wever, W.; Rajale, T.; Li, G., Research Article: Asymmetric Hydrophosphylation of Chiral N-Phosphonyl Imines Provides an Efficient Approach to Chiral α-Amino Phosphonates. *Chemical Biology & Drug Design* **2010,** *76* (4), 314-319.
42. Zhang, S.; Bedi, D.; Cheng, L.; Unruh, D. K.; Li, G.; Findlater, M., Cobalt(II)-Catalyzed Stereoselective Olefin Isomerization: Facile Access to Acyclic Trisubstituted Alkenes. *Journal of the American Chemical Society* **2020,** *142* (19), 8910-8917.
43. Zhang, S.; Liao, J.-S.; Unruh, D. K.; Li, G.; Findlater, M., Cobalt- and iron-catalyzed regiodivergent alkene hydrosilylations. *Organic Chemistry Frontiers* **2021,** *8* (10), 2174-2181.
44. Calò, V.; Nacci, A.; Monopoli, A.; Montingelli, F., Pd Nanoparticles as Efficient Catalysts for Suzuki and Stille Coupling Reactions of Aryl Halides in Ionic Liquids. *The Journal of Organic Chemistry* **2005,** *70* (15), 6040-6044.
45. Molander, G. A.; Biolatto, B., Palladium-Catalyzed Suzuki−Miyaura Cross-Coupling Reactions of Potassium Aryl- and Heteroaryltrifluoroborates. *The Journal of Organic Chemistry* **2003,** *68* (11), 4302-4314.
46. Migliorini, A.; Oliviero, C.; Gasperi, T.; Loreto, M. A., The Suzuki Reaction Applied to the Synthesis of Novel Pyrrolyl and Thiophenyl Indazoles. *Molecules* **2012,** *17* (4), 4508-4521.
47. Prabakaran, K.; Nawaz Khan, F.; Jin, J. S., Ligand-free, PdCl2(PPh3)2 catalyzed, microwave-assisted Suzuki coupling of 1-chloro-3-phenylisoquinoline in the synthesis of

diversified 1,3-disubstituted isoquinolines. *Research on Chemical Intermediates* **2012,** *38* (2), 337-346.
48. Rossi, R.; Bellina, F.; Carpita, A., Palladium Catalysts for the Suzuki Cross-Coupling Reaction: An Overview of Recent Advances. *Synthesis* **2004,** *2004* (15), 2419-2440.
49. Marion, N.; Navarro, O.; Mei, J.; Stevens, E. D.; Scott, N. M.; Nolan, S. P., Modified (NHC)Pd(allyl)Cl (NHC = N-Heterocyclic Carbene) Complexes for Room-Temperature Suzuki−Miyaura and Buchwald−Hartwig Reactions. *Journal of the American Chemical Society* **2006,** *128* (12), 4101-4111.
50. Sirindil, F.; Pertschi, R.; Naulin, E.; Hatey, D.; Weibel, J.-M.; Pale, P.; Blanc, A., trans-Dichlorobis(XPhos)palladium(II) Precatalyst for Suzuki–Miyaura Cross-Coupling Reactions of Aryl/Vinyl Sulfonates/Halides: Scope, Mechanistic Study, and Synthetic Applications. *ACS Omega* **2022,** *7* (1), 1186-1196.
51. Almond-Thynne, J.; Blakemore, D. C.; Pryde, D. C.; Spivey, A. C., Site-selective Suzuki–Miyaura coupling of heteroaryl halides – understanding the trends for pharmaceutically important classes. *Chemical Science* **2017,** *8* (1), 40-62.
52. Jeon, Y.-K.; Lee, J.-Y.; Kim, S.-E.; Kim, W.-S., Highly Selective Room-Temperature Suzuki–Miyaura Coupling of Bromo-2-sulfonyloxypyridines for Unsymmetrical Diarylpyridines. *The Journal of Organic Chemistry* **2020,** *85* (11), 7399-7412.
53. Widenhoefer, R. A.; Buchwald, S. L., Formation of Palladium Bis(amine) Complexes from Reaction of Amine with Palladium Tris(o-tolyl)phosphine Mono(amine) Complexes. *Organometallics* **1996,** *15* (16), 3534-3542.
54. Widenhoefer, R. A.; Buchwald, S. L., Halide and Amine Influence in the Equilibrium Formation of Palladium Tris(o-tolyl)phosphine Mono(amine) Complexes from Palladium Aryl Halide Dimers. *Organometallics* **1996,** *15* (12), 2755-2763.
55. Barder, T. E.; Buchwald, S. L., Insights into Amine Binding to Biaryl Phosphine Palladium Oxidative Addition Complexes and Reductive Elimination from Biaryl Phosphine Arylpalladium Amido Complexes via Density Functional Theory. *Journal of the American Chemical Society* **2007,** *129* (39), 12003-12010.
56. Xia, Y.; Wang, J.; Dong, G., Suzuki–Miyaura Coupling of Simple Ketones via Activation of Unstrained Carbon–Carbon Bonds. *Journal of the American Chemical Society* **2018,** *140* (16), 5347-5351.
57. Whitaker, L.; Harb, H. Y.; Pulis, A. P., One-pot borylation/Suzuki–Miyaura sp2–sp3 cross-coupling. *Chemical Communications* **2017,** *53* (67), 9364-9367.
58. Neese, F., The ORCA program system" Wiley Interdisciplinary Reviews: Computational Molecular Science. 2012; Vol. 2, pp 73-78.
59. Perdew, J. P.; Burke, K.; Ernzerhof, M., Generalized Gradient Approximation Made Simple. *Physical Review Letters* **1996,** *77* (18), 3865-3868.
60. Kohn, W.; Sham, L. J., Self-Consistent Equations Including Exchange and Correlation Effects. *Physical Review* **1965,** *140* (4A), A1133-A1138.
61. Grimme, S.; Ehrlich, S.; Goerigk, L., Effect of the damping function in dispersion corrected density functional theory. *Journal of Computational Chemistry* **2011,** *32* (7), 1456-1465.
62. Grimme, S.; Antony, J.; Ehrlich, S.; Krieg, H., A consistent and accurate ab initio parametrization of density functional dispersion correction (DFT-D) for the 94 elements H-Pu. *The Journal of Chemical Physics* **2010,** *132* (15), 154104.
63. Weigend, F., Accurate Coulomb-fitting basis sets for H to Rn. *Physical Chemistry Chemical Physics* **2006,** *8* (9), 1057-1065.

64. Pantazis, D. A.; Chen, X.-Y.; Landis, C. R.; Neese, F., All-Electron Scalar Relativistic Basis Sets for Third-Row Transition Metal Atoms. *Journal of Chemical Theory and Computation* **2008,** *4* (6), 908-919.

2. Experimental and Computational Studies of Phosphine Ligand Displacement in Iridium–Pincer Complexes Employing Pyridine or Acetonitrile

Modified with the permission of the ACS
https://doi.org/10.1021/acs.organomet.0c00202
Aneelman Brar, Sara Shaeifi Haghighi, Michael Findlater, Anthony F. Cozzolino, Daniel K Unruh

2.1. Introduction

Group 9 metal–pincer complexes of general formula [(pincer)–M(L)] (L = weakly bound ligand) can be used to prepare reactive 14-electron species, which are widely applied in a variety of catalytic transformations.[1, 2] Among the numerous available ligand backbones known to support iridium–pincer complexes, POCOP has received sustained interest arising from both facile and highly modular syntheses.[3-9] Moreover, the iridium complexes of POCOP ligands have found application in numerous catalytic transformations.[2, 10-16] As a fundamental transformation in coordination/catalysis chemistry, the displacement of labile donor ligands from iridium and other metal centers has been studied by many groups. In 1976, Garrou and Hartwell reported an intermolecular ligand exchange between a halide, CO, and organophosphine ligand in the four-coordinate $M(CO)(X)L_2$ [M = Rh, Ir; X = Cl, Br; L = PPh_3 and others] complexes. It was proposed that exchange between CO and X occurs via a four-center associative process while the organophosphine exchange takes place through a dissociative pathway.[17] Later, Atwood described a ligand-exchange process between the *trans*-$Ir(CO)L_2X$ (L = P(*p*-tolyl)$_3$ and $PMePh_2$, X = Cl, Me, or OMe). Three species were observed: *trans*-$Ir(CO)(P(p\text{-tolyl})_3)_2X$, *trans*-$Ir(CO)(PMePh_2)_2X$, and *trans*-$Ir(CO)(PMePh_2)(P(p\text{-tolyl})_3)X$ upon reaction between *trans*-$Ir(CO)(P(p\text{-tolyl})_3)_2X$ and *trans*-$Ir(CO)(PMePh_2)_2X$.[18] The Oro group prepared cationic iridium complexes, $[IrClH(P^iPr_3)(NCCH_3)_3]BF_4$ and $[IrH_2(P^iPr_3)(NCCH_3)_3]BF_4$, and studied the rates of exchange between free and bound acetonitrile using NMR spectroscopy. Oro and co-workers proposed fluxional five-coordinate intermediates to be involved in this exchange, arising from dissociation of one acetonitrile ligand trans to hydride in both complexes.[19] Milstein and co-workers reported an exchange study at a ^{Pyr}PCP-based rhodium(I) center. It was demonstrated that treatment of either $Rh^I(^{Pyr}PCP)PPh_3$ or $Rh^I(^{Pyr}PCP)PPyr_3$ (Pyr = pyrrolyl, NC_4H_4) with an equivalent of $PPyd_3$ (Pyd = pyrrolydinyl, NC_4H_8) led to the formation of $Rh^I(^{Pyr}PCP)PPyd_3$ with release of either PPh_3 or $PPyr_3$, respectively. However, addition of either 1 equiv of $PPyr_3$ to $Rh^I(^{Pyr}PCP)PPh_3$ or 1 equiv of PPh_3 to $Rh^I(^{Pyr}PCP)PPyr_3$ afforded an equilibrium between two complexes, shifted toward formation of $Rh^I(^{Pyr}PCP)PPyr_3$ at 295 K.[20] One year later, the Brookhart group demonstrated ligand interchange of N_2 with small molecules (CO, NH_3, C_2H_4, H_2, and O_2) could occur within single crystals of the POCOP–Ir^I–(N_2) complex. Significantly, an associative mechanism was observed, and exchange occurred with no apparent loss of crystallinity.[21]Later, Weller and co-workers prepared a series of cationic $[(PNP^R)Rh(PCy_3)]^+$ (R = Ph, Cy, Mes, ^{t}Bu; Mes =2,4,6-$Me_3C_6H_2$) complexes and studied the displacement of the PCy_3 ligand from the rhodium center by using CO, CH_2CH_2, MeCN, acetone, H_2, and N_2, resulting in a suite of new Rh(I)–pincer complexes.[1] In a related study, Fujita's group reported on the equilibrium and kinetics of the coordination of

several small molecules (N_2, H_2, D_2, and C_2H_4) to PCP rhodium(I) complexes in different organic solvents by a combination of kinetic flash photolysis methods, NMR equilibrium studies, and density functional theory (DFT) calculations.[22] In 2015, the Zargarian research group synthesized a range of nickel–pincer complexes of type [(R-POCOP$^{R'}$)Ni(NCMe)][OSO_2CF_3] and investigated the effect of R and R′ groups on equilibrium constants for ligand exchange reactions in both ionic and neutral bromo complexes. It was shown that nickel-bound acetonitrile can be easily displaced by bromide and triflate anions, especially for the more electrophilic (cationic) Ni center.[23]

More recently, the MacLachlan group synthesized a square-planar pincer macrocyclic palladium complex and its corresponding open form, in which the palladium center is coordinated to a tridentate, NNN pincer bis(amido)pyridine and the final coordination site is occupied by an acetonitrile ligand. Acetonitrile exchange was studied by using six different ligands in which kinetic studies revealed that ligand substitution follows an associative pathway. Thus, an increase in steric bulk near the palladium center could prevent the ligand exchange reaction.[24]

Surprisingly, given their popularity in organometallic chemistry, to the best of our knowledge there is still a lack of comparable ligand exchange studies employing iridium–pincer complexes.[21] Previously, our group has reported the synthesis of (^{tBu}POCOP)Ir(L) (L = MeCN (**5**), pyridine (**6**)) complexes (**Scheme 2.1**),[25] which we viewed as excellent test beds for such fundamental ligand exchange studies. Herein, we report on our experimental and computational studies of ligand exchange chemistry between (^{tBu}POCOP)Ir(PPh_3) (**7**) and exogenous ligand, L (L = MeCN, pyridine).

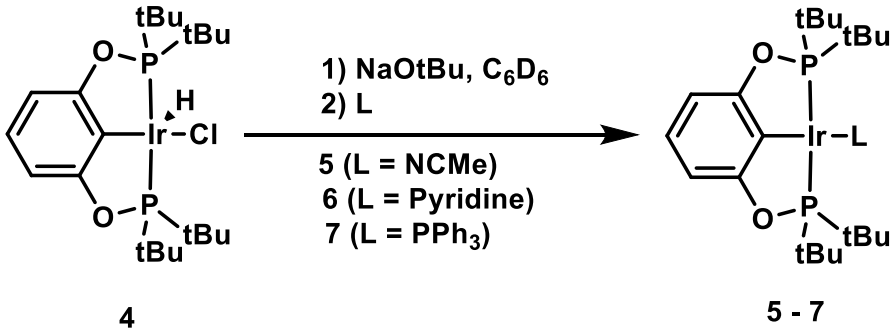

Scheme 2.1. Synthesis of complexes **5-7**

2.2. Ligand-Exchange Studies by Spectroscopy and DFT calculation

2.2.1. By NMR Spectroscopy

Our group[25] demonstrated that addition of CO or C_2H_4 to **7** resulted in the formation of the known complexes (^{tBu}POCOP)Ir(CO) (**8**)[26] and (^{tBu}POCOP)Ir- (C_2H_4) (**9**)[27] at room temperature and 75 °C, respectively, and 1 equiv of free PPh_3.[25] In the present work, we attempted to displace PPh_3 with both acetonitrile and pyridine under ambient conditions. However, at room temperature no reaction was observed even after addition of 2 equiv of

exogenous lewis base and extended reaction times (~1 week). Subsequently, we decided to warm the reaction mixtures to 75 °C, which led to the generation of an equilibrium mixture of **7** with **5** or **7** with **6**, respectively. These results suggested, somewhat to our surprise, that coordination of CO and C_2H_4 to the iridium center is thermodynamically more favored than coordination of either MeCN or pyridine. With these results in hand, we further studied the exchange of PPh_3 by pyridine or MeCN at differing concentration of incoming ligand in an effort to more fully understand the underlying ligand substitution mechanism. The exchange of phosphine can occur via dissociative or associative pathways. Thus, to gain insight into the mechanism of the ligand substitution, NMR and UV studies were performed to evaluate the effects of concentration on the equilibrium and the time required to reach equilibrium (**Figure 2.1**). Upon using 2 equiv of either acetonitrile or pyridine at 75 °C, we observed the formation of a mixture of **7:6/5** in a 1:1 ratio after the reaction reached equilibrium. Increasing the amount of added base to 4, 8, and 16 equiv shifted the equilibrium to the product side and afforded mixtures of complex **7** with either complex **6** or **5** in a 1:2, 1:4, or 1:8 ratio, respectively (**Scheme 2.2 and Figure 2.1**). The ^{31}P and ^{1}H NMR spectra for displacement of PPh_3 with MeCN are as shown in **Figure 2.6 and 2.7** respectively.

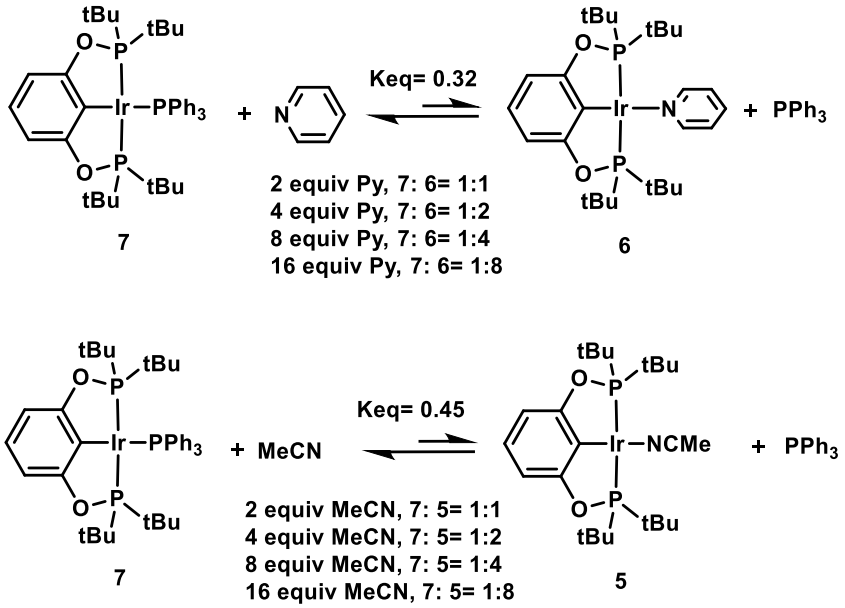

Scheme 2.2. Displacement of PPh_3 with the exogenous ligand (top) pyridine and (bottom) acetonitrile.

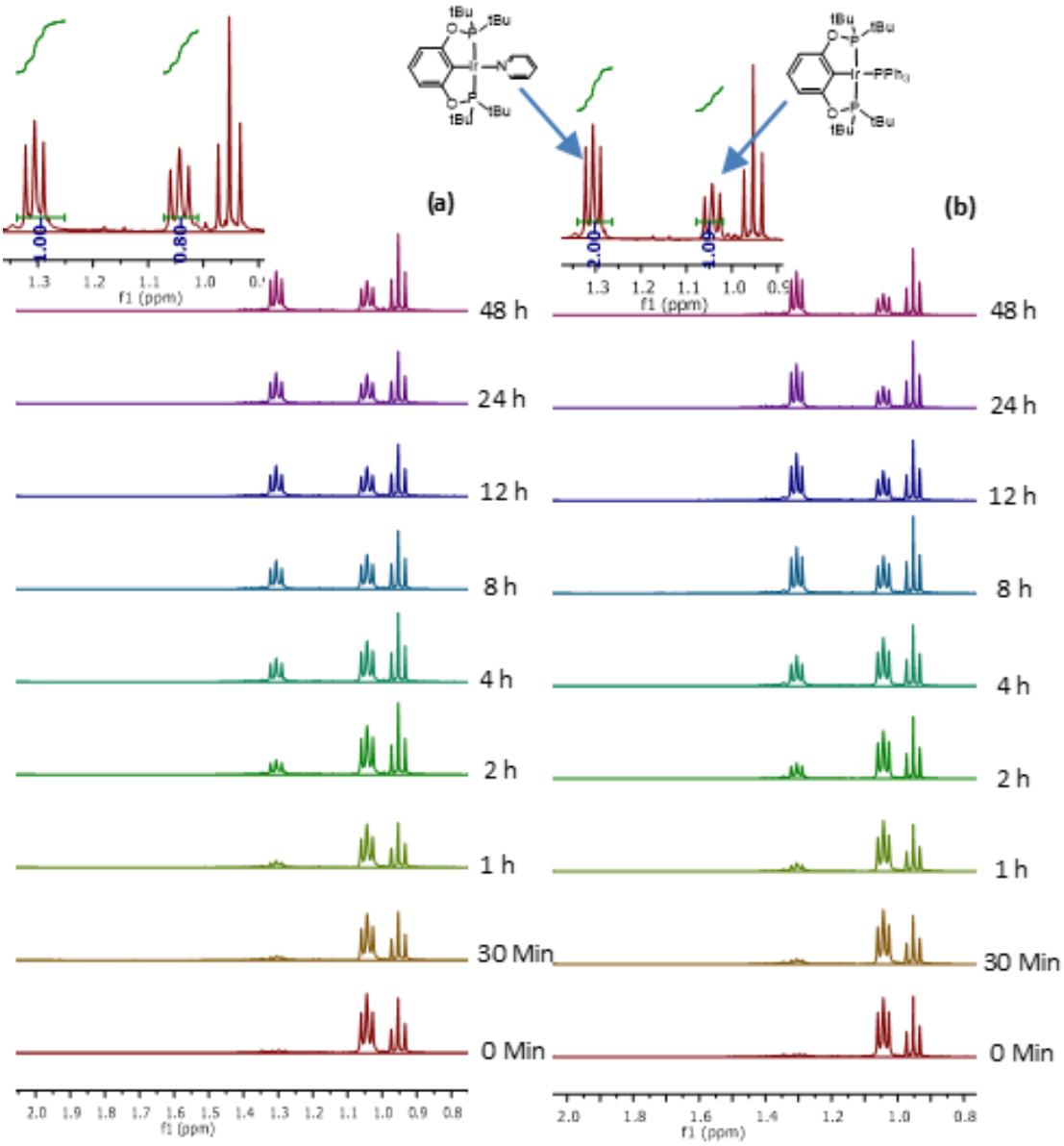
(a)
(b)
48 h
24 h
12 h
8 h
4 h
2 h
1 h
30 Min
0 Min
f1 (ppm)

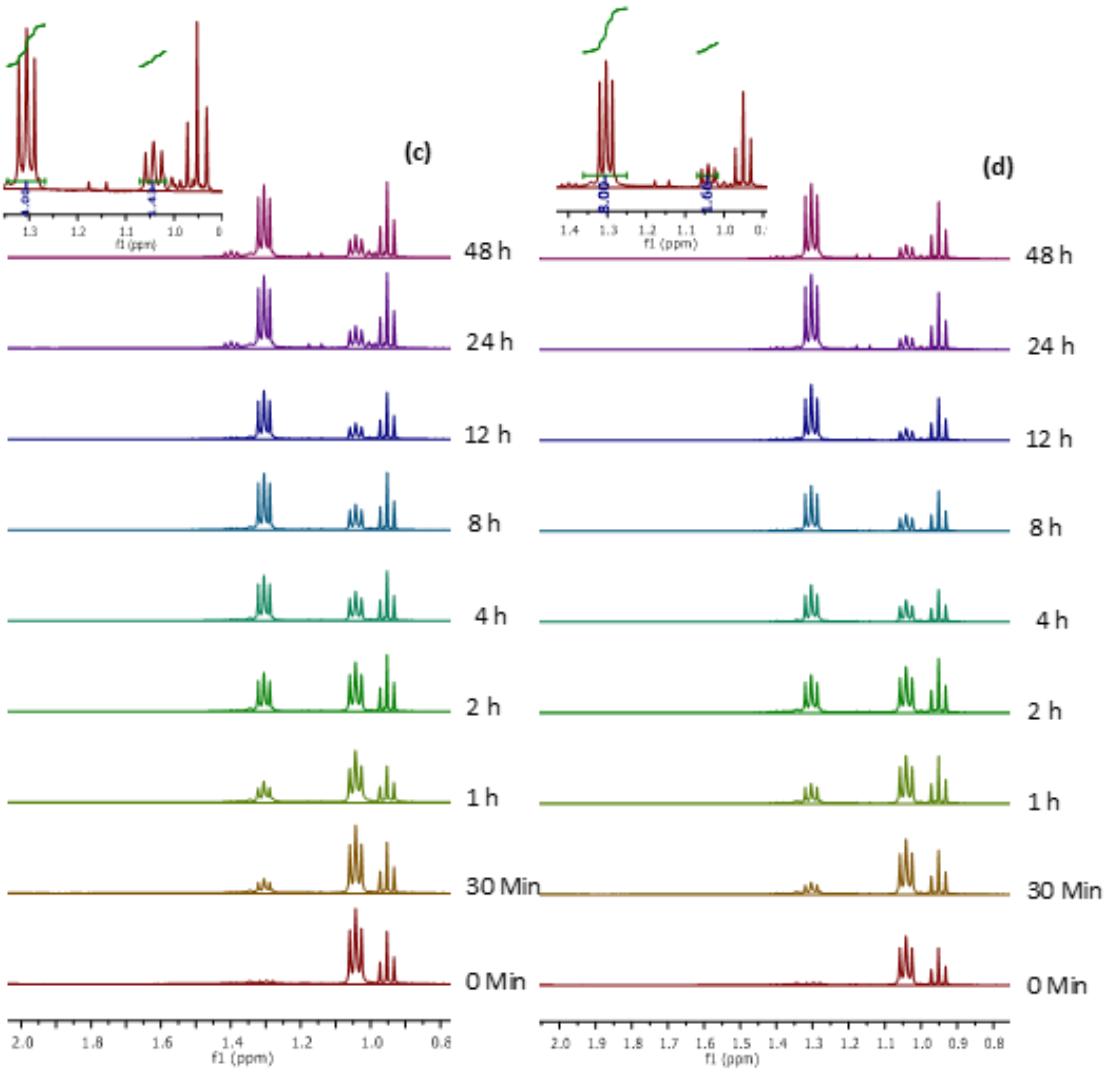

Figure 2.1. Stacked ^{1}H NMR spectra of (a) (^{tBu}POCOP)Ir(PPh$_3$) and (^{tBu}POCOP)Ir(Py) at 75 °C obtained in situ by addition of 2 equiv. pyridine in toluene-d_8, (b) (^{tBu}POCOP)Ir(PPh$_3$) and (^{tBu}POCOP)Ir(Py) at 75 °C obtained in situ by addition of 4 equiv. pyridine in toluene-d_8, (c) (^{tBu}POCOP)Ir(PPh$_3$) and (^{tBu}POCOP)Ir(Py) at 75 °C obtained in situ by addition of 8 equiv. pyridine in toluene-d_8, (d) (^{tBu}POCOP)Ir(PPh$_3$) and (^{tBu}POCOP)Ir(Py) at 75 °C obtained in situ by addition of 16 equiv. pyridine in toluene-d_8.

From our in-situ NMR measurements (performed by former group member Dr. Sara Shafiei), the kinetic profile of the displacement of PPh$_3$ with MeCN or Py was generated by plotting the initial rate of product formation versus concentration of exogenous base; the reaction is clearly dependent on the concentration of Py or MeCN but appears to be less than first order (**Figure 2.2**).

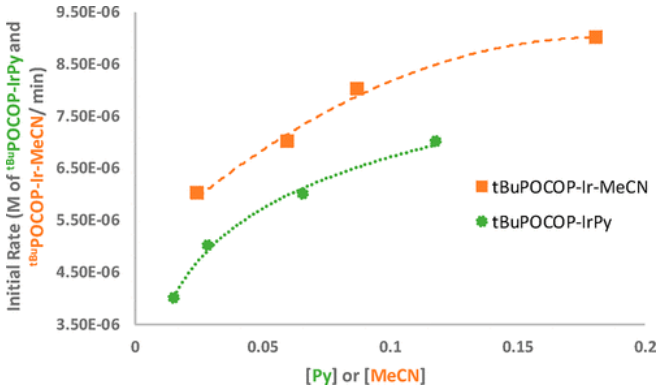

Figure 2.2. Plot of (a) [Py] and (b) [MeCN] vs reaction rate ($K_{initial}$); reaction follows first order dependance upon exogeneous base.

Because changing the concentration of pyridine or MeCN shows an increase in initial rate of reaction, this strongly implies that the rate of the reaction is dependent on concentration of added ligand; hence, the substitution displays characteristics of an associative pathway.[20] To provide further support that an associative mechanism is at play, the displacement of PPh_3 was attempted by using sterically encumbered 2,6-lutidine (**Scheme 2.3**). In this case, even after prolonged reaction times, no phosphine displacement was observed. We attribute this lack of reactivity to the increase in steric hindrance, arising from methyl substitution in the ortho-positions of 2,6-lutidine which would preclude an associative pathway. Furthermore, we probed the effects of addition of free phosphine on the position of the equilibrium.

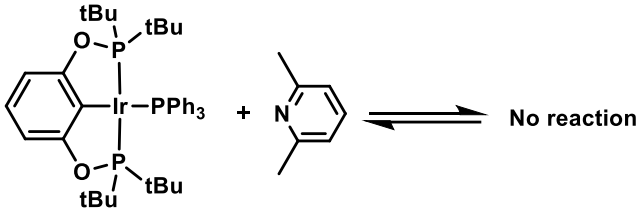

7

Scheme 2.3. Displacement of PPh_3 with 2,6- Lutidine.

Addition of excess PPh_3 shifted the equilibrium to the reactant side, confirming the presence of an equilibrium. Based upon the NMR spectroscopic data for complexes **5 – 7**, the coordination environment around the iridium center is consistent with pseudo-square-planar geometry with time averaged C_{2v} symmetry.[25] The associative mechanism is considered to be more common in 16e, d^8 square-planar complexes and is more likely to occur for electron-deficient metal centers; this mechanism therefore avoids formation of electron-deficient 14e species.[20] However, in 2002, Goldman and co-workers, showed that because of repulsive interactions between the HOMO of the complex and the HOMO of an incoming ligand in square-planar d^8 ML_4 iridium complexes, the addition of a fifth ligand is not favored.[28] Previous theoretical studies by the Hoffmann group revealed that the addition of a fifth ligand can happen if it occurs through a bent ML_4 geometry.[29]

Moreover, this effect will be enhanced by the presence of π-accepting ligands which facilitate the coordination of the fifth ligand.[30] The equilibrium constant and Gibb's free energy were measured experimentally using NMR spectroscopy. To measure the concentration of the complexes **6** and **7**, tetraethylsilane was used as an internal standard when reaction reached equilibrium 24 hr. Knowing the total concentration of starting complex and added ligands, the relative concentrations of free ligands (Py, MeCN) were also measured. The average equilibrium constant value when Py is used as incoming ligand is determined to be 0.32 and 0.45 in the case of MeCN as incoming ligand (**Eq.1**). It should be noted that the free energy change of the reaction is equivalent to the difference in the free energies of binding of the incoming ligand Py/MeCN and the PPh_3 ligand to POCOP–Ir–PPh_3.[22]

$$K_{eq} = [(POCOP)\text{-}Ir(L)][PPh_3]/[(POCOP)\text{-}Ir(PPh_3)][L] \qquad (\textbf{Eq.1})$$

Finally, the reverse reaction, displacement of pyridine and acetonitrile with PPh_3, was investigated by using 1 equiv of PPh_3 in combination with either complex **5** or **6** (**Scheme 2.4**).

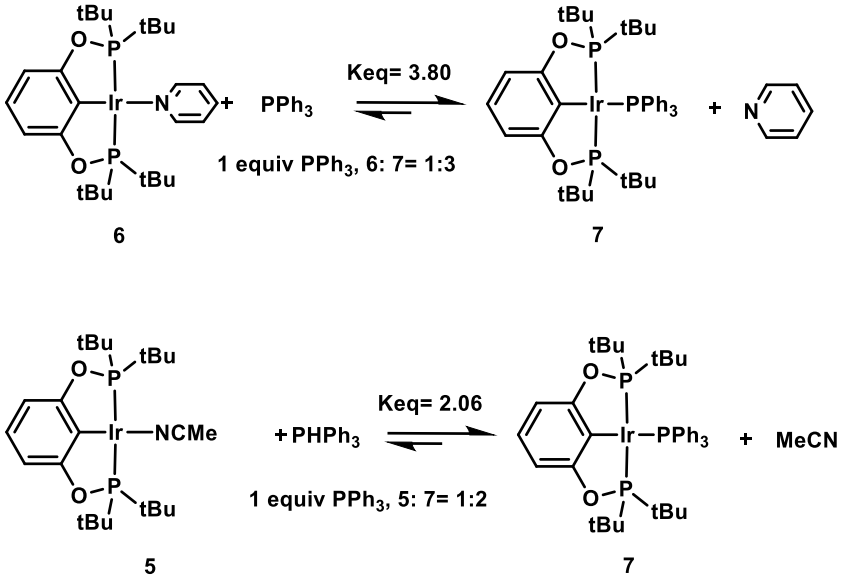

Scheme 2.4. Displacing Py and Acetonitrile with PPh_3.

The K_{eq} values for displacement of pyridine or acetonitrile with PPh_3 are both >1 and are therefore fully consistent with the conclusion that addition of PPh_3 to POCOP–Ir–L (L = MeCN or Py) is thermodynamically favored.

2.2.2.DFT calculations

DFT calculations (PBE, ZORA, CPCM) were performed to gain insight into the reaction mechanism for the ligand exchange reaction with **7**. The geometric parameters of the optimized structures were compared with the experimentally determined values.[31] The geometry of the coordination sphere was well-reproduced, with bond distances within 0.04 Å and bond angles within 1° (**Table 2.1**) by using the TZVP basis set. Frequency calculations confirmed that the structures are energetic minima and allowed for the calculation of free energies. The Gibbs free energy values for the replacement of triphenylphosphine with acetonitrile or pyridine were calculated to be 3.3 and 5.8 kcal mol^{-1}, respectively. These values suggest that acetonitrile binding is more favorable than pyridine, and this is consistent with the relative ordering of the binding constants obtained from the solution NMR study, although the absolute values appear to underestimate the free energy of the product. To elucidate the mechanism, both associative and dissociative pathways were explored (**Scheme 2.5**). The dissociative pathway was modeled by elongating the $Ir–P_{phosphine}$ distance. The energy reached a maximum upon complete dissociation to give three coordinated iridium (path I), the presumed transition state for this pathway. The free energy barrier for this pathway is estimated as 42.2 kcal mol^{-1}, too high to proceed at room temperature.

An associative mechanism is more complicated to model as various angles of approach can be considered. Furthermore, an isomerization step is necessary, so the reaction can proceed by association, then isomerization or isomerization, and then association. Following pathway II, the ligand was stepped in at a right angle to the CP_2IrP plane to give a pseudo-square-pyramidal geometry. It was found that this pathway encounters a reaction barrier of 50.2 kcal mol^{-1}, effectively ruling it out as a viable alternative to a dissociative pathway. Assuming that both ligands follow the same mechanism, we also ruled out this pathway for the acetonitrile ligand. Considering an isomerization-first pathway (path III), the potential energy surface for the isomerization of the $C–Ir–P_{phosphine}$ bond from 170° to 90° was mapped. A potential energy surface was then mapped out by varying the Ir–N and Ir–P distances while fixing the C(39)–Ir(1)–P(3) angle at 120°. A transition state search was performed starting near the saddle point on this surface, and a geometry with a single imaginary vibrational mode was found. This transition state occurred at a calculated energy barrier (**Figure 2.2**) of 26.04 and 20.95 kcal mol^{-1} for pyridine and acetonitrile, respectively. These barriers, which are less than that calculated for the dissociative pathway, appear to support the ligand exchange occurring through an associative mechanism.

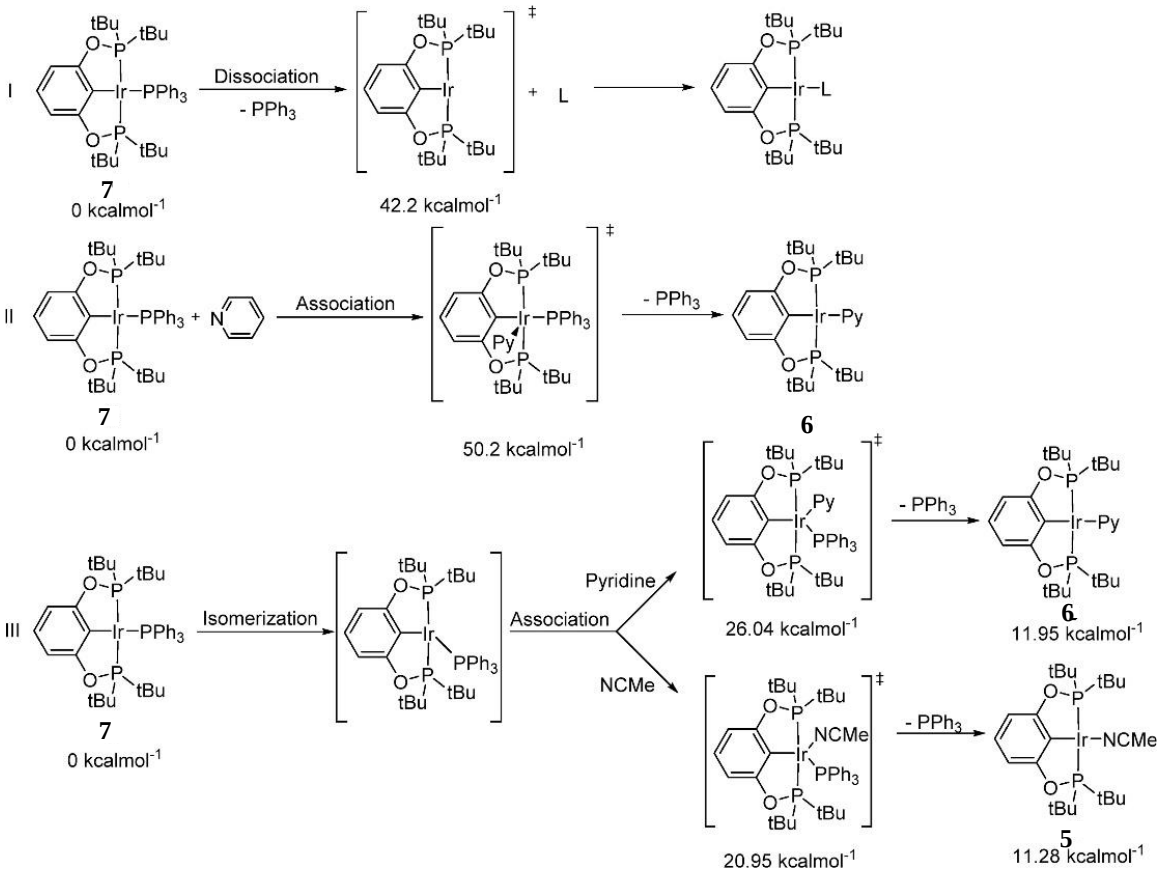

Scheme 2.5. Possible Pathways for Ligand Exchange Reaction

2.2.3. By UV–Vis Spectroscopy

It proved possible to also monitor ligand exchange processes employing UV–vis spectroscopy. The changes observed in the UV−vis spectra were monitored as a function of time while varying the temperatures (65, 75, or 85 °C) and concentrations of pyridine or acetonitrile. **Figure 2.3**. represents the changes observed in absorbance as the pyridine or acetonitrile reacts with **7** in toluene. The change in absorbance at ~515.505 nm was found to be the greatest in both reactions and was chosen as a wavelength to monitor to evaluate the kinetics.

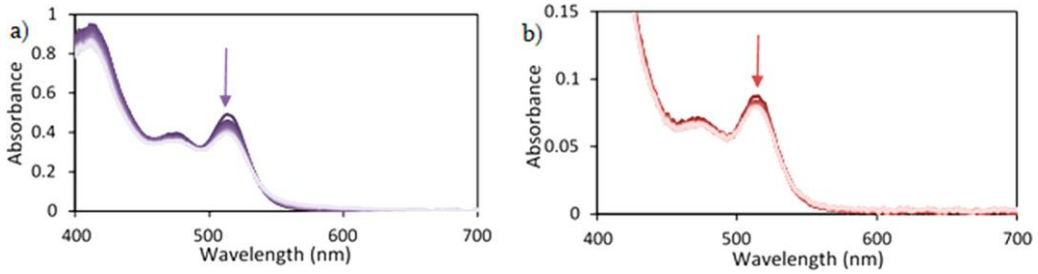

Figure 2.3. Plot of change in absorption with a) pyridine and b) acetonitrile as exogeneous ligand.

The molar absorptivity values (**Figure 2.3**) of 1670, 492, and 450 M^{-1} cm^{-1} were acquired for **7, 5,** and **6**, respectively. Both the DFT calculations and the absence of an observable exchange reaction with lutidine (discussed previously) were consistent with an associative mechanism. However, when a solution of **7** was heated in toluene and monitored by UV–vis spectroscopy, it became clear that phosphine ligand dissociation from **7** was occurring even in the absence of exogenous ligand, strongly indicating the presence of a dissociative mechanism (**Figure 2.15**). Notably, the intensity increased toward the original value once the heating was turned off, suggesting a return to the original complex **7**. Given the apparently conflicting results, we opted to fit the ligand exchange data with two models: (1) dissociative (first order in complex concentration with forward and reverse rate constants) and (2) associative (first order in all species with forward and reverse rate constants. Fitting the data by using the first kinetic model resulted in different initial rates being obtained, and overall, this model provided a poor fit for the data (**Figure 2.14**). Fitting the data with the second kinetic model led to a better fit, but with some residual negative dependence on the concentration of incoming ligands. The inability to obtain a perfect fit with either model leads us to believe that at elevated temperatures it is possible to access both associative and dissociative pathways. The rate constants from the second kinetic model obtained by fitting the data at three different temperatures (**Table 2.1**) afforded a linear Eyring plot (**Figure 2.4**), and a Gibbs free energy of activation of 24.5 and 24.0 kcal mol^{-1} was determined for pyridine and acetonitrile, respectively.

Table 2.1. The forward rate constants (*k1*) for pyridine and acetonitrile at different temperatures are calculated using Eq. 5 (Associative mechanism)

S.no	Ligand	Temperature (°C)	100 eq	200 eq	300 eq
1	Pyridine	65	1.61E-03	5.13E-04	3.52E-04
2	Pyridine	75	3.56E-03	2.81E-03	1.50E-03
3	Pyridine	85	2.32E-03	9.21E-03	5.40E-03
4	Acetonitrile	65	3.43E-03	1.29E-03	7.38E-04
5	Acetonitrile	75	8.91E-03	4.38E-03	2.16E-03
6	Acetonitrile	85	2.94E-02	1.37E-02	9.89E-03

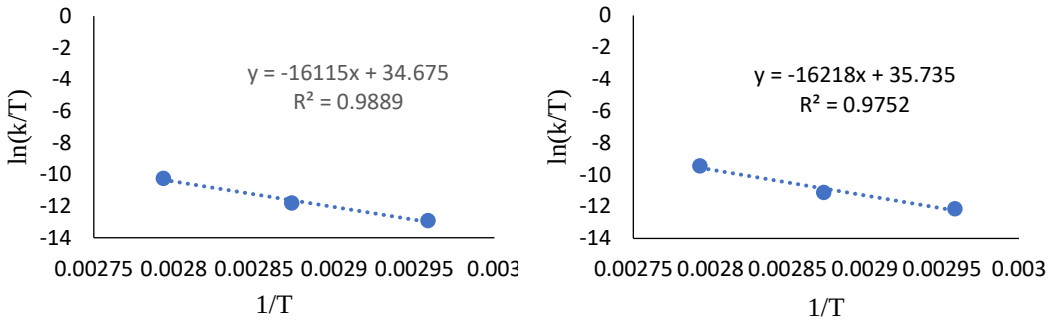

Figure 2.4. The eyring plot for kinetic run a) Py (left) and b) acetonitrile (right)

The entropy of activation was determined to be positive which is consistent with a dissociative process. We attribute the seemingly at odds positive enthalpy of activation and exogenous ligand dependence in the rate law to a mixture of associative and dissociative pathways being accessible under these conditions. This sheds some light on the disparate results from the previously reported CO and C_2H_4 exchange with PPh_3. The ability of CO to displace PPh_3 at room temperature suggests that the small size and high nucleophilicity of the CO allow for an associative pathway. Heating is required for the replacement of PPh_3 with C_2H_4. This suggests that a higher energy dissociative pathway needs to be accessed in order for the exchange to take place.

2.3. Conclusion

We have conducted equilibrium and kinetic studies for the ligand exchange of pyridine and acetonitrile with triphenylphosphine from complex **7** by NMR and UV–vis spectroscopy. The equilibrium (NMR) and DFT studies are consistent with an associative mechanism for the displacement of PPh_3 by these ligands, but reaction kinetics as monitored by UV–vis spectroscopy revealed that both associative and dissociative mechanisms are viable and likely taking place.

2.4. Experimental Section

2.4.1. General Considerations

All manipulations were performed by using standard Schlenk, high-vacuum, and glovebox techniques. Argon was purified by passage through columns of BASF R3-11 (chemalog) and 4 Å molecular sieves. Anhydrous benzene and toluene were purchased from Sigma-Aldrich. Proton and carbon nuclear magnetic resonance spectra (^{1}H NMR and ^{13}C NMR

spectra) were recorded on a Jeol 400 MHz spectrometer with Me_4Si or solvent resonance as the internal standard (^1H NMR, Me_4Si at 0 ppm, $CHCl_3$ at 7.24 ppm; ^{13}C NMR, Me_4Si at 0 ppm, $CDCl_3$ at 77.0 ppm). The relaxation delay time was set to 5s, and the initial wait was 1s in ^1H NMR of all the equilibria. All reagents, unless otherwise noted, were purchased from commercial vendors, and used without further purification. The syntheses of the phosphinite complexes, (^{tBu}POCOP)Ir(H)(Cl)[26] and (^{tBu}POCOP)Ir(PPh_3),[31] have been previously described in the literature.

2.4.2. Computational Method

Density functional theory (DFT) calculations were performed by using the ORCA 4.1.0 quantum chemistry program package from the development team at the Max Planck Institute for Bioinorganic Chemistry.[32] All calculations were performed by using the exchange correlation functional proposed by Perdew, Becke, and Ernzerhof (PBE)[33] with the zeroth-order regular approximation (ZORA).[34, 35] Spin-restricted Kohn–Sham determinants were chosen to describe the closed shell wave functions, employing the RI approximation and the tight SCF convergence criteria provided by ORCA.[36] The atom-pairwise dispersion correction with the Becke–Johnson damping scheme (D3) were utilized for all calculations,[37, 38] and the def2-SVP, def2-TZVP, and SARC/J auxiliary basis sets were used for all atoms.[39-43] The effect of solvent were also included by employing the conductor-like polarizable continuum model (C-PCM).[44] The energetics were calculated by the equation

$$\Delta \boldsymbol{G} = \Delta \boldsymbol{H} - \boldsymbol{T}\Delta \boldsymbol{S} + \boldsymbol{ZPE} + \boldsymbol{BSSE} + \Delta \boldsymbol{E}(\boldsymbol{solv})$$

The ZPE is the zero-point energy, BSSE is the basis-set superposition error which was evaluated by the method given by Boys and Bernardi,[45] and ΔE_{solv} is the energy change associated with the C-PCM calculation. Analytical frequency calculations were performed on all low-energy conformations and revealed no negative frequencies. The entropy, ZPE, and BSSE values obtained from the gas-phase calculations were used for all reported values.

2.4.3. UV-Vis Kinetics

The control experiments were run where we heated the (^{tBu}POCOP)Ir(PPh_3) complex in toluene for the duration of kinetic experiments at 75 and 85 °C to observe any background reactivity or changes. At the end of the time heat was turned off to reduce temperature back to 25 °C, and subsequent changes were monitored (**Figure 2.15**). To study the kinetics of ligand exchange, stock solutions of (^{tBu}POCOP)Ir(PPh_3) (0.020 M), pyridine (5.00 M), and acetonitrile (5.00 M) were prepared. The exchange was monitored at three different temperatures with three (100, 200, and 300) equivalents of ligand. Inside the glovebox, the cuvette was charged with 2.00 mL of toluene, (25.00 μL, 0.020 M) of (^{tBu}POCOP)Ir(PPh_3), and pyridine (10.00 μL, 100 equiv; 20.00 μL, 200 equiv; 30.00 μL, 300 equiv) from the prepared stock solution of 5.00 M. A similar procedure was followed for kinetic run with acetonitrile. The reaction mixture was heated to temperature (65, 75, and 85 °C) with the stirring speed of 1200 rpm. The relevant spectra(s) were recorded over the range of 400–

800 nm wavelength. The wavelength of 515.505 nm was chosen as the optimal wavelength for the investigation of kinetics of reaction between (^{tBu}POCOP)IrPPh$_3$ and incoming ligand. After the solution reached equilibrium the intensity data extracted at ~515.505 nm was fit to a calculated intensity by varying the rate constant for the particular integrated rate law by using the solver function in excel. From these rate constants, the Gibbs free energy of activation was determined by using the Eyring equation.

2.5. Appendix

2.5.1 Spectral data for displacement of PPh$_3$ with pyridine

Equilibrium between (tBuPOCOP)Ir(PPh$_3$) and (tBuPOCOP)Ir(Py) using 2 equiv of Pyridine: δH (400 MHz; toluene-d$_8$): δ 9.10 (d, J= 5.2 Hz, 1H, Ir-py), 8.45 (brs, 4H, py), 8.02 (t, J= 8.0 Hz, 3H, Ir-PPh$_3$), 7.32 (m, 3H, PPh$_3$), 7.12 (m, 1H, Ir-PP$_3$), 7.03-7.00 (m, 9H, Ir-PPh$_3$, PPh$_3$, Ir-py, py), 6.83 (t, J= 8.0 Hz, 1H, Ir-PPh$_3$), 6.73-6.70 (m, 4H, py), 6.67-6.65 (m, 1H, Ir-py), 6.43 (t, J= 6.4 Hz, 1H, Ir-py), 1.29 (t, J= 6.4 Hz, 18H, Ir-py), 1.04 (t, J= 6.4 Hz, 18H, Ir-PPh$_3$). 31P {^{1}H} (162 MHz, toluene-d8): δ 180.6 (d, J= 6.5 Hz, 2P, Ir-PPh$_3$), 172.6 (s, 2P, Ir-py), 15.64 (t, J= 5.8 Hz, 1P, Ir-PPh$_3$), 4.69 (s, 1P, PPh$_3$).

Equilibrium between (tBuPOCOP)Ir(PPh$_3$) and (tBuPOCOP)Ir(Py) using 4 equiv of Pyridine: δH (400 MHz; toluene-d8): δ 9.06 (d, J= 4.8 Hz, 1H, Ir-py), 8.49 (d, J= 4.0 Hz, 8H, py), 8.06 (t, J= 8.4 Hz, 2H, Ir-PPh$_3$), 7.34-7.30 (m, 4H, PPh$_3$), 7.10 (s, 1H, Ir-PPh$_3$), 7.07-7.00 (m, 11H, Ir-PPh$_3$, PPh$_3$, Ir-py, py), 6.94-6.90 (m, 1H, Ir-py), 6.82 (dd, J= 7.6 Hz, 1H, Ir-PPh$_3$), 6.79-6.77 (m, 1H, Ir-py), 6.69-6.66 (m, 8H, py), 6.33 (dq, J= 6.4 Hz, 1H, Ir-py), 1.30 (t, J= 6.4 Hz, 24H, Ir-py), 1.04 (t, J= 6.4 Hz, 12H, Ir-PPh$_3$). 31P {1H} (162 MHz, toluene-d8): δ 180.6 (d, J= 6.5 Hz, 2P, Ir-PPh$_3$), 172.6 (s, 1P, Ir-py), 15.64 (t, J= 5.7 Hz, 1P, Ir-PPh$_3$), 4.69 (s, 1P, PPh$_3$).

Equilibrium between (tBuPOCOP)Ir(PPh$_3$) and (tBuPOCOP)Ir(Py) using 8 equiv of Pyridine: δH (400 MHz; toluene-d8): δ 9.04 (d, J= 4.8 Hz, 1H, Ir-py), 8.48 (d, J= 4.0 Hz, 20H, py), 8.04 (t, J= 9.2 Hz, 1H, Ir-PPh$_3$), 7.34-7.30 (m, 4H, PPh$_3$), 7.13 (s, 1H, Ir-PPh$_3$), 7.07-7.02 (m, 15H, Ir-PPh$_3$, PPh3, Ir-py, py), 6.94-6.90 (m, 1H, Ir-py), 6.82 (dd, J= 8.0 Hz, 1H, Ir-PPh$_3$), 6.78-6.77 (m, 1H, Ir-py), 6.69-6.66 (m, 20H, py), 6.34 (dq, J= 6.2 Hz, 1H, Ir-py), 1.30 (t, J= 6.4 Hz, 27H, Ir-py), 1.04 (t, J= 6.4 Hz, 9H, Ir-PPh$_3$). 31P {1H} (162 MHz, toluene-d8): δ 180.6 (d, J= 5.7 Hz, 1P, Ir-PPh$_3$), 172.6 (s, 4P, Ir-py), 15.62 (t, J= 5.5 Hz, 1P, Ir-PPh$_3$), 4.69 (s, 2P, PPh$_3$).

Equilibrium between (tBuPOCOP)Ir(PPh$_3$) and (tBuPOCOP)Ir(Py) using 16 equivalents of Pyridine: δH (400 MHz; toluene-d8): δ 9.04 (d, J= 4.8 Hz, 1H, Ir-py), 8.48 (d, J= 4.0 Hz, 32H, py), 8.04 (t, J= 8.0 Hz, 1H, Ir-PPh$_3$), 7.34-7.30 (m, 5H, PPh$_3$), 7.13 (s, 1H, Ir-PPh$_3$), 7.07-7.00 (m, 21H, Ir-PPh$_3$, PPh$_3$, Ir-py, py), 6.93-6.89 (m, 1H, Ir-py), 6.82 (dd, J= 7.6 Hz, 1H, Ir-PPh$_3$), 6.78-6.76 (m, 1H, Ir-py), 6.68 (dq, J= 7.8 Hz, 32H, py), 6.35 (dq, J= 6.4 Hz, 1H, Ir-py), 1.30 (t, J= 6.4 Hz, 32H, Ir-py), 1.04 (t, J= 6.4 Hz, 4H, Ir-PPh$_3$). 31P {^{1}H} (162 MHz, toluene-d8): δ 180.6 (d, J= 6.0 Hz, 1P, Ir-PPh$_3$), 172.6 (s, 8P, Ir-py), 15.60 (t, J= 5.8 Hz, 1P, Ir-PPh$_3$), 4.69 (s, 4P, PPh$_3$).

2.5.2 Spectral data for Displacement of PPh_3 by acetonitrile

Equilibrium between (tBuPOCOP)Ir(PPh_3) and (tBuPOCOP)Ir($NCCH_3$) using 2 equiv of acetonitrile: δH (400 MHz; toluene-d_8): δ 8.04 (t, J= 9.2 Hz, 3H, Ir-PPh_3), 7.34-7.30 (m, 3H, PPh_3), 7.13 (s, 1H, Ir-PPh_3), 7.08-7.01 (m, 9H, Ir-PPh_3, PPh_3), 6.88-6.84 (m, 1H, Ir-$NCCH_3$), 6.82 (dd, J= 7.6 Hz, 1H, Ir-PPh_3), 6.77-6.75 (m, 1H, Ir-$NCCH_3$), 1.45 (t, J= 6.8 Hz, 18H, Ir-$NCCH_3$), 1.04 (t, J= 6.8 Hz, 18H, Ir-PPh_3), 0.68 (s, 7H, $NCCH_3$). 31P {1H} (162 MHz, toluene-d_8): δ 180.6 (d, J= 6.0 Hz, 2P, Ir-PPh_3), 179.5 (s, 2P, Ir-$NCCH_3$), 15.62 (t, J= 5.7 Hz, 1P, Ir-PPh_3), 4.68 (s, 1P, PPh_3).

Equilibrium between (tBuPOCOP)Ir(PPh_3) and (tBuPOCOP)Ir($NCCH_3$) using 4 equivalents of acetonitrile: δH (400 MHz; toluene-d_8): δ 8.06-8.01 (m, 2H, Ir-PPh_3), 7.34-7.30 (m, 4H, PPh_3), 7.13 (s, 1H, Ir-PPh_3), 7.09-7.03 (m, 9H, Ir-PPh_3, PPh_3), 6.88-6.84 (m, 1H, Ir-$NCCH_3$), 6.81 (dd, J= 7.8 Hz, 1H, Ir-PPh_3), 6.76-6.74 (m, 1H, Ir-$NCCH_3$), 1.44 (t, J= 6.8 Hz, 24H, Ir-$NCCH_3$), 1.04 (t, J= 6.4 Hz, 12H, Ir-PPh_3), 0.69 (s, 16H, $NCCH_3$). 31P {1H} (162 MHz, toluene-d_8): δ 180.5 (d, J= 5.7 Hz, 1P, Ir-PPh_3), 179.4 (s, 2P, Ir-$NCCH_3$), 15.48 (t, J= 5.8 Hz, 1P, Ir-PPh_3), 4.8 (s, 1P, PPh_3).

Equilibrium between (tBuPOCOP)Ir(PPh_3) and (tBuPOCOP)Ir($NCCH_3$) using 8 equiv of acetonitrile: δH (400 MHz; toluene-d8): δ 8.03 (t, J= 9.4 Hz, 1H, Ir-PPh_3), 7.34-7.30 (m, 4H, PPh_3), 7.13 (s, 1H, Ir-PPh_3), 7.07-7.02 (m, 9H, Ir-PPh_3, PPh_3), 6.87-6.83 (m, 1H, Ir-$NCCH_3$), 6.80 (dd, J= 8.0 Hz, 1H, Ir-PPh_3), 6.76-6.74 (m, 1H, Ir-$NCCH_3$), 1.44 (t, J= 6.8 Hz, 27H, Ir-$NCCH_3$), 1.04 (t, J= 6.4 Hz, 9H, Ir-PPh_3), 0.71 (s, 30H, $NCCH_3$). 31P {1H} (162 MHz, toluene-d_8): δ 180.63 (d, J= 6.0 Hz, 1P, Ir-PPh_3), 179.54 (s, 4P, Ir-$NCCH_3$), 15.55 (t, J= 5.7 Hz, 1P, Ir-PPh_3), 4.71 (s, 2P, PPh_3).

Equilibrium between (tBuPOCOP)Ir(PPh_3) and (tBuPOCOP)Ir($NCCH_3$) using 16 equivalents of acetonitrile: δH (400 MHz; toluene-d_8): δ 8.0 (t, J= 8.2 Hz, 1H, Ir-PPh_3), 7.31-7.27 (m, 4H, PPh_3), 7.11 (s, 1H, Ir-PPh_3), 7.05-7.0 (m, 9H, Ir-PPh_3, PPh_3), 6.83-6.80 (m, 1H, Ir-$NCCH_3$), 6.76 (dd, J= 8.0 Hz, 1H, Ir-PPh_3), 6.71-6.69 (m, 1H, Ir-$NCCH_3$), 1.41 (t, J= 6.8 Hz, 32H, Ir-$NCCH_3$), 1.01 (t, J= 6.0 Hz, 4H, Ir-PPh_3), 0.73 (s, 52H, $NCCH_3$). 31P {1H} (162 MHz, toluene-d_8): δ 180.54 (d, J= 6.1 Hz, 1P, Ir-PPh_3), 179.47 (s, 8P, Ir-$NCCH_3$), 15.44 (t, J= 5.7 Hz, 1P, Ir-PPh_3), 4.81 (s, 4P, PPh_3).

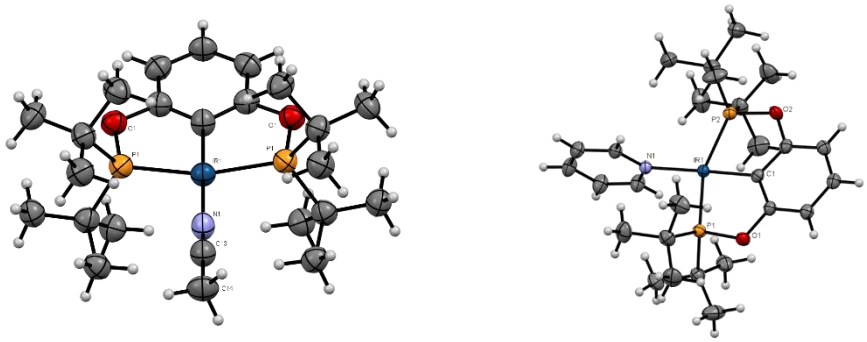

Figure 2.5. The crystal structure for (^{tBu}POCOP)Ir-MeCN (left) and (^{tBu}POCOP)Ir-Py (right).

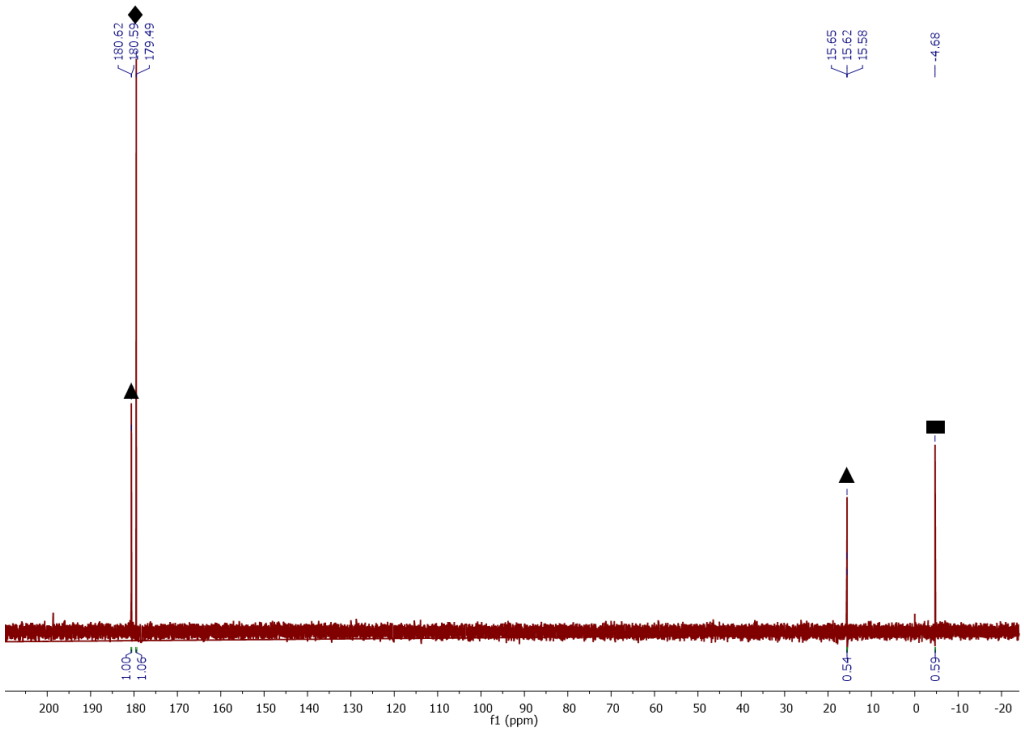

Figure 2.6. ^{31}P NMR of (^{tBu}POCOP)Ir(PPh_3) and (^{tBu}POCOP)Ir($NCCH_3$) equilibrium after 24h, using 2 equivalents of MeCN. (▲) represents (^{tBu}POCOP)Ir(PPh_3) , (◆) represents (^{tBu}POCOP)Ir($NCCH_3$) and (■) represents PPh_3.

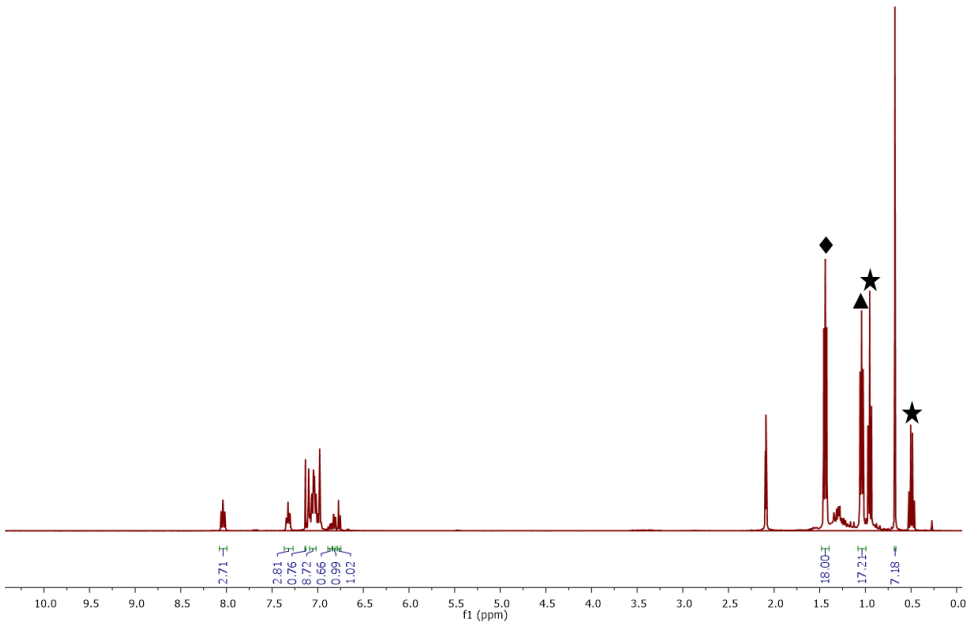

Figure 2.7. ^{1}H NMR of (^{tBu}POCOP)Ir(PPh$_3$) and (^{tBu}POCOP)Ir(NCCH$_3$) equilibrium after 24h, using 2 equivalents of MeCN. (♦) represents (^{tBu}POCOP)Ir(NCCH$_3$),(▲) represents (^{tBu}POCOP)Ir(PPh$_3$) and (★) represents internal standard.

Table 2.1. Comparison of experimental and DFT calculations in terms of bond parameters and energy [a] is for [(^{tBu}POCOP)Ir(NCCH$_3$)] and [b] is for [(^{tBu}POCOP)Ir(Py)].

Structural parameters	Crystal structure	Geometry optimized
Ir (1)- P(2)[a]	2.246 (2)Å	2.276 Å
Ir (1)- P(1)[a]	2.246 (2)Å	2.276 Å
Ir(1)- C(40)[a]	2.010 (11) Å	2.022 Å
C(40)- Ir(1)-P(3)[a]	178.90° (4)	178.44°
P(1)- Ir(1)-P(2)[a]	159.40° (15)	158.55°
Ir (1) – N (1)[a]	2.054 (10) Å	1.99 Å
Ir (1) – N (1)[b]	2.133 (2)Å	2.133 Å
Ir (1) – P (1)[b]	2.256 (6) Å	2.283 Å
Ir (1) – P (2)[b]	2.255 (6) Å	2.282 Å
Ir (1) – C (1)[b]	2.004 (3) Å	2.019 Å
C(39)- Ir(1)-P(3)[b]	178.8° (9)	179.91°
P(1)- Ir(1)-P(2)[b]	158.92° (2)	158.14°

Table 2.2. Energy Values for Reaction w.r.t. SVP, TZVP, TZVPP basis set (in kcal.mol^{-1})

Reaction	ΔG (SVP)	ΔG (TZVP)	ΔG (TZVPP)
Displacement of PPh_3 with MeCN	2.294	3.295	4.231
Displacement of PPh_3 with pyridine	4.695	5.788	6.060

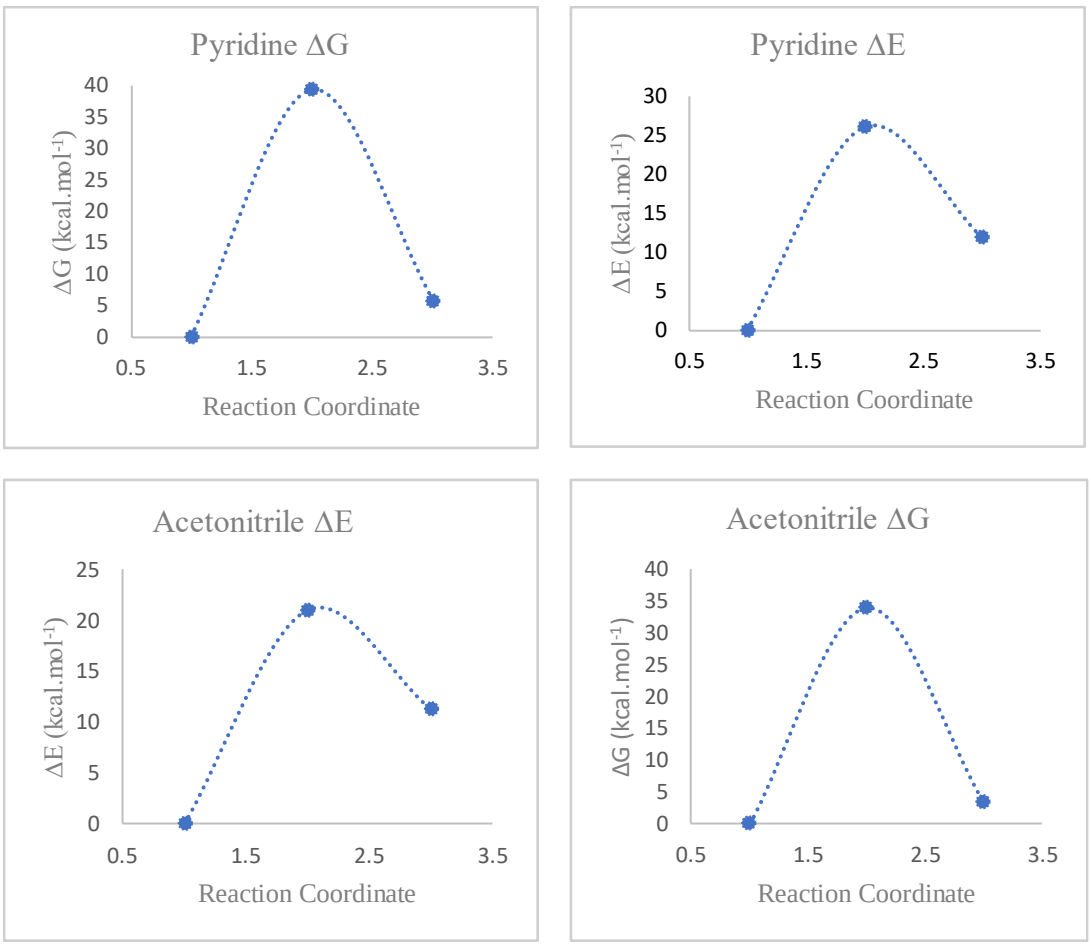

Figure 2.8. Calculated Energy barriers (ΔE and ΔG) for pyridine and acetonitrile. The dotted lines were added for visual aid.

2.5.3. UV-Vis Kinetic Data Collection and Fitting

Data Collection:
UV-vis spectra were collected on Silver-Nova Super Range TEC spectrometer, with SL1 Tungsten Halogen Lamp (visible and near-IR region) as the light source. The spectrometer was equipped with a CUV-TEMP cuvette holder (qpod 2e) with a path length of 1.0 cm. The spectra were collected at three different temperatures (65 °C, 75 °C, 85 °C) with a stir rate of 1200 rpm.
Before each kinetic run, a dark spectrum, and a blank spectrum (of toluene) were collected. Inside a glove box, the cuvette was charged with 2.00 mL of the (^{tBu}POCOP)IrPPh$_3$ solution and appropriate amounts of pyridine or acetonitrile stock solutions to achieve the desired concentrations. The cuvettes had a Chemglass stopper with an o-ring to ensure air-free conditions over the course of the experiments. The (^{tBu}POCOP)IrPPh$_3$ stock solutions were prepared at concentrations of 0.020 M or 0.004225 M for the pyridine or acetonitrile experiments, respectively. The stock solutions of Pyridine and Acetonitrile were prepared in toluene at a concentration of 5.00 M. For the kinetic run, each time cuvette was charged

with 25 µL of (^{tBu}POCOP)IrPPh$_3$ in 2 ml Toluene followed by 10.00 µL (100 eq), 20.00 µL (200 eq), 30.00 µL (300 eq) of pyridine and acetonitrile stock solution.

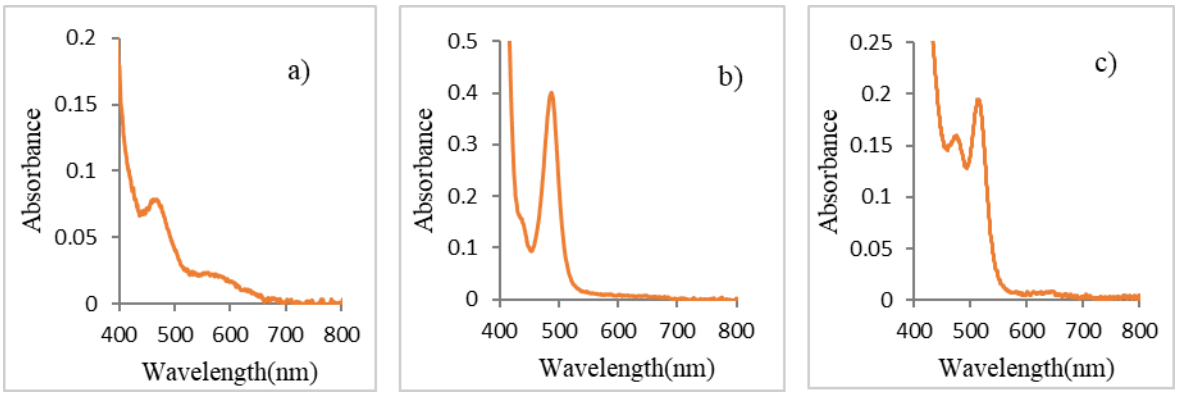

Figure 2.9. Plot of Absorbance Vs Wavelength for a) (^{tBu}POCOP)Ir(Py), b) (^{tBu}POCOP)Ir(NCCH$_3$), c) (^{tBu}POCOP)Ir(PPh$_3$)

Data Fitting

The intensity data at 515.505 nm was extracted and plotted as a function of time. Kinetic rate laws were used to fit the intensity data by adjusting the value of the rate. For the fit, we chose the time frame where continuous smooth decrease was observed. The employed models are discussed below and correspond to the following equilibrium:

$$ML + L' \rightleftharpoons ML' + L$$

1. Dissociative Mechanism; Reversible reaction with 1st order dependence on metal complexes only: In this reaction we assume that forward and reverse reaction have no dependence on the concentration of exogenous ligand. The differential equation expressing this model is as follow:

$$\frac{dx(t)}{dt} = k_1[C_{ML} - x(t)] - k_2[C_{ML'} + x(t)] \qquad \textbf{[Eq. 2]}$$

The following integrated rate law was determined using MathCAD:

$$x(t) = \left[\frac{(k_1 C_{ML} + k_2 C_{ML'})}{k_1 + k_2}\right]\left[1 - e^{-(k_1+k_2)}\right] \qquad \textbf{[Eq. 3]}$$

2. Associative Mechanism; Reversible reaction with 1st order dependence on all species: The reversible bimolecular transformation above could have the following rate law where k_1 and k_2 are the forward and backward rate constants, respectively. The value x(t) represents the change as a function of time.

$$\frac{dx(t)}{dt} = k_1[C_{ML} - x(t)][C_{L'} - x(t)] - k_2[C_{ML'} + x(t)][C_L + x(t)] \qquad \textbf{[Eq.4]}$$

The integrated rate law was determined using the Maple software package and it was simplified further by symbols:

$$x(t) = 2\tan(\lambda t/2)\left[\frac{\delta}{\lambda + (\gamma.\tan(\gamma t/2))}\right] \qquad \textbf{[Eq. 5]}$$

where $\beta = k_1 - k_2$; $\delta = k_1 C_{ML} C_{L'} - k_2 C_{ML'} C_L$; $\gamma = k_1 (C_{ML} + C_{L'}) + k_2 (C_{ML'} + C_L)$ and $\lambda = \sqrt{4\beta\delta - \gamma^2}$

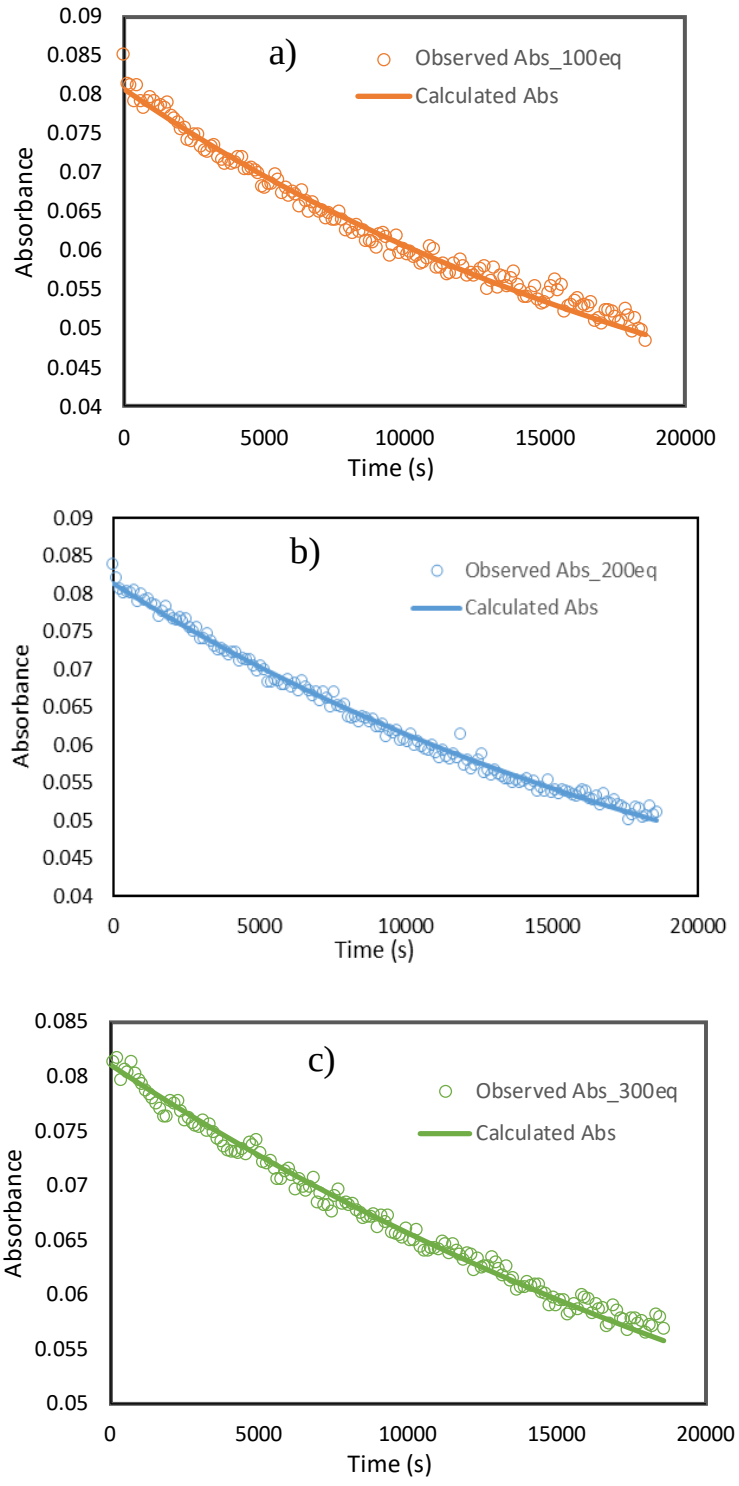

Figure 2.10. Kinetic run plot for a) 100 eq b) 200 eq, c) 300 eq of Acetonitrile at 65 °C.

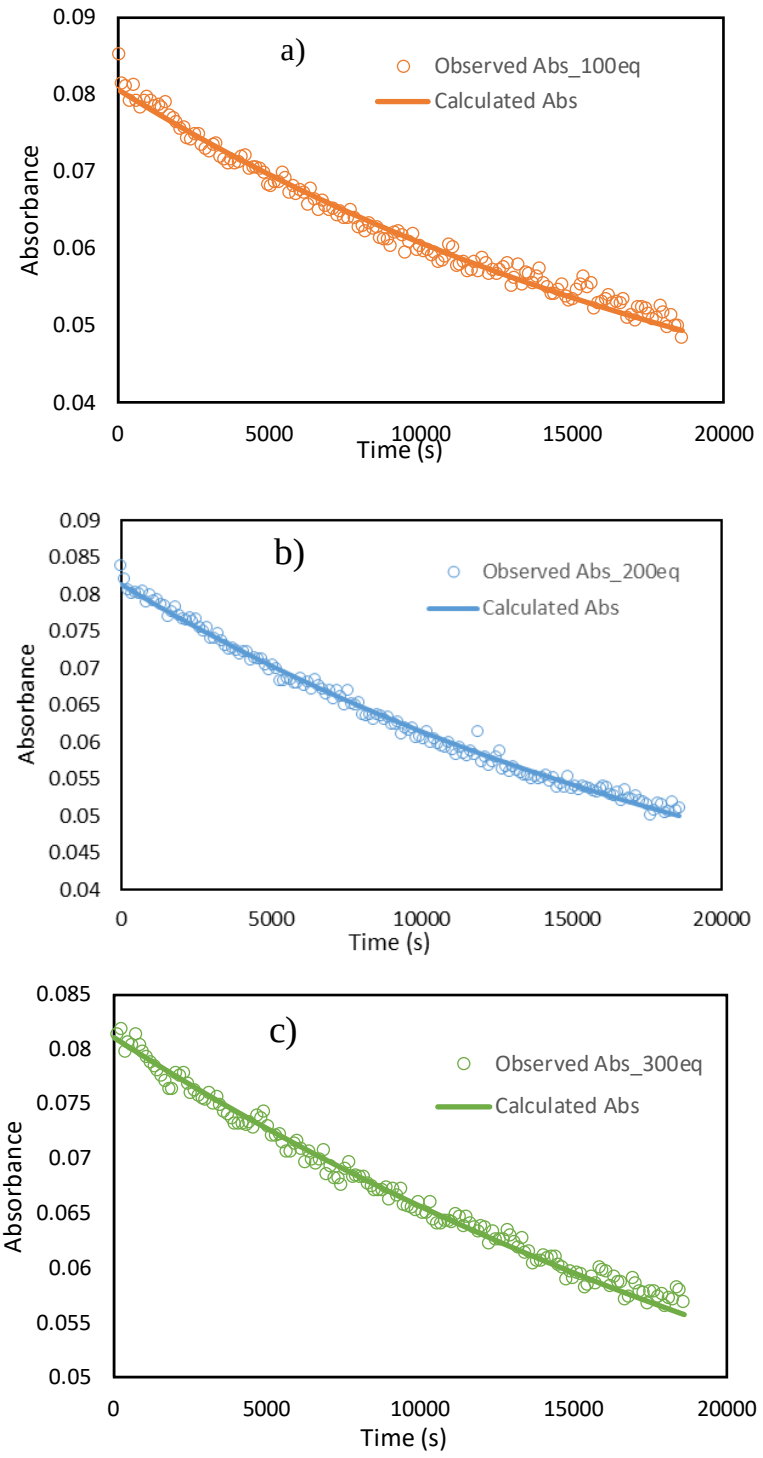

Figure 2.11. Kinetic run plot for a) 100 eq b) 200 eq, c) 300 eq of Acetonitrile at 75 °C.

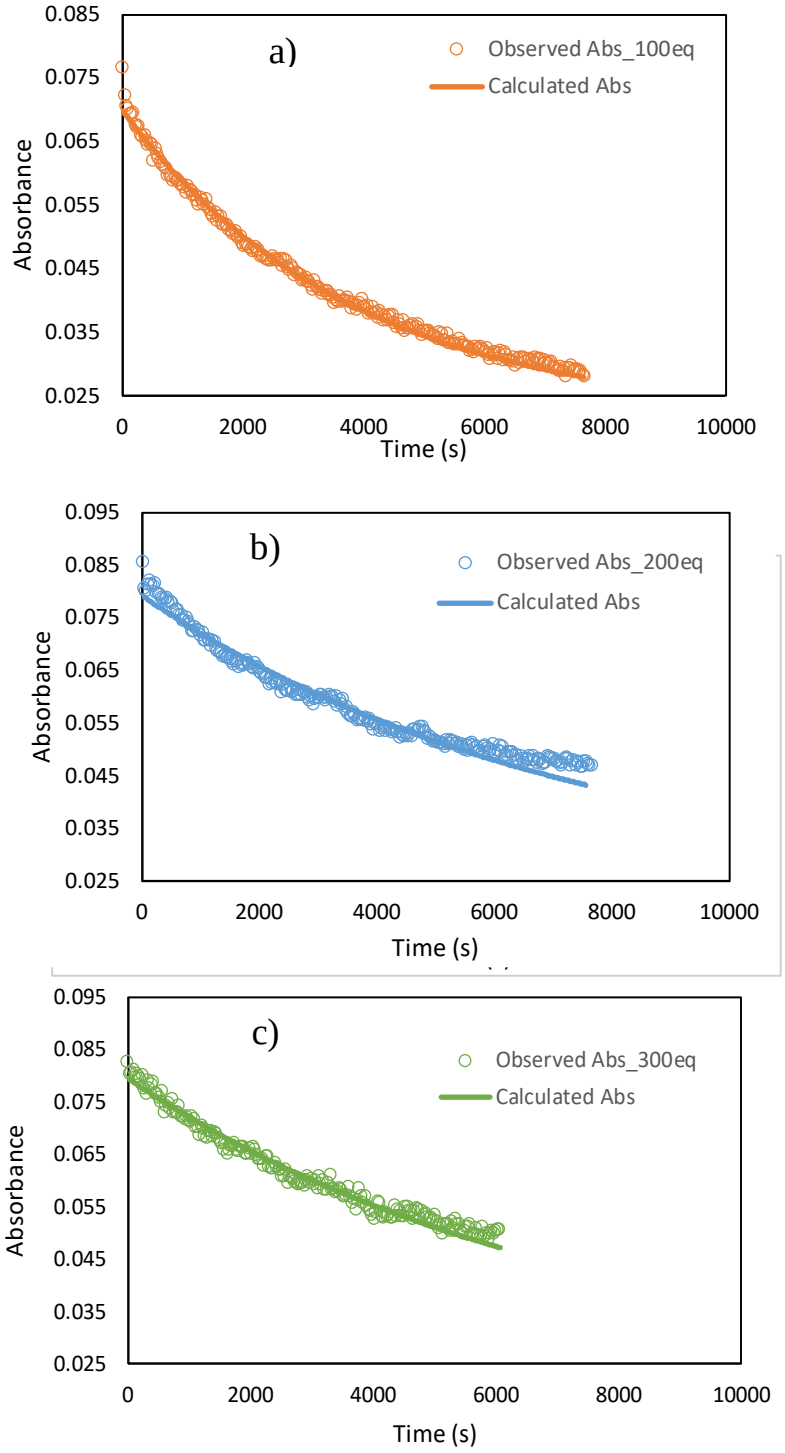

Figure.2.12. Kinetic run plot for a) 100 eq b) 200 eq, c) 300 eq of Acetonitrile at 85 °C.

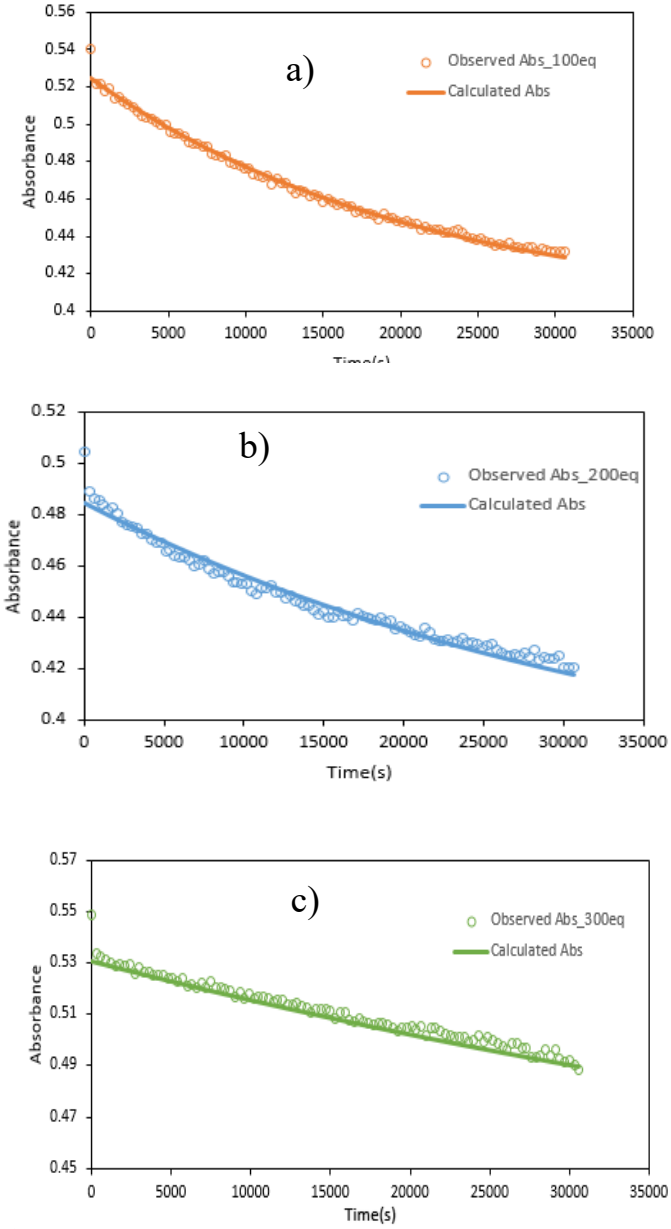

Figure 2.13. Kinetic run plot for a) 100 eq b) 200 eq, c) 300 eq of Pyridine at 65 ^{o}C.

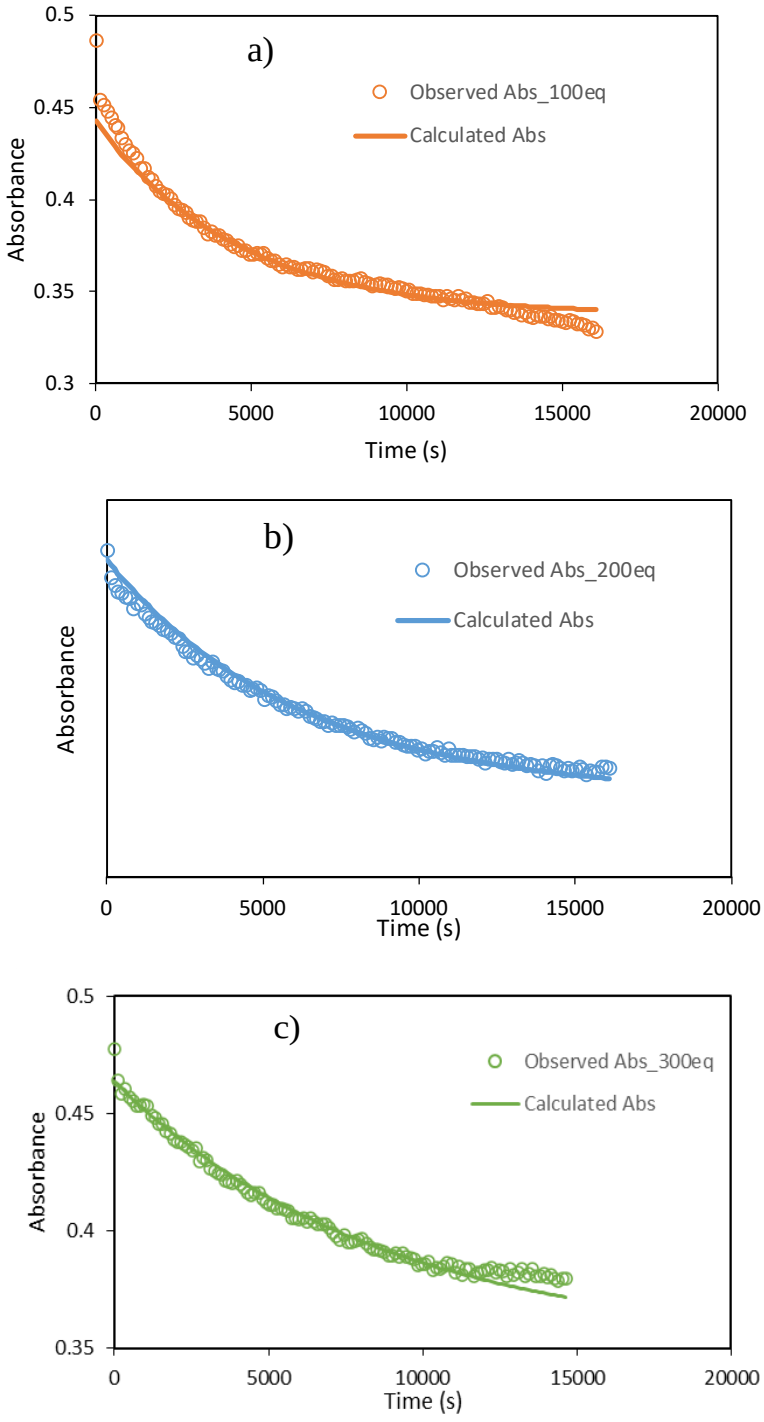

Figure 2.14. Kinetic run plot for a) 100 eq b) 200 eq, c) 300 eq of Pyridine at 75 °C.

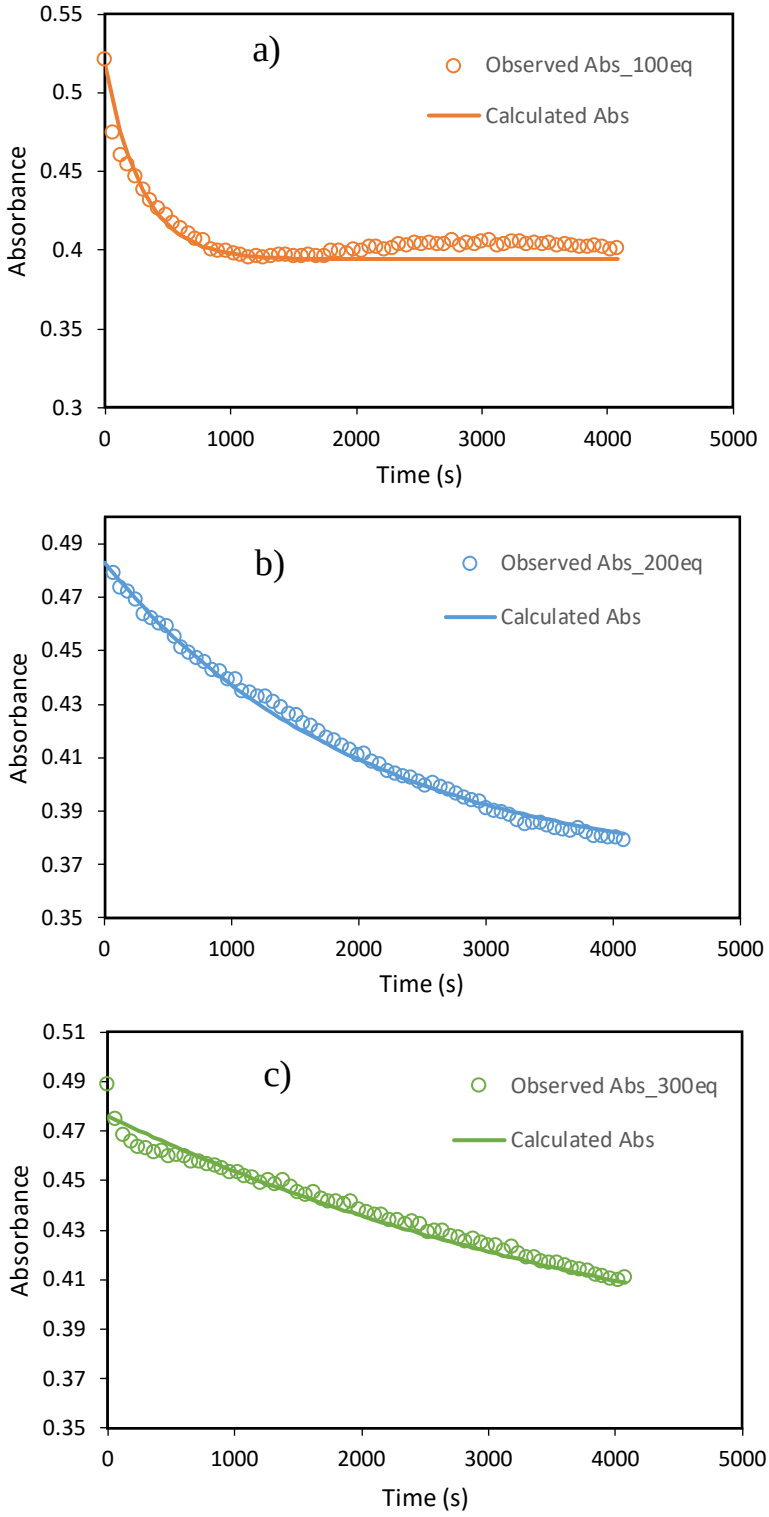

Figure 2.15. Kinetic run plot for a) 100 eq, b) 200 eq, c) 300 eq of Pyridine at 85 °C.

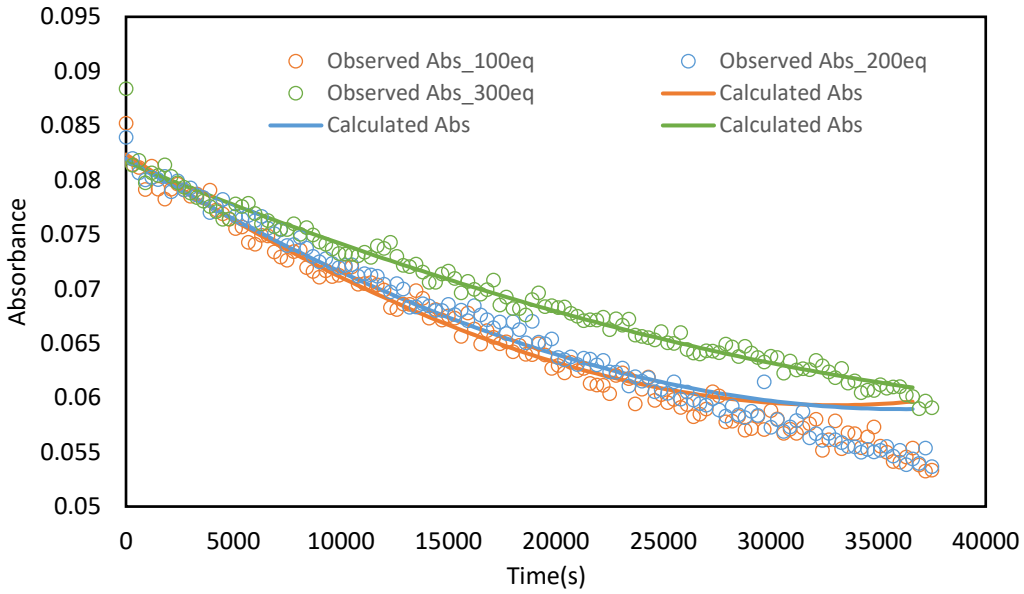

Figure 2.16. Kinetic run plot of acetonitrile according to Dissociation model at 75 °C

Determination of rate constants
Absorbance = εCl, where ε is molar absorptivity, C is concentration and l is path length of the cuvette. In this, UV-Vis path length is 1 cm.

$Absorbance_{obs} = \varepsilon_{ML}[ML] + \varepsilon_{ML'}[ML']$

ε_{ML} is the molar absorptivity of the (^{tBu}POCOP)Ir(PPh_3)

$\varepsilon_{ML'}$ is the molar absorptivity of (^{tBu}POCOP)Ir(L) where L is pyridine or acetonitrile)

Activation Parameters
The enthalpy of activation and the entropy of activation were determined by evaluating the rate constants at different temperatures and plotting the data according to the Eyring equation:

$$ln\left(\frac{k}{T}\right) = -\frac{\Delta H^{\ddagger}}{RT} + ln\frac{k'}{h} + \frac{\Delta S^{\ddagger}}{R}$$

k is rate constant, T is temperature in K, R is molar gas constant (8.314 J K^{-1} mol^{-1}), k′ is Boltzmann Constant (1.381*10^{-23} J K^{-1}), h is planck constant (6.626* 10^{-34} J s). The Gibbs energy of activation was obtained using

$$\Delta G^{\ddagger} = \Delta H^{\ddagger} - T\Delta S^{\ddagger}.$$

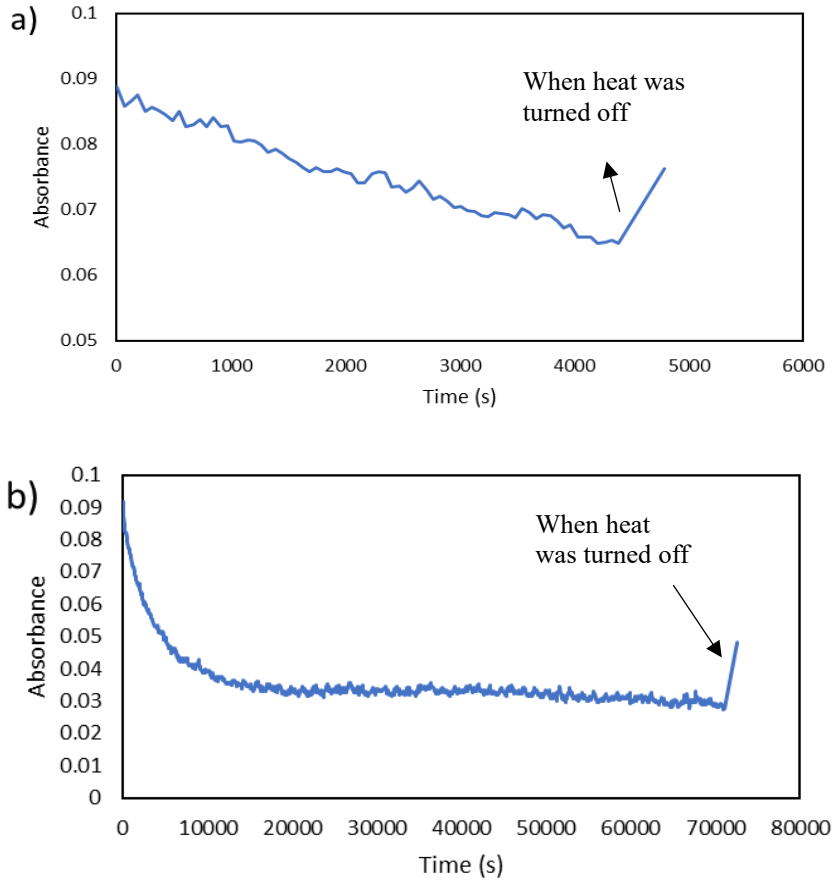

Figure 2.17. Plot of Absorbance vs Time for (^{tBu}POCOP)Ir(PPh$_3$) at a) 75 ºC and b) 85 ºC

2.6. References

1. Chaplin, A. B.; Weller, A. S., [Rh{NC$_5$H$_3$-2,6-(CH$_2$P^{t}Bu$_2$)$_2$}(PCy$_3$)][BAr$^{F\,4}$]: A Latent Low-Coordinate Rhodium(I) PNP Pincer Compound. *Organometallics* **2011,** *30* (16), 4466-4469.
2. Press, L. P.; Kosanovich, A. J.; McCulloch, B. J.; Ozerov, O. V., High-Turnover Aromatic C–H Borylation Catalyzed by POCOP-Type Pincer Complexes of Iridium. *Journal of the American Chemical Society* **2016,** *138* (30), 9487-9497.
3. Bhattacharya, P.; Krause, J. A.; Guan, H., Iron Hydride Complexes Bearing Phosphinite-Based Pincer Ligands: Synthesis, Reactivity, and Catalytic Application in Hydrosilylation Reactions. *Organometallics* **2011,** *30* (17), 4720-4729.
4. Bhattacharya, P.; Krause, J. A.; Guan, H., Activation of Dihydrogen and Silanes by Cationic Iron Bis(phosphinite) Pincer Complexes. *Organometallics* **2014,** *33* (21), 6113-6121.

5. Chen, T.; Yang, L.; Li, L.; Huang, K.-W., Homocoupling of benzyl halides catalyzed by POCOP–nickel pincer complexes. *Tetrahedron* **2012,** *68* (31), 6152-6157.
6. Li, Y.; Krause, J. A.; Guan, H., Cobalt POCOP Pincer Complexes via Ligand C–H Bond Activation with Co₂(CO)₈: Catalytic Activity for Hydrosilylation of Aldehydes in an Open vs a Closed System. *Organometallics* **2018,** *37* (13), 2147-2158.
7. Morales-Espinoza, E. G.; Coronel-García, R.; Valdés, H.; Reyes-Martínez, R.; German-Acacio, J. M.; Aguilar-Castillo, B. A.; Toscano, R. A.; Ortiz-Pastrana, N.; Morales-Morales, D., Synthesis, characterization and catalytic evaluation of non-symmetric Pd(II)-POCOP pincer compounds derived from 2′,4′-Dihydroxyacetophenone. *Journal of Organometallic Chemistry* **2018,** *867*, 155-160.
8. Pell, C. J.; Ozerov, O. V., Catalytic dehydrogenative borylation of terminal alkynes by POCOP-supported palladium complexes. *Inorganic Chemistry Frontiers* **2015,** *2* (8), 720-724.
9. Timpa, S. D.; Fafard, C. M.; Herbert, D. E.; Ozerov, O. V., Catalysis of Kumada–Tamao–Corriu coupling by a (POCOP)Rh pincer complex. *Dalton Transactions* **2011,** *40* (20), 5426-5429.
10. Morales-Morales, D., Pincer complexes: applications in catalysis. *Revista de la Sociedad Química de México* **2004,** *48* (4), 338-346.
11. Kosanovich, A. J.; Press, L. P.; Ozerov, O. V., Boryl transfer reactivity of a POCOP-supported Ir-diboryl: Reduction of CO2 to CO and borylation of other small molecules. *Journal of Organometallic Chemistry* **2017,** *845*, 19-24.
12. Goldberg, J. M.; Goldberg, K. I.; Heinekey, D. M.; Burgess, S. A.; Lao, D. B.; Linehan, J. C., Detection of an Iridium–Dihydrogen Complex: A Proposed Intermediate in Ionic Hydrogenation. *Journal of the American Chemical Society* **2017,** *139* (36), 12638-12646.
13. Goldberg, J. M.; Berman, J. L.; Kaminsky, W.; Goldberg, K. I.; Heinekey, D. M., Oxidative addition of iodine to (tBu)4(POCOP)Ir(CO) complexes. *Journal of Organometallic Chemistry* **2017,** *845*, 171-176.
14. Ahmed Foskey, T. J.; Heinekey, D. M.; Goldberg, K. I., Partial Deoxygenation of 1,2-Propanediol Catalyzed by Iridium Pincer Complexes. *ACS Catalysis* **2012,** *2* (6), 1285-1289.
15. Park, S.; Bézier, D.; Brookhart, M., An Efficient Iridium Catalyst for Reduction of Carbon Dioxide to Methane with Trialkylsilanes. *Journal of the American Chemical Society* **2012,** *134* (28), 11404-11407.
16. Park, S.; Brookhart, M., Hydrosilylation of Carbonyl-Containing Substrates Catalyzed by an Electrophilic η¹-Silane Iridium(III) Complex. *Organometallics* **2010,** *29* (22), 6057-6064.
17. Garrou, P. E.; Hartwell, G. E., Redistribution reactions of organometallic complexes. Carbonyl, halogen, and organophosphine exchange between coordinately unsaturated rhodium (I) and iridium (I) complexes. *Inorganic Chemistry* **1976,** *15* (3), 646-650.
18. Thompson, J. S.; Atwood, J. D., Rapid intermolecular ligand exchange between square-planar iridium(I) complexes: trans-Ir(CO)L2X (X = Cl or Me, L = P(p-tolyl)3 or PMePh2). *Journal of the American Chemical Society* **1991,** *113* (19), 7429-7430.
19. Sola, E.; Navarro, J.; López, J. A.; Lahoz, F. J.; Oro, L. A.; Werner, H., Labile Hydrido Complexes of Iridium(III): Synthesis, Dynamic Behavior in Solution, and Reactivity toward Alkenes. *Organometallics* **1999,** *18* (17), 3534-3546.
20. Kossoy, E.; Rybtchinski, B.; Diskin-Posner, Y.; Shimon, L. J. W.; Leitus, G.; Milstein, D., Structure and Reactivity of Rhodium(I) Complexes Based on Electron-Withdrawing Pyrrolyl-PCP-Pincer Ligands. *Organometallics* **2009,** *28* (2), 523-533.
21. Huang, Z.; White, P. S.; Brookhart, M., Ligand exchanges and selective catalytic hydrogenation in molecular single crystals. *Nature* **2010,** *465* (7298), 598-601.

22. Doherty, M. D.; Grills, D. C.; Huang, K.-W.; Muckerman, J. T.; Polyansky, D. E.; Van Eldik, R.; Fujita, E., Kinetics and Thermodynamics of Small Molecule Binding to Pincer-PCP Rhodium(I) Complexes. *Inorganic Chemistry* **2013,** *52* (8), 4160-4172.
23. Lapointe, S.; Vabre, B.; Zargarian, D., POCOP-Type Pincer Complexes of Nickel: Synthesis, Characterization, and Ligand Exchange Reactivities of New Cationic Acetonitrile Adducts. *Organometallics* **2015,** *34* (14), 3520-3531.
24. Carta, V.; Mehr, S. H. M.; Maclachlan, M. J., Controlling Ligand Exchange through Macrocyclization. *Inorganic Chemistry* **2018,** *57* (6), 3243-3253.
25. Shafiei-Haghighi, S.; Singer, L. M.; Tamang, S. R.; Findlater, M., Synthesis, characterization and reactivity of iridium pincer complexes. *Polyhedron* **2018,** *143*, 126-131.
26. Göttker-Schnetmann, I.; White, P. S.; Brookhart, M., Synthesis and Properties of Iridium Bis(phosphinite) Pincer Complexes (p-XPCP)IrH₂, (p-XPCP)Ir(CO), (p-XPCP)Ir(H)(aryl), and {(p-XPCP)Ir}₂{μ-N₂} and Their Relevance in Alkane Transfer Dehydrogen. *Organometallics* **2004,** *23* (8), 1766-1776.
27. Goldman, A. S.; Roy, A. H.; Huang, Z.; Ahuja, R.; Schinski, W.; Brookhart, M., Catalytic Alkane Metathesis by Tandem Alkane Dehydrogenation-Olefin Metathesis. *Science* **2006,** *312* (5771), 257-261.
28. Krogh-Jespersen, K.; Czerw, M.; Zhu, K.; Singh, B.; Kanzelberger, M.; Darji, N.; Achord, P. D.; Renkema, K. B.; Goldman, A. S., Combined Computational and Experimental Study of Substituent Effects on the Thermodynamics of H2, CO, Arene, and Alkane Addition to Iridium. *Journal of the American Chemical Society* **2002,** *124* (36), 10797-10809.
29. Saillard, J. Y.; Hoffmann, R., Carbon-hydrogen and hydrogen-hydrogen activation in transition metal complexes and on surfaces. *Journal of the American Chemical Society* **1984,** *106* (7), 2006-2026.
30. Kossoy, E.; Iron, M. A.; Rybtchinski, B.; Ben-David, Y.; Shimon, L. J. W.; Konstantinovski, L.; Martin, J. M. L.; Milstein, D., ?-Accepting-Pincer Rhodium Complexes: An Unusual Coordination Mode of PCP-Type Systems. *Chemistry - A European Journal* **2005,** *11* (8), 2319-2326.
31. Sykes, A. C.; White, P.; Brookhart, M., Reactions of Anilines and Benzamides with a 14-Electron Iridium(I) Bis(phosphinite) Complex: N−H Oxidative Addition versus Lewis Base Coordination. *Organometallics* **2006,** *25* (7), 1664-1675.
32. Neese, F., The ORCA program system" Wiley Interdisciplinary Reviews: Computational Molecular Science. 2012; Vol. 2, pp 73-78.
33. Perdew, J. P.; Burke, K.; Ernzerhof, M., Generalized Gradient Approximation Made Simple. *Physical Review Letters* **1996,** *77* (18), 3865-3868.
34. Lenthe, E. v.; Baerends, E. J.; Snijders, J. G., Relativistic regular two-component Hamiltonians. *The Journal of Chemical Physics* **1993,** *99* (6), 4597-4610.
35. J -L Heully, I. L., E Lindroth, S Lundqvist and A -M Martensson-Pendrill, Diagonalisation of the Dirac Hamiltonian as a basis for a relativistic many-body procedure. *Journal of Physics B: Atomic and Molecular Physics,* **1986,** *19*, 2799.
36. Kohn, W.; Sham, L. J., Self-Consistent Equations Including Exchange and Correlation Effects. *Physical Review* **1965,** *140* (4A), A1133-A1138.
37. Grimme, S.; Antony, J.; Ehrlich, S.; Krieg, H., A consistent and accurate ab initio parametrization of density functional dispersion correction (DFT-D) for the 94 elements H-Pu. *The Journal of Chemical Physics* **2010,** *132* (15), 154104.
38. Grimme, S.; Ehrlich, S.; Goerigk, L., Effect of the damping function in dispersion corrected density functional theory. *Journal of Computational Chemistry* **2011,** *32* (7), 1456-1465.

39. Weigend, F., Accurate Coulomb-fitting basis sets for H to Rn. *Physical Chemistry Chemical Physics* **2006,** *8* (9), 1057-1065.
40. Pantazis, D. A.; Chen, X.-Y.; Landis, C. R.; Neese, F., All-Electron Scalar Relativistic Basis Sets for Third-Row Transition Metal Atoms. *Journal of Chemical Theory and Computation* **2008,** *4* (6), 908-919.
41. Pantazis, D. A.; Neese, F., All-Electron Scalar Relativistic Basis Sets for the Lanthanides. *Journal of Chemical Theory and Computation* **2009,** *5* (9), 2229-2238.
42. Pantazis, D. A.; Neese, F., All-Electron Scalar Relativistic Basis Sets for the Actinides. *Journal of Chemical Theory and Computation* **2011,** *7* (3), 677-684.
43. Pantazis, D. A.; Neese, F., All-electron scalar relativistic basis sets for the 6p elements. *Theoretical Chemistry Accounts* **2012,** *131* (11), 1292.
44. Barone, V.; Cossi, M., Quantum Calculation of Molecular Energies and Energy Gradients in Solution by a Conductor Solvent Model. *The Journal of Physical Chemistry A* **1998,** *102* (11), 1995-2001.
45. Boys, S. F.; Bernardi, F., The calculation of small molecular interactions by the differences of separate total energies. Some procedures with reduced errors. *Molecular Physics* **1970,** *19* (4), 553-566.

3. Examining the reactivity of pincer-based iridium hydride complexes for reduction of carbamates

Aneelman Brar, Michael Findlater

3.1. Introduction

Carbon dioxide is the major greenhouse gas emitted by human activities.[1] When CO_2 is released into the atmosphere due to the consumption of fossil fuels from industrial/residential emissions, it traps the heat and warms the Earth surface, i.e., global climate change. It is known that global warming leads to a range of negative impacts such as rising sea levels, intense heat waves, droughts, flood and severe weather events.[2] It is imperative that measures be enacted to reduce these emissions. Two approaches to reducing CO_2 levels which have been explored are – carbon capture and sequestration (CCS) and carbon capture and utilization (CCU). Where CCS involves the capture of CO_2 and storage in underground geological formations or in the deep oceans, alternatively CCU involves capturing and converting CO_2 into valuable products. Alongside the advantages associated with CCS and CCU, they both suffer from problems and the relative value of such approaches has become a topic for debate. For example, there are problematic factors inherent to storage solutions such as a limitation to suitable areas where CO_2 can be stored underground, the cost associated with building the massive steel pipeline network for transportation and storage and requirement of substantial thermal energy to release carbon dioxide from capture agents associated with the CCS and CCU technology respectively.[3-5] Despite the technology's advanced stage of readiness, extensive research is still being conducted to improve its economic feasibility and to reduce the environmental footprint of such technology. An alternative approach to this energy intensive process would be direct reaction of the captured CO_2. The process of direct reaction of captured carbon dioxide to produce a valuable added chemicals/products or fuels has been termed as*reactive capture of carbon dioxide (RCC)*.[6] For example, theoretical calculations of the energy costs for electrochemical CO production through RCC predicted an energy savings of 146kJ per mole of product, or 20 % in comparison to sequential CCU.[7] However, both RCC and sequential CCU costs are understated because this estimate relies on a pure stream of concentrated CO_2. Hence, there are significant knowledge gaps that must be filled to accelerate RCC technology.

On an academic level, where many different approaches such as photo-, thermo- and electrochemical catalysts have been employed to reduce CO_2 into chemical targets such as formic acid (FA), methanol and acrylic acid, only a handful of reports exist describing thermal routes for RCC. [8-19] The electrochemical reduction of CO_2 is in principal a clean and efficient route for carbon dioxide utilization because of mild operating conditions and the possibility of developing tailored reaction pathways. There has been a wealth of research on the electrocatalytic reduction of pure and concentrated carbon dioxide to chemical feedstocks or fuels and one of the most promising approaches for conversion of carbon dioxide is via the use of transition metal catalysts.[8, 10] When carbon dioxide binds to many transition metals, in some cases the coordination of carbon dioxide weakens the strong C=O double bond and helps to facilitate further transformation.[15] Another approach

for activating and reducing carbon dioxide; mostly driven by thermodynamic factors is insertion of carbon dioxide into metal-element σ bonds (such as M-H, M-OR, M-NR_2 and M-CR_3 bonds).[20, 21] In this project, the insertion of carbon dioxide into late transition *metal-hydride* σ bond will be explored, as it plays a vital role in the catalytic cycle for converting CO_2 into products such as CO, formate, methanol and ethylene, which are critical feedstocks for the chemical and fuel industries.

3.2. Translating the electrochemical reduction of CO_2 chemistry to carbamate chemistry

Carbon dioxide is naturally only available in dilute streams and most methods of capture and concentration are inefficient. Direct electrocatalytic reduction of absorbed CO_2 has energetic advantages compared to sequential capture and concentration followed by reduction. At this point, only a few studies have been performed that examine how our understanding of CO_2 reduction translates when captured CO_2 is used as the substrate. However, of note is a report from Saouma and coworkers that described a change in product selectivity when an amine-captured CO_2 was reduced by a Mn electrocatalyst that has high selectivity for CO_2 reduction to CO.[22] The most heavily studied homogeneous CO_2 sorbent for capture from flue gas (5 - 15% CO_2) are amines. The familiarity with the properties of amines such as binding constants, solubility and impurity tolerance provides leverage over the possible capture agents. We can tailor the amines for RCC without the requirement of high temperature stability. Amines react with CO_2 in a 2:1 stoichiometry to form the corresponding carbamates as shown in **Scheme 3.1**. There are several routes for the production of carbamates, but we chose commercially available carbamates as our model substrates, i.e., ammonium carbamate (AC) and dimethyl ammonium dimethyl carbamate (DMADMC).

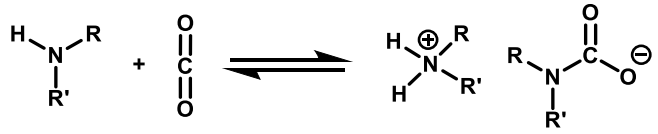

Scheme.3.1. CO_2 captured by amine to form the carbamate salt.

AC and DMADMC are obtained from the reaction of CO_2 with two equivalents of ammonia and dimethyl amine respectively. To better understand the factors involved in selective ammonium carbamate reduction, we explored its use as a substrate with pincer ligand-based iridium metal complexes. Pincer ligands are extensively employed in modern organometallic chemistry and for good reason, they yield highly robust and modular coordination complexes capable of catalyzing the wide range of organic transformations. **Figure 3.1** illustrates the diversity of ligand platforms and our ability to tailor the ligand at will. As an example, in $^{t\text{Bu}}$POCOP ligand, the phosphorus atom participates in back bonding, hence stabilizing the metal in low oxidation state. The four bulky *tert*-butyl groups in these pincer ligands provide considerable amount of steric shielding that prevent the dimerization of the complex even when coordinatively unsaturated. Finally, many

pincer complexes are efficient hydrogenation catalysts, making them plausible candidates for preliminary research into electrocatalytic reduction mechanisms.

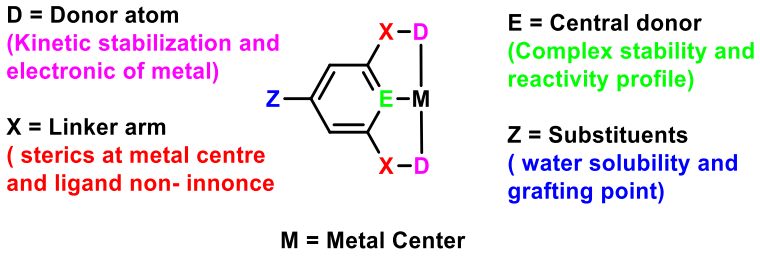

Figure 3.1. Pincer ligand anatomy

In the literature, many pincer ligand based electrocatalysts have been reported for the conversion of CO_2 into valuable products and fuels. Nozaki and coworkers **(Scheme 3.2)** reported the six coordinate 18e$^-$ Ir(III) pincer trihydride complex which reacts with THF at 25 ^oC yielding the formate complex.[23] Later Hazari and coworkers (**Scheme 3.2**) disclosed a six-coordinate Ir(III) pincer trihydride complex reacts with CO_2 to form an adduct, in which hydrogen bonding is the driving force for the formation of the adduct.[24] The formate product was obtained in both the Nozaki and Hazari systems under basic conditions. Later Brookhart (**Scheme 3.2**) and coworkers reported the five-coordinate, 16e$^-$ Ir(III) pincer dihydride which readily inserts CO_2 and selectively reduces the CO_2 to formate or formic acid electrochemically.[25] Given the long standing interest of our lab in pincer chemistry we decided to probe the reactivity of Brookhart's catalyst, i.e. [(^{tBu}POCOP)Ir(H)(NCCH$_3$)$_2$][B(Ar^F)$_4$](^{tBu}(POCOP) = 2, 6 bis(di-tert-butyl-phosphonito)) (**10**).

Complex **10** exhibits high selectivity towards CO_2 reduction in both acetonitrile and water, with 85% and 15% Faradaic efficiency for formic acid and hydrogen formation, respectively.[25] In this work, the complex (**10**) was selected among others to initiate the testing of the electrochemical reduction of carbamates.

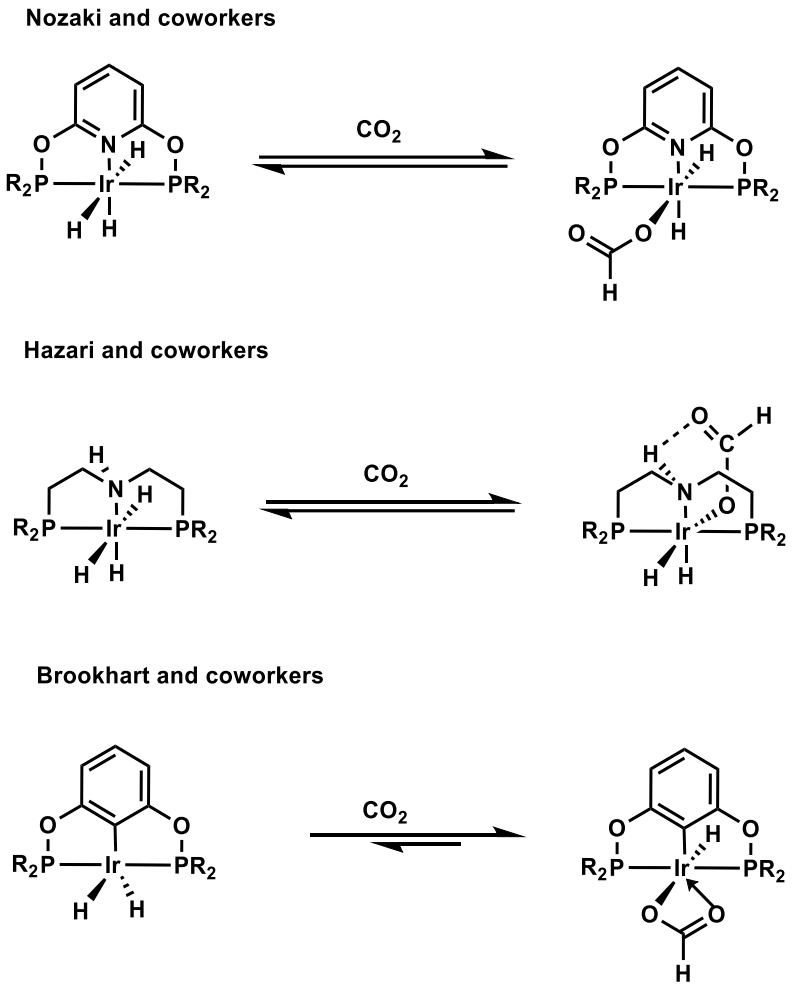

Scheme 3.2. CO_2 insertion by iridium pincer hydrido complexes

3.3. Results and Discussion

Complex **10** was synthesized according to prior literature reports.[25] The identity of the synthesized complex was established using ^{1}H and ^{31}P NMR spectroscopy (**Figure 3.4**). We subsequently investigated the electrocatalytic reduction of carbamate by cyclic voltammetry (CV) and controlled potential electrolysis (CPE) experiments. The catalytic reduction activity towards the reduction of our model substrate ammonium carbamate was performed in 95:5 CH_3CN/H_2O (0.1 M tetrabutylammonium hexafluorophosphate ($TBAPF_6$)) employing 1mM **10** catalyst. The voltammograms were taken with and without substrate to explore any reaction between the carbamate and the electrocatalyst **10**. From the cyclic voltammogram of **10** and AC, qualitative analysis was obtained by the observed change in catalytic current; suggesting catalytic reduction activity. To get quantitative analysis of reactivity and products formed, CPE was performed, and post electrolysis analyses were carried out using GC and NMR techniques.

In the absence of substrate AC, a two electron irreversible reduction wave at a cathodic peak potential ($E_{p,c}$) of -1.4 V Vs NHE was observed under Argon in acetonitrile (**Figure 3.2**), in good agreement with the reported literature values of this catalyst.[25]

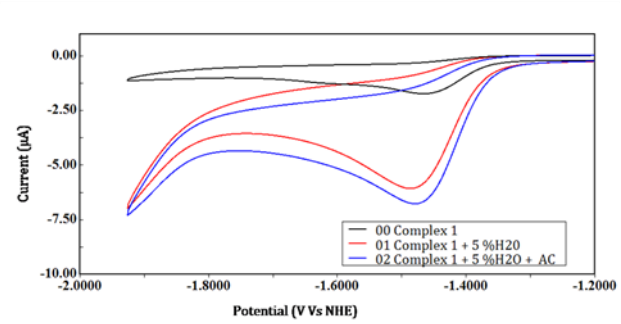

Figure 3.2. Cyclic voltammetry of **10** under argon in CH_3CN, 95:5 CH_3CN: H_2O, and in 95:5 CH_3CN: H_2O with 10 mM ammonium carbamate.

During the titration studies, a slight increase in current was observed with each added equiv of AC, until 15 equiv. of model substrate AC as shown in **Figure 3.3**. Later CPE (**Figure 3.5**) was performed at -2.15 V (Vs $Ag/AgNO_3$) in 95:5 CH_3CN: H_2O solvent system employing 1mM catalyst **10** (0.1M $TBAPF_6$, 10 mM AC). 14.71C (Coulombs) of current were passed, (25 equivalents of electrons per iridium complex). The post electrolysis solution and headspace were analyzed for hydrogen and carbon-based products. However, this catalyst **10** is known for formate production with carbon dioxide, only H_2 was detected in this system with the FE of 85-90 %

When no reduced product was obtained and only hydrogen evolution was observed in the system, we began to speculate as to the cause (or causes) of the lack of desired reactivity. We formulated two plausible reasons to explain the decrease in selectivity for catalyst **10** when AC was used as substrate instead of carbon dioxide. Firstly, the ammonium cation present in the system alters the selectivity of the reaction through modification of the proton activity. In the study by Brookhart and coworkers, a solution of 95:5 CH_3CN:H_2O under 1 atm of carbon dioxide affords carbonic acid, which has a pKa of 23.4.[26] The ammonium cation, formed by reaction of two equivalents of an amine with carbon dioxide, results in a solution that is significantly more acidic. Ammonium has a pK_a of ~18 in acetonitrile and ~9.25 in water. In the mixed solvent, the pK_a is expected to be intermediate between these values, yielding the strongest acid in solution.

Secondly, carbamate is a very challenging substrate to reduce as compared to carbon dioxide. Though perhaps controversial, the idea that Y-shaped conjugation in e.g. guanidine-type molecules is a new form of acyclic aromaticity, called Y-aromaticity, is four decades old now.[27] Literature reports a few computational studies on this unusual stability.[28, 29]Whether this Y shaped aromaticity is really a new form of aromaticity, carbamates being a Y shaped and conjugated molecule is expected to be more difficult to reduce than carbon dioxide.

To dig deeper into the reactivity between the carbamates and catalyst **10**, we attempted to perform stoichiometric studies between catalyst (**10**) and AC in acetonitrile and 95:5 CH_3CN: H_2O systems. It is now well established that acetonitrile is an ancillary ligand that helps sustain the electrocatalysis and it supports both the regeneration of catalyst at the end of the catalytic cycle and dissociation of formate.[25]

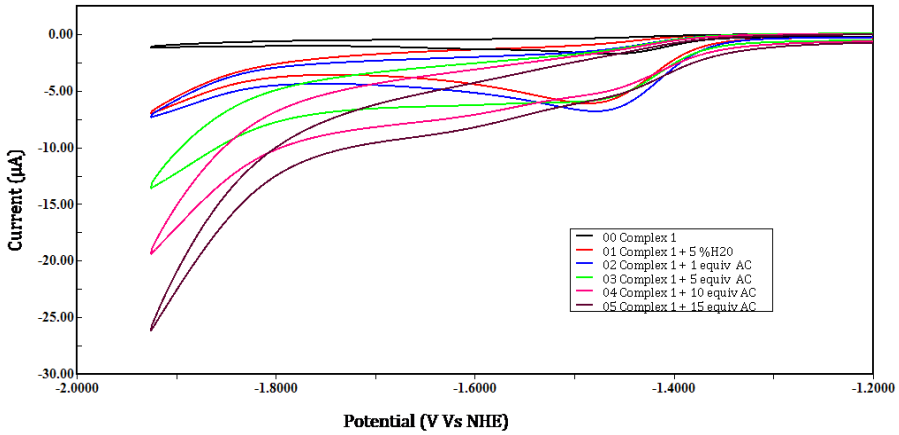

Figure 3.3. Cyclic voltammograms of (**10**) with different equiv of AC under argon in 95:5 CH_3CN: H_2O

In NMR studies, it was observed that the acetonitrile ligand was playing an important role in the reactivity. The cis and trans acetonitrile peaks in catalyst **10** were observed at 2.15 and 1.83 ppm respectively.[30] During the course of the reaction, the intensity of the peak corresponding to the cis acetonitrile ligand diminished over time and eventually disappeared, creating a vacant coordination site around the octahedral iridium center. We hypothesize that carbamate binds to the vacant coordination site to maintain an octahedral geometry at the iridium center, and results in two triplets at -20.03 and -21.00 ppm, observed by NMR spectroscopy.

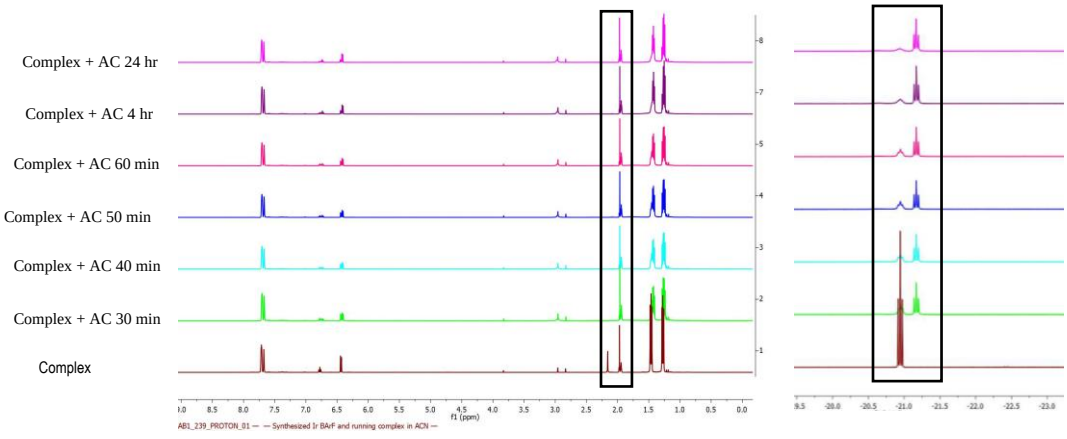

Figure 3.4. Stoichiometric reaction of AC and $[(^{tBu}POCOP)Ir(H)(NCCH_3)_2][B(Ar^F)_4]$ in acetonitrile.

To support our first supposition that ammonium ion generates a more acidic reaction medium and is solely responsible for hydrogen production, we performed the same controlled potential electrolysis using ammonium hexafluorophosphate under an atmosphere of carbon dioxide. After passing 63.7 C (100 equivalent per Ir catalyst), two products; H_2 and formate were formed in 82% and 2% faradic efficiency respectively. The faradic efficiency was obtained from headspace and solution analyses. There was no observation of any other carbon-based product.

Despite the presence of carbon dioxide in the catalytic system, the sole production of hydrogen suggests that addition of a stronger acid (ammonium) under electrolytic conditions promotes hydrogen evolution, compromising the selectivity for carbon-based products. One significant outcome which emerges from these studies is that employing a known CO_2 reduction catalyst does not *a priori* mean it will be effective in the reduction of captured CO_2; indeed, mechanistic studies using catalyst (**10**) suggest unfavorable kinetics for hydrogen evolution.[31] This experiment neither excludes nor quantifies the degree to which carbamate reduction is 'more difficult' than carbon dioxide reduction. Yet, from **Scheme 3.1**, using amines as capture agents for carbon dioxide will always produce an equivalent of ammonium acid. As a result, selectivity may be more difficult in general when carbon dioxide is substituted for amine-captured CO_2 as the substrate for catalysts that are typically highly selective for CO_2 reduction. Moreover, Saouma and coworkers described a recent study that in the presence of ammonium a change in product selectivity is observed. Additional strategies or modified complexes/clusters are required that favor carbamate reduction specifically. We intended to explore the possibility of other known (reduces CO_2 efficiently) electrocatalyst for the electrochemical reduction of carbamates.

3.4. Electrochemical reduction of carbamate with another established catalysts

In 2015, Berben and coworkers[32] reported that an iron carbonyl cluster $[Fe_4N(CO)_{12}]^-$ selectively reduces carbon dioxide electrochemically to formate in a CO_2-saturated buffer water solution. In pure acetonitrile a mixture of hydrogen and formate was obtained, whereas formate product could be selectively obtained in 95:5 CH_3CN:H_2O mixture albeit at a slower rate. They rationalized the observed selectivity in both systems depending upon thermochemical data (hydricity). The small amount of hydrogen observed in the system was attributed as background hydrogen evolution taking place at glassy carbon electrode and not due to the cluster itself. In their subsequent reports, they outlined the modification of iron cluster by introducing neutral/charge ligands in the primary or secondary coordination sphere and studied the inductive vs electrostatic effects on the reactivity.[33] They attempted the synthetic modification of cluster complex through substitution of carbonyl ligands with various different phosphine and monitored the synthesis using ^{31}P and IR spectroscopy. [33] They reported series of isoelectronic phosphine substituted cluster using the modified literature procedures.[34] As expected, phosphine substitution tends to increase the cluster core electron density and decrease carbonyl stretching frequency.[34] Later on, Dmitry *et al*,[35] mentioned the formation of sterically hindered carbonyl based complex, i.e. [N,N'- bid(2,6 diisopropylphenyl)-acenaphthene-1,2-diimine-$1\kappa^2$N,N']-heptacarbonyl-1κC,$2\kappa^3$C,$3\kappa^3$C-di-μ_3-tellurido-triiiron(II)(2 Fe—Fe). After reading through literature reports on substituted iron cluster, we learned that ligand substitution had an

effect on the reactivity towards electrochemical reduction. We intended to examine the reactivity of iron cluster after substituting the carbonyl with bulky redox active BIAN ligand, N,N'-bis-(2,6-diisopropylphenyl)acenaphthene-1,2-diimine (**Scheme 3.3**).

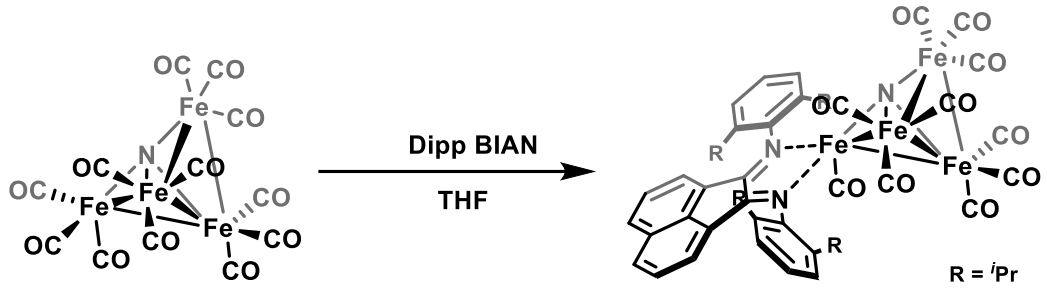

Scheme 3.3. Synthesis of BIAN substituted iron cluster.

We hypothesize that coordination of dpp-BIAN will influence the iron-carbonyl core electronic properties (enhancing the electron density at one of the iron centers), altering its catalytical activity towards the electrochemical reduction of carbon dioxide and eventually could be employed for carbamate reduction. Following the literature procedure, an effort was made to synthesize the BIAN substituted iron carbonyl cluster. All the reactions were characterized using IR spectroscopy. When no reaction was observed between the iron carbonyl cluster and BIAN at room temperature then we investigated the thermochemical and photochemical approach. The reaction was heated at 60 °C but no observable shift was seen in the carbonyl stretching frequency in the IR spectroscopy. Finally, switching to photochemical approach for substitution. After 3 hours of exposure of reaction mixture to light (370 nm), a shift was observed in the carbonyl stretching frequency from 1989 to 1979 cm^{-1} (**Figure 3.5**)

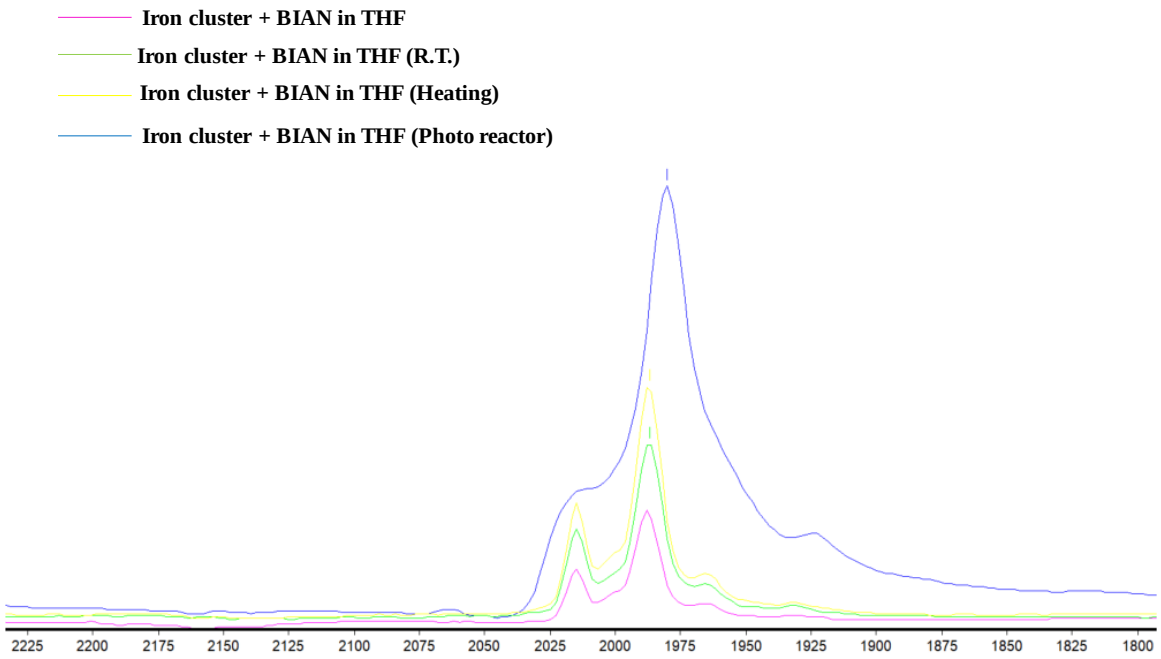

Figure 3.5. Shift in stretching frequency of carbonyl observed by the IR spectroscopy.

3.5. Future Directions

When the well-established electrocatalyst for carbon dioxide reduction failed to yield the desired formate with carbamate reduction, then we decided to switch to other electrochemical systems. It would be interesting to study the behavior of electrocatalyst when carbamate will be utilized as substrate instead of carbon dioxide. Firstly, the synthesized carbonyl substituted cluster will be optimized electrochemically, and then test electrochemical reduction of carbon dioxide and eventually carbamate. Because of improved sterics and electron density at meal center, we aim better selectivity of carbon-based products with carbon dioxide and carbamate.

3.6. General Considerations

All syntheses and manipulations were carried out under an inert Argon atmosphere in glovebox or using standard Schlenk techniques. Anhydrous organic solvents used during synthesis were purchased from Sigma and were degassed by sparging with argon and dried by passing through columns of neutral alumina or molecular sieves and stored over activated 3 Å molecular sieves. Water was obtained from a Barnstead Nanopure filtration system and was degassed under an active vacuum. Deuterated solvents were purchased from Sigma and Cambridge Isotope Laboratories, Inc. Deuterated solvents used for nuclear magnetic resonance (NMR) spectroscopic characterization were degassed via three freeze-pump-thaw (FPT) cycles and stored over activated 3 Å molecular sieves prior to use. All solvents and reagents were purchased from commercial vendors (Sigma and Alfa aesar) and used without further purification unless otherwise noted. Electrochemical studies under pure CO_2 atmospheres were performed using ultra high purity (99.999%) CO_2 that was passed through a VICI carbon dioxide purification column to eliminate residual H2O, O_2, CO, halocarbons, and sulfur compounds. ^{1}H and ^{31}P NMR were recorded on 400 MHz and 500 MHz Bruker and Varian instruments at 300K unless otherwise stated.

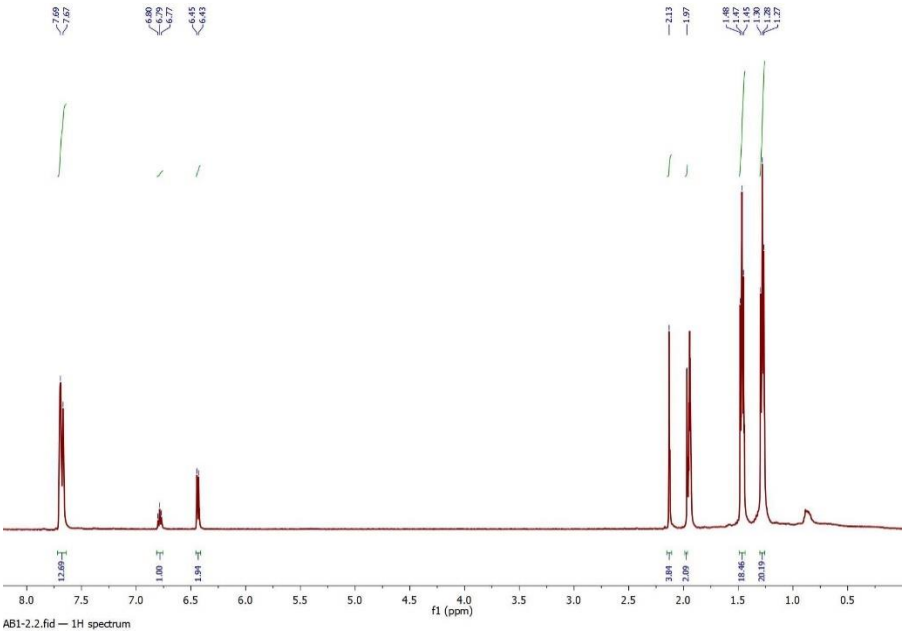

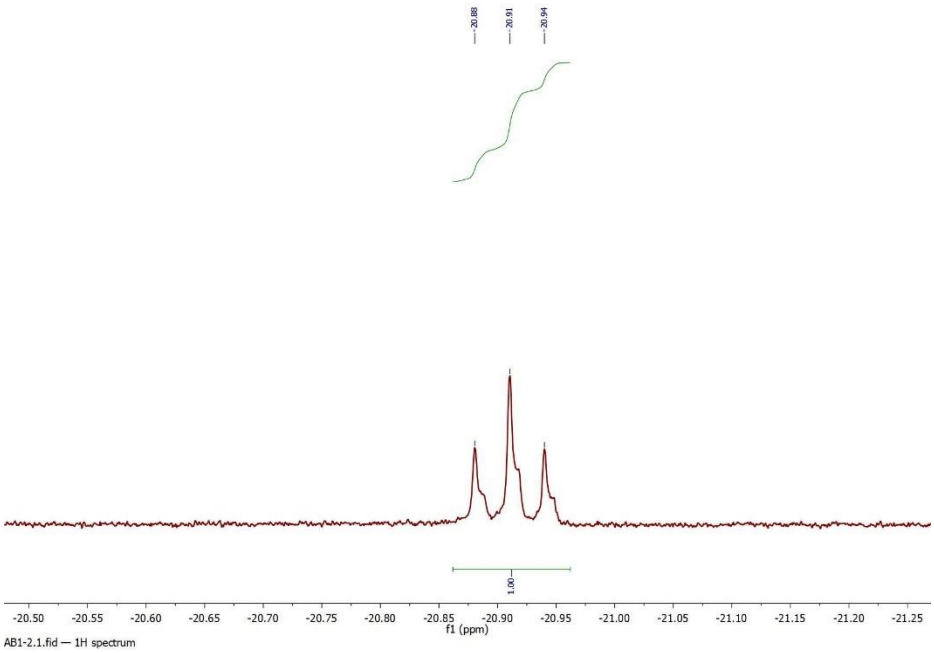

Figure3.6. ^{1}H NMR of $[(^{tBu}POCOP)Ir(H)(NCCH_3)_2][B(Ar^F)_4]$ catalyst

3.6.1. Electrochemistry set up for controlled potential electrolysis and cyclic voltammograms.

All measurements were performed on a Pine Wavedriver 10 bipotentiostat. Cyclic voltammetry was performed with a 1 mm diameter glassy carbon disc working electrode, a glassy carbon rod counter electrode, and a $Ag/AgNO_3$ reference electrode. All experiments were performed in degassed aqueous solutions with 1 mM catalyst and 0.1 M tetrabutylammonium hexafluorophosphate; as supporting electrolyte. Samples for electrochemical studies performed under CO_2 atmosphere were prepared by sparging the analyte solution with solvent saturated carbon dioxide gas prior to measurement and the headspace above the solution was blanketed with CO_2 during each measurement. Controlled potential electrolysis experiments were performed in a custom H-cell with the working and counter compartments (16.1 and 8.0 mL respectively) separated by a medium S4 porosity glass frit. The working and counter compartments were sealed with GL25 and GL18 open top caps with silicone/PTFE septa from Ace Glass. The working compartment contained: 1.0 mM catalyst, 10 mM Ammonium Carbamate, 0.1M $TBAPF_6$, a glassy carbon cloth as working electrode, the $Ag/AgNO_3$ reference electrode. The counter compartment contained an aqueous solution of 0.1 M $TBAPF_6$ and a 1” x 2.25” piece of carbon fabric as the counter electrode. After the electrolysis period, the volume in the working compartment was measured. The formate concentration was determined by ^{1}H NMR after addition of an internal standard (benzene) to a known volume of electrolysis solution. The headspace of the working compartment was sampled with a Restek A-2 Luer

lock gas-tight syringe. Headspace hydrogen was quantified by gas chromatography on an Agilent 7890B instrument with a HP-PLOT Molesieve column (19095P-MS6, 30m x 0.530 mm, 25 mm) and TCD detector.

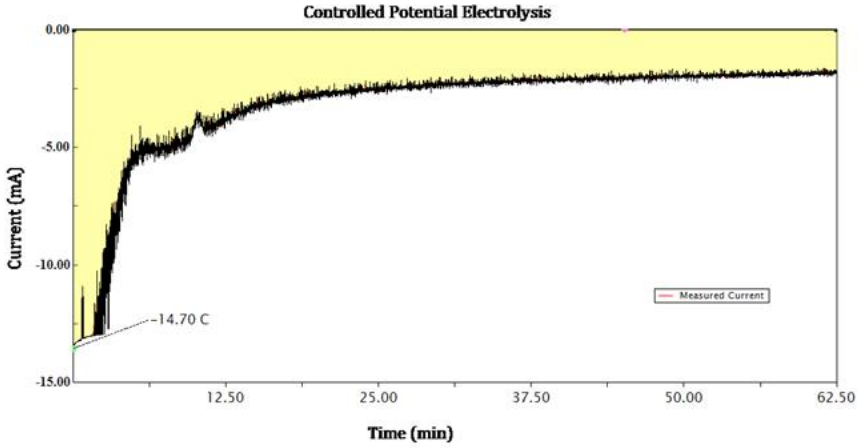

Figure 3.7. Controlled Potential Electrolysis - Ammonium Carbamate

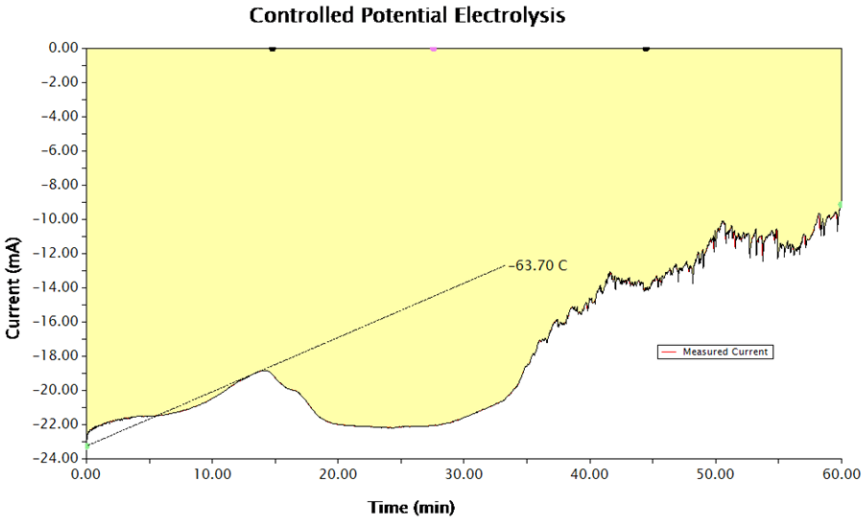

Figure 3.8. Controlled Potential Electrolysis - Ammonium hexafluorophosphate + CO_2

Synthesis of [Ir(^{tBu}POCOP)(H)(MeCN)$_2$][B(Ar^F)$_4$]and [(^{tBu}POCOP)Ir(H)(Cl)] was done following the published procedures.[25] To a 10mL chlorobenzene solution of [(^{tBu}POCOP)Ir(H)(Cl)] (42mg) was added 1.1 eq. Na(BAr$^F{}_4$)and added 15-20 drops of MeCN slowly and the solution was stirred for 1h. The reaction mixture was passed through a Teflon syringe filter, and the solvent was then removed under vacuum, yielding a light-yellow solid.

Synthesis of BIAN substituted iron cluster was done using the modified literature procedure.[34] – Inside the globe box, Schlenk flask was charged with 1:1 ratio of $[Fe_4N(CO)_{12}][Na(diglym)_2]$ and BIAN ligand in THF. The reaction was monitored by IR spectroscopy and looked for changes associated with carbonyl stretching frequency. In absence of observed reaction at room temperature, the reaction was heated to 60 °C or exposed to light (370nm) for 3 hours. Once the reaction was completed, the reaction mixture was through celite plug, followed by salt metathesis with 1 equiv of tetraethylammonium chloride at room temperature for 2 hours.

3.7. Appendix

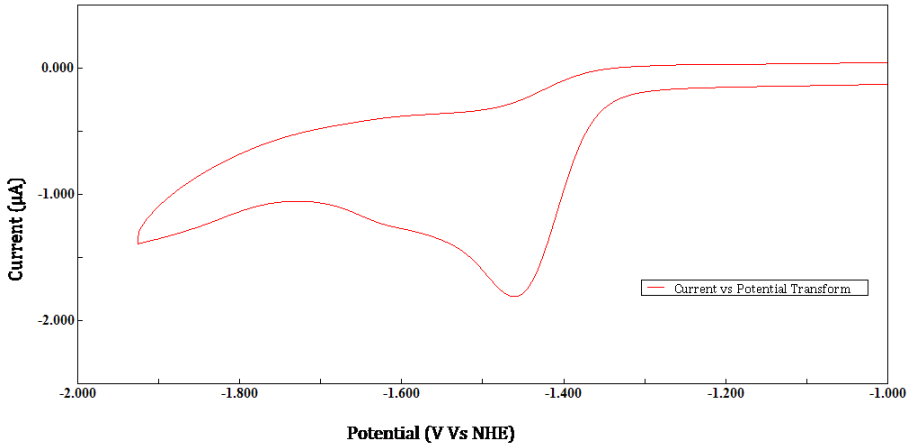

Figure 3.9. Cyclic Voltammogram of $[Ir(^{tBu}POCOP)(H)(MeCN)_2][B(Ar^F)_4]$ Complex

3.8. References

1. National Research Council Advancing the Science of Climate change. The National Academics Press, Washington, DC,USA: 2010.
2. Climate Change Indicators: Weather and Climate https://www.epa.gov/climate-indicators/weather-climate.
3. Gao, N.; Quiroz-Arita, C.; Diaz, L. A.; Lister, T. E., Intensified co-electrolysis process for syngas production from captured CO2. *Journal of CO2 Utilization* **2021,** *43*, 101365.
4. Pérez-Gallent, E.; Vankani, C.; Sánchez-Martínez, C.; Anastasopol, A.; Goetheer, E., Integrating CO2 Capture with Electrochemical Conversion Using Amine-Based Capture Solvents as Electrolytes. *Industrial & Engineering Chemistry Research* **2021,** *60* (11), 4269-4278.
5. Chen, L.; Li, F.; Zhang, Y.; Bentley, C. L.; Horne, M.; Bond, A. M.; Zhang, J., Electrochemical Reduction of Carbon Dioxide in a Monoethanolamine Capture Medium. *ChemSusChem* **2017,** *10* (20), 4109-4118.

6. Olah, G. A.; Prakash, G. K. S.; Goeppert, A., Anthropogenic Chemical Carbon Cycle for a Sustainable Future. *Journal of the American Chemical Society* **2011,** *133* (33), 12881-12898.
7. Lee, G.; Li, Y. C.; Kim, J.-Y.; Peng, T.; Nam, D.-H.; Sedighian Rasouli, A.; Li, F.; Luo, M.; Ip, A. H.; Joo, Y.-C.; Sargent, E. H., Electrochemical upgrade of CO2 from amine capture solution. *Nature Energy* **2020,** *6* (1), 46-53.
8. Federsel, C.; Jackstell, R.; Beller, M., State-of-the-Art Catalysts for Hydrogenation of Carbon Dioxide. *Angewandte Chemie International Edition* **2010,** *49* (36), 6254-6257.
9. Börjesson, M.; Moragas, T.; Gallego, D.; Martin, R., Metal-Catalyzed Carboxylation of Organic (Pseudo)halides with CO2. *ACS Catalysis* **2016,** *6* (10), 6739-6749.
10. Riduan, S. N.; Zhang, Y., Recent developments in carbon dioxide utilization under mild conditions. *Dalton Transactions* **2010,** *39* (14), 3347-3357.
11. Peters, M.; Köhler, B.; Kuckshinrichs, W.; Leitner, W.; Markewitz, P.; Müller, T. E., Chemical Technologies for Exploiting and Recycling Carbon Dioxide into the Value Chain. *ChemSusChem* **2011,** *4* (9), 1216-1240.
12. Cokoja, M.; Bruckmeier, C.; Rieger, B.; Herrmann, W. A.; Kühn, F. E., Transformation of Carbon Dioxide with Homogeneous Transition-Metal Catalysts: A Molecular Solution to a Global Challenge? *Angewandte Chemie International Edition* **2011,** *50* (37), 8510-8537.
13. Fan, T.; Chen, X.; Lin, Z., Theoretical studies of reactions of carbon dioxide mediated and catalysed by transition metal complexes. *Chemical Communications* **2012,** *48* (88), 10808-10828.
14. Schneider, J.; Jia, H.; Muckerman, J. T.; Fujita, E., Thermodynamics and kinetics of CO2, CO, and H+ binding to the metal centre of CO2reductioncatalysts. *Chemical Society Reviews* **2012,** *41* (6), 2036-2051.
15. Appel, A. M.; Bercaw, J. E.; Bocarsly, A. B.; Dobbek, H.; DuBois, D. L.; Dupuis, M.; Ferry, J. G.; Fujita, E.; Hille, R.; Kenis, P. J. A.; Kerfeld, C. A.; Morris, R. H.; Peden, C. H. F.; Portis, A. R.; Ragsdale, S. W.; Rauchfuss, T. B.; Reek, J. N. H.; Seefeldt, L. C.; Thauer, R. K.; Waldrop, G. L., Frontiers, Opportunities, and Challenges in Biochemical and Chemical Catalysis of CO2 Fixation. *Chemical Reviews* **2013,** *113* (8), 6621-6658.
16. Wang, W.-H.; Himeda, Y.; Muckerman, J. T.; Manbeck, G. F.; Fujita, E., CO2 Hydrogenation to Formate and Methanol as an Alternative to Photo- and Electrochemical CO2 Reduction. *Chemical Reviews* **2015,** *115* (23), 12936-12973.
17. Yadav, M.; Linehan, J. C.; Karkamkar, A. J.; van der Eide, E.; Heldebrant, D. J., Homogeneous Hydrogenation of CO2 to Methyl Formate Utilizing Switchable Ionic Liquids. *Inorganic Chemistry* **2014,** *53* (18), 9849-9854.
18. Kothandaraman, J.; Heldebrant, D. J., Catalytic coproduction of methanol and glycol in one pot from epoxide, CO2, and H2. *RSC Advances* **2020,** *10* (69), 42557-42563.
19. Khusnutdinova, J. R.; Garg, J. A.; Milstein, D., Combining Low-Pressure CO2 Capture and Hydrogenation To Form Methanol. *ACS Catalysis* **2015,** *5* (4), 2416-2422.
20. Yin, X.; Moss, J. R., Recent developments in the activation of carbon dioxide by metal complexes. *Coordination Chemistry Reviews* **1999,** *181* (1), 27-59.
21. Aresta, M.; Dibenedetto, A., Utilisation of CO2 as a chemical feedstock: opportunities and challenges. *Dalton Transactions* **2007,** (28), 2975.
22. Bhattacharya, M.; Sebghati, S.; VanderLinden, R. T.; Saouma, C. T., Toward Combined Carbon Capture and Recycling: Addition of an Amine Alters Product Selectivity from CO to Formic Acid in Manganese Catalyzed Reduction of CO2. *Journal of the American Chemical Society* **2020,** *142* (41), 17589-17597.
23. Tanaka, R.; Yamashita, M.; Nozaki, K., Catalytic Hydrogenation of Carbon Dioxide Using Ir(III)−Pincer Complexes. *Journal of the American Chemical Society* **2009,** *131* (40), 14168-14169.

24. Schmeier, T. J.; Dobereiner, G. E.; Crabtree, R. H.; Hazari, N., Secondary Coordination Sphere Interactions Facilitate the Insertion Step in an Iridium(III) CO2 Reduction Catalyst. *Journal of the American Chemical Society* **2011,** *133* (24), 9274-9277.
25. Kang, P.; Cheng, C.; Chen, Z.; Schauer, C. K.; Meyer, T. J.; Brookhart, M., Selective Electrocatalytic Reduction of CO2 to Formate by Water-Stable Iridium Dihydride Pincer Complexes. *Journal of the American Chemical Society* **2012,** *134* (12), 5500-5503.
26. Matsubara, Y.; Grills, D. C.; Kuwahara, Y., Thermodynamic Aspects of Electrocatalytic CO2 Reduction in Acetonitrile and with an Ionic Liquid as Solvent or Electrolyte. *ACS Catalysis* **2015,** *5* (11), 6440-6452.
27. Brown, I. D., Prediction of angles in tetrahedral complexes and pseudotetrahedral complexes with stereoactive pairs. *Journal of the American Chemical Society* **1980,** *102* (6), 2112-2113.
28. Gobbi, A.; Frenking, G., Y-Conjugated compounds: the equilibrium geometries and electronic structures of guanidine, guanidinium cation, urea, and 1,1-diaminoethylene. *Journal of the American Chemical Society* **1993,** *115* (6), 2362-2372.
29. Kleinpeter, E.; Klod, S.; Rudorf, W.-D., Electronic State of Push−Pull Alkenes: An Experimental Dynamic NMR and Theoretical ab Initio MO Study. *The Journal of Organic Chemistry* **2004,** *69* (13), 4317-4329.
30. Durin, G.; Berthet, J.-C.; Nicolas, E.; Thuéry, P.; Cantat, T., The Role of (tBuPOCOP)Ir(I) and Iridium(III) Pincer Complexes in the Catalytic Hydrogenolysis of Silyl Triflates into Hydrosilanes. *Organometallics* **2022,** *41* (14), 1786-1796.
31. Johnson, S. I.; Nielsen, R. J.; Goddard, W. A., III, Selectivity for HCO2– over H2 in the Electrochemical Catalytic Reduction of CO2 by (POCOP)IrH2. *ACS Catalysis* **2016,** *6* (10), 6362-6371.
32. Taheri, A.; Thompson, E. J.; Fettinger, J. C.; Berben, L. A., An Iron Electrocatalyst for Selective Reduction of CO2 to Formate in Water: Including Thermochemical Insights. *ACS Catalysis* **2015,** *5* (12), 7140-7151.
33. Pattanayak, S.; Loewen, N. D.; Berben, L. A., Using Substituted [Fe4N(CO)12]− as a Platform To Probe the Effect of Cation and Lewis Acid Location on Redox Potential. *Inorganic Chemistry* **2023,** *62* (5), 1919-1925.
34. Loewen, N. D.; Pattanayak, S.; Herber, R.; Fettinger, J. C.; Berben, L. A., Quantification of the Electrostatic Effect on Redox Potential by Positive Charges in a Catalyst Microenvironment. *The Journal of Physical Chemistry Letters* **2021,** *12* (12), 3066-3073.
35. Piryazev, D. A.; Ogienko, M. A.; Virovets, A. V.; Pushkarevsky, N. A.; Konchenko, S. N., [N,N'-Bis(2,6-diisopropylphenyl)acenaphthene-1,2-diimine-1[kappa]2N,N']heptacarbonyl-1[kappa]C,2[kappa]3C,3[kappa]3C-di-[mu]3-tellurido-triiiron(II)(2 Fe-Fe). *Acta Crystallographica Section C* **2012,** *68* (11), m320-m322.

4. Theoretical Studies of pnictogen family chemistry

4.1. A computational chemistry approach to the study of arsenic tautomerization

Arsenic is a toxic metalloid which is widely dispersed in the environment. It is a pollutant that is accessible to humans through the air, water, soil and food, owing to both natural and anthropogenic activities.[1] Seafood is the main source of human exposure to arsenic.[2] It enters the food chain through a process called bioaccumulation, i.e., over time in the marine environment it accumulates in the tissues of organisms such as fish and shellfish. The increasing demand for seafood consumption is driven by several factors which include both environmental and societal changes. Recent data shows that in 2019, consumption of seafood by the American populace was 19.2 pounds per capita.[3] Given these toxicity concerns and the increasing prevalence of arsenic in diets, it is important to define the types of arsenic which pose the greatest exposure and toxicological risks. In the marine environment, arsenic exists in both inorganic and organic forms, including arsenate, arsenite and various arsenosugars and arsenolipids. Amongst these forms, 70% of arsenic occurs in the form of arsenolipids.[4] Arsenohydrocarbons (As-HCs; e.g. As-HC332 and As-HC360) (**Figure 4.1**) are a prevalent sub class of arsenolipid compounds and have been found in concentration ranges from 33 to 40 ppb in sea foods.[5]

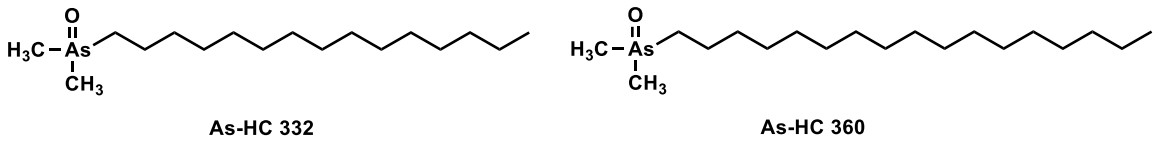

Figure 4.1. Structure of As-HC 332 and As-HC 360 with dimethyl -As group on one end and long hydrocarbon on another end.

It is known that inorganic arsenic is the more toxic form of the element and is found in various compounds such as arsenite and dimethylarsinic acid (DMA) but the organoarsenical As-HC360 is 5 times more toxic than inorganic As (iAs), which is regulated in water at 10 ppb and in infant cereals at 100 ppb[6-8] - As-HC332 is 3.7 times more toxic than iAs. Hence, due to their potential for bioaccumulation in the brain and the impairment of central nervous system function, As-HCs have become an emerging species of interest with respect to neurodevelopment disorders (NDs).

Studies have shown that in Drosophila melanogaster,[9] these As HCs can pass through physiological barriers including cell membranes and the intestinal and blood brain barriers, but similar research in a mammalian model system has yet to be performed. Results from in vitro research on human neuronal cells has shown that, As-HCs trigger apoptosis and disrupt the neuronal network. Numerous epidemiological studies have demonstrated a link between arsenic exposure and the manifestation of NDs; associations with attention-deficit/hyperactivity disorder (AD/HD), autism spectrum disorder (ASD), obsessive compulsive disorders (OCD) and learning disabilities are consistently and frequently reported.[10-14] It has also been proposed that As-HCs can be metabolized to dimethyl arsinic

acid (DMA(V)) which can cross the blood-brain barrier and, along with its metabolites, e.g., dimethylmonothioarsinic acid (DMMTA(V)), can result in oxidative stress, inflammation, mitochondrial dysfunction, apoptosis and impaired protein degradation [15, 16] - causal mechanisms underlying NDs. Altogether, this data suggests that As HCs exposure is responsible, at least in part, for the development of NDs.

A major constraint to the experimental investigation of As-HCs and their toxicity is a lack of standard and certified reference materials, which are required from an analytical perspective in the development of strategies for compound identification and quantification. References materials are also required, for assessment of toxicological endpoints, metabolic pathways, and toxicity mechanisms. Finally, from a regulatory perspective, the safe and effective monitoring of arsenic levels in food products requires accurate analytical standard materials. Several synthetic routes have been reported in the literature for the preparation of As-HCs, unfortunately they are both time and labor intensive and typically proceed in low to moderate overall yield.[17] This results in the increased cost for purchasing As-HC standards; which are only available from a limited number of laboratories.

The lack of efficient and robust synthetic procedures in the literature prompted us to propose two new methods for the preparation of As-HCs, involving fewer chemical steps and providing broader access to a range of As-HCs and their derivatives. Hydroarsinylation is an atom economical approach to the preparation of organoarsenic compounds (Route a; **Scheme 4.1**) in which the addition of an As-H bond across an unsaturated C=C double bond may occur, typically in the presence of a transition metal-based catalyst.[18-20] Alternatively, borrowing an approach from analogous phosphorus chemistry,[21] a nucleophilic arsenic precursor (Route b; **Scheme 4.1**) can be employed to displace a bromide ion from an appropriate alkyl bromide to afford the desired As HC. It soon became readily apparent that a secondary arsine oxide (SAO) (shown below) intermediate was key to both synthetic strategies.

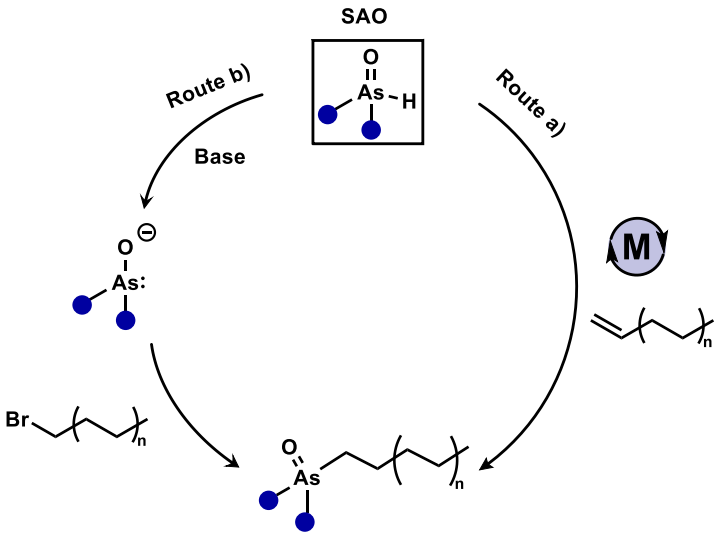

Scheme 4.1. Two proposed routes to access the targeted As-HCs. Route a) employs a metal-catalyzed hydroarsinylation strategy whilst route b) envisions a direct nucleophilic attack on an appropriate alkyl halide reagent. Key to both routes is the generation of a secondary arsine oxide (SAO) to be utilized as a starting material.

The use of a SAO intermediate requires the preparation and isolation of an "As^{V}-H" moiety. Thus, this approach relies on the relative stability of As^{III} versus As^{V} oxidation states and directly begs the question: will such species undergo tautomerization? Tautomerization is a rearrangement which involves the interconversion of constitutional isomers (tautomers). The very first tautomerization one learns in sophomore organic chemistry is keto-enol tautomerization, but prototropy is a common subclass, where a hydrogen atom moves from one atom to another. The SAO (**1**) shown below may undergo prototropic tautomerism to afford the "As-OH" species (**1´**). We hypothesize that if the As(III) oxidation state is accessible, this would open a second synthetic strategy to access As-HCs; tautomer **1'** features a nucleophilic lone pair at the As center which facilitates S_N2-type reaction chemistry. This can be exploited in a simple displacement reaction of a C-X bond to furnish the targeted As-HCs from commercially available alkyl bromides. If feasible, an easy and high yielding synthetic approach to AsHCs via a secondary arsine oxide will facilitate access to an AsHCs compound library, which would be useful for biomedical researchers investigating the toxicological consequences in mammalian model systems.

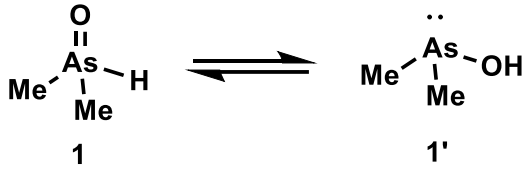

Scheme 4.2. Arsenic tautomerization from As^{v} to As^{III}.

In phosphorus chemistry, a lighter group 15 congener of arsenic, the equilibrium is expected to lie far towards the higher P(V) oxidation state. [22, 23] In contrast, the relative stability of As(III) means that it is likely the predominant species under equilibrium conditions. Before embarking on a lab-based, experimental campaign, we decided to explore the relative stability of a range of substituted SAOs using computational techniques. Our goal being to understand the influence of substituents on the position of the equilibrium i.e. can we control the tendency to form As(III) or As(V) species through manipulation of electron-donating or electron-withdrawing substituents.

4.2 Results and Discussion

Computational Method - Initial benchmark work was carried out by comparing three different functionals (B3LYP, M062X, and ωB97XD) and six basis sets [6-311G(d,p), cc-pVDZ, cc-pVTZ, aug-cc-pVDZ, def2tzvp and def2tzvpp], resulting in 18 different model chemistries.[24-26] Results from these benchmark calculations are summarized in **Table 4.1**. Following a thorough examination of these results we determined that ωB97XD/cc-pVTZ

model chemistry best reproduced the literature reported phosphorus results.[21] We also ran additional augmented basis set to see if energy values are improved and make remarkable difference using bigger basis set as compared to cc-pVTZ, but since large difference was not observed so less expensive basis set was chosen for further calculations.

With these findings in hand, we began by optimizing the geometry of the As=O and As-OH tautomeric forms and subsequently probed their relative stability. As preliminary calculations, the energetics associated with $R^1R^2As(O)H$ and $R^1R^2As(OH)$ equilibrium was calculated in the gas phase as summarized in **Figure 4.2.** We determined the relative stability of the tautomer's using the Gibb's free energy difference between two species (**Table 4.1**). To explore the impact of substituents on the relative stability of the tautomeric forms, a wide range of stereo electronically differentiated groups were explored. Both electronically donating groups (R = methyl (Me), ethyl (Et), butyl (Bu), octyl (Oct), ethoxy (OEt)) and electronically withdrawing groups (R = phenyl (Ph), trifluoromethyl (CF_3), cyanide (CN)) were selected for study.

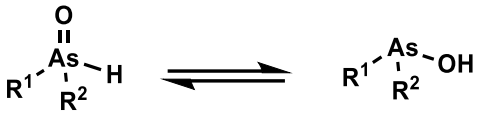

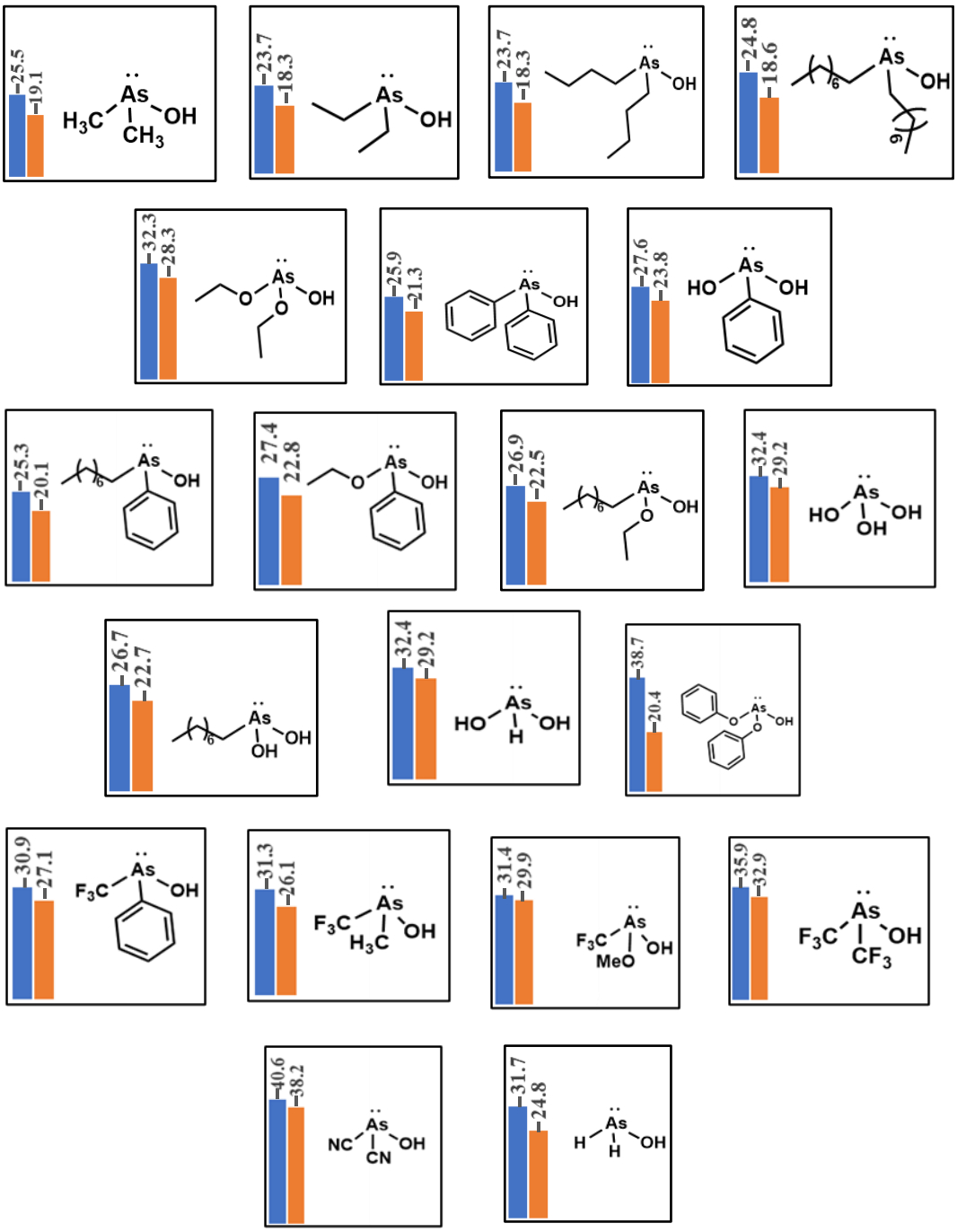

Figure 4.2. ΔE values obtained for tautomeric equilibria associated with organoarsenical in the gas and solvent phases represented by blue and orange bars, respectively. .

In the gas phase calculations, it was found that when substituted with electron releasing groups, the equilibrium of tautomerization shifted toward the As^{V} form, although the As^{III} oxidation state was still energetically preferred. In contrast, when electron withdrawing groups are used, the equilibrium favors the As^{III} form even more strongly. To produce a more realistic dataset and possibly more relevant results to help guide future experimental work, we performed the calculations in a universal continuum solvation model (SMD) employing dichloromethane as solvent.

Based upon our preliminary DFT work, it appears that no (reasonable) substitution patterns will overcome the inherent stability of As^{III}. Thus, an As^{V} hydroarsinylation approach may not be feasible. With this conclusion in hand, we decided to explore the next steps in a putative 'nucleophilic arsine' approach. We subsequently performed calculations to estimate the energy associated with deprotonation (**Figure 4.3**) of the As-OH moiety. Dimethyl arsane was chosen as a model substrate for the calculations. We assumed that deprotonation would likely be an energetically demanding process and calculated an (energy difference) ΔE of 320 kcal/mol. We carried out a preliminary screen of substituent effects to explore their influence on the energy barrier in the hopes that more feasible experimental systems could be found which allow deprotonation to occur. When both substituents are electron releasing, the energy requirement increased (more positive ΔE was observed). In contrast, when electron withdrawing substituents were employed, a small lowering of the energy barrier was obtained, but still too large to be accessible under standard thermochemical conditions. Gibb's free energy data is assembled in **Table 4.2.**

While exploring possible routes to prepare As-HCs using SAOs we were intrigued by a recent publication by Lee and coworkers.[27] Using an exogenous Lewis acid, this strategy allowed the authors to successfully alkylate a phosphine oxide and we were curious to learn if a similar approach could be deployed in the analogous arsenic chemistry. We chose BBr_3 as a starting point for our exploration of Lewis acid-assisted stabilization of As^{V} species (**Figure 4.4)**. To our delight, when the As^{V} was trapped by the Lewis acid, the calculated energy difference was -45 kcal/mol, which is drastically lower than the ΔE requirement for deprotonation of As^{III}. Once again, we decided to explore the role of substituents on the arsenic center by systematically varying the attached groups with both electron releasing and electron withdrawing moieties. Our calculated values revealed a trend in stability in which electron releasing groups would provide increased stabilization of an As^{V} species. We were encouraged by these results and that they, perhaps, point the way to a feasible synthetic method to in the laboratory. The corresponding ΔG values for this reaction are provided in **Table 4.3.** Overall, we conclude that to access the As-HC's Lewis acid-assisted strategy will be one we pursue in synthetic efforts moving forward.

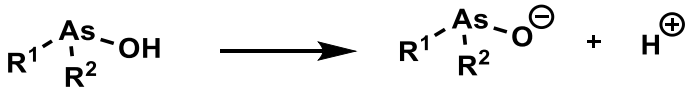

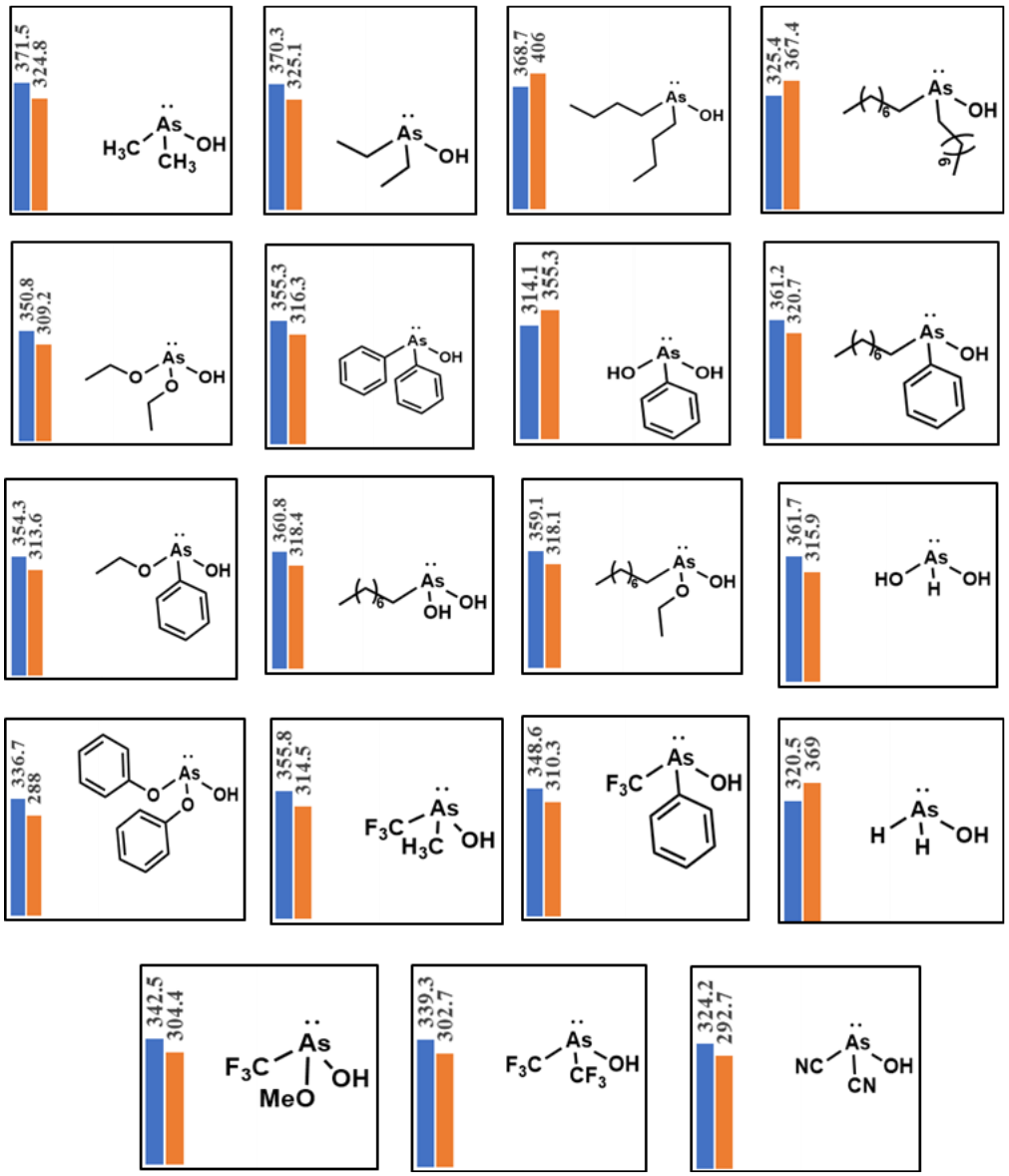

Figure 4.3. ΔE values obtained for deprotonation of As^{III} species in gas and solvent phase represented by blue and orange bars respectively.

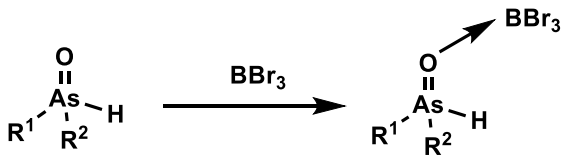

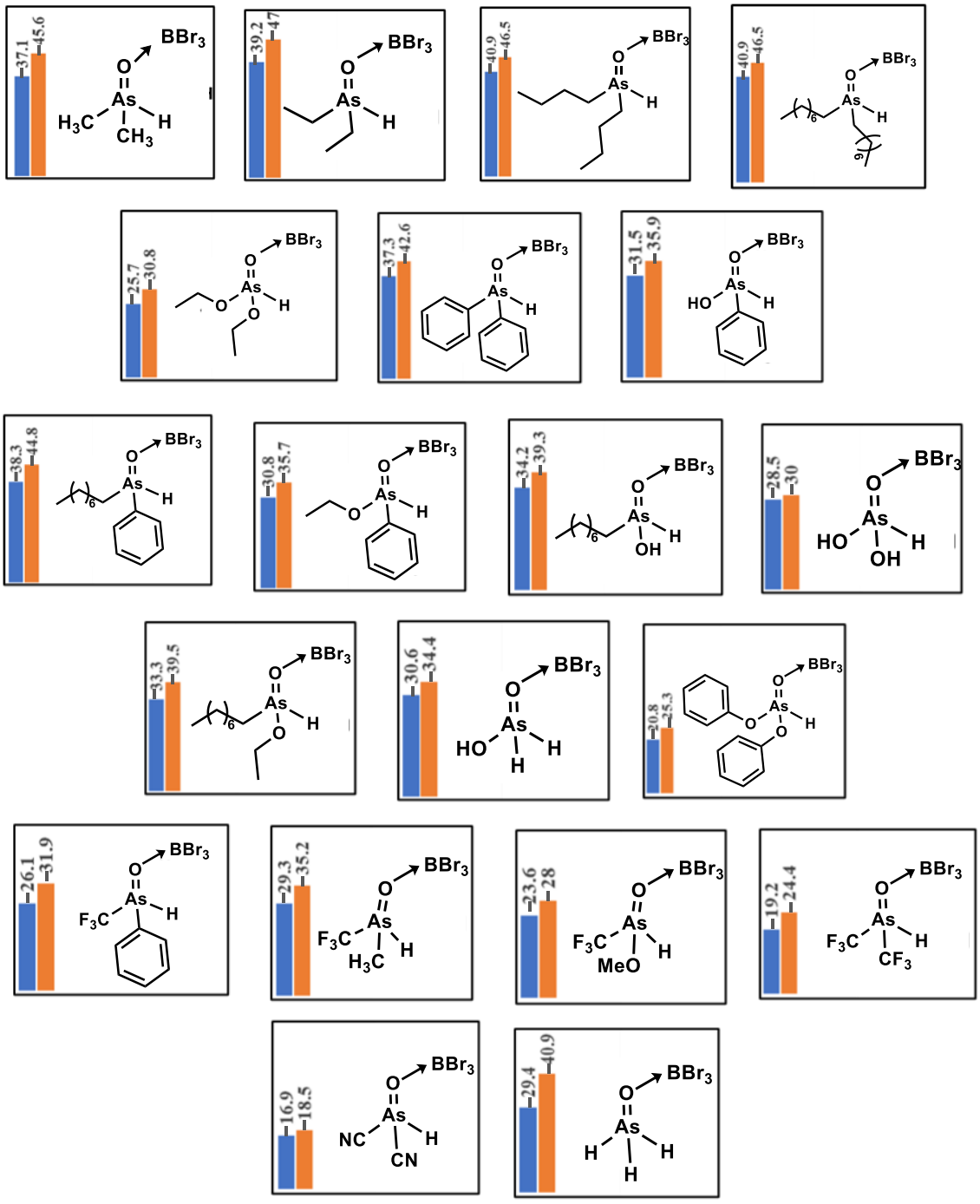

Figure 4.4. ΔE values obtained for lewis acid association with As^{V} species in gas and solvent phase represented by blue and orange bars respectively.

Table 4.1. Gibb's free energy obtained for tautomeric equilibria between As^{V} and As^{III} species.

Entry	R^1	R^2	ΔG^a (kcal/mol)[a]	ΔG^b (kcal/mol)[b]
1	Me	Me	-25.69	-19.68
2	Et	Et	-24.61	-19.41
3	Bu	Bu	-23.59	-18.16
4	Oct	Oct	-25.04	-19.71
5	OEt	OEt	-32.74	-28.84
6	Ph	Ph	-26.67	-21.83
7	OH	Ph	-27.39	-23.54
8	OEt	Ph	-28.01	-23.62
9	Oct	Ph	-24.58	-20.04
10	OH	Oct	-26.44	-23.08
11	OEt	Oct	-27.20	-22.79
12	OH	OH	-32.74	-29.37
13	OH	H	-38.44	-20.25
14	OPh	OPh	-36.77	-33.38
15	CF_3	Ph	-31.20	-27.11
16	CF_3	Me	-31.18	-25.95
17	CF_3	OMe	-31.46	-30.79
18	CF_3	CF_3	-37.41	-34.49
19	CN	CN	-40.98	-38.46
20	H	H	-32.68	-25.20

[a] Gas Phase [b] Solvent Phase - DCM

Table 4.2. Gibb's free energy required for deprotonation of As^{III} species.

Entry	R^1	R^2	ΔG (kcal/mol)[a]	ΔG (kcal/mol)[b]
1	Me	Me	371.83	325.47
2	Et	Et	370.72	326.32
3	Bu	Bu	369.38	325.39
4	Oct	Oct	366.84	326.35
5	OEt	OEt	351.01	309.73
6	Ph	Ph	356.70	317.33
7	OH	Ph	355.33	314.18
8	OEt	Ph	354.81	313.83
9	Oct	Ph	361.22	320.43
10	OH	Oct	360.79	318.38
11	OEt	Oct	359.96	318.67
12	OH	H	367.81	309.95
13	OPh	OPh	336.37	301.72
14	CF_3	Ph	349.01	310.83
15	CF_3	Me	355.94	314.74
16	CF_3	OMe	343.06	304.76
17	CF_3	CF_3	339.16	302.80
18	CN	CN	324.33	292.67
19	H	H	369.37	336.47

[a] Gas phase [b] Solvent phase (DCM)

Table 4.3. Gibb's free energy obtained from stabilization of As^V species with lewis acid BBr_3.

Entry	R^1	R^2	ΔG^a (kcal/mol)[a]	ΔG^b (kcal/mol)[b]
1	Me	Me	-25.76	-34.45
2	Et	Et	-28.40	-34.94
3	Bu	Bu	-27.09	-34.16
4	Oct	Oct	-29.08	-34.74
5	OEt	OEt	-12.98	-18.32
6	Ph	Ph	-25.08	-30.61
7	OH	Ph	-19.07	-23.56
8	OEt	Ph	-19.43	-23.13
9	Oct	Ph	-25.68	-33.01
10	OH	Oct	-21.87	-29.58
11	OEt	Oct	-20.51	-25.17
12	OH	OH	-15.92	-17.36
13	OH	H	-18.45	-23.02
14	OPh	OPh	-8.21	-13.89
15	CF_3	Ph	-13.82	-18.51
16	CF_3	Me	-17.75	-22.37
17	CF_3	OMe	-11.76	-16.55
18	CF_3	CF_3	-8.37	-12.26
19	CN	CN	-5.07	-7.00
20	H	H	-18.76	-30.06

[a] Gas Phase [b] Solvent Phase - DCM

4.3. Antimony Bismuth Host Guest Chemistry

4.3.1. Pnictogen Bonding

Pnictogen bonding is a type of non-covalent interaction that occurs between molecules containing an electrophilic region (or regions) on an element from group 15 (or pnictogens) of the periodic table (the PnB donor), including phosphorus (P), arsenic (As), antimony (Sb), and bismuth (Bi), and a suitable nucleophile (PnB acceptor). *Triple pnictogen bonding* is the capability of a pnictogen atom to participate in three pnictogen bonds simultaneously with a complementary partner through a single pnictogen atom. [28, 29] The strength of pnictogen bonding can be influenced by the geometry and electronic structure of the molecules involved.[30] It can play a significant role in host guest chemistry (yielding supramolecular structures), which refers to the interaction between a molecule or ion (the "guest") and a larger molecular structure (the "host"). The host can selectively bind specific guest molecules within the cavity of a host molecule.[31] With pnictogen bond donors, this selectivity arises from the ability of pnictogen atoms to form directional interactions with

lone pair electrons on the guest molecule, resulting in a specific orientation and positioning of the guest molecule within the host cavity.

4.3.2. Anion recognition

Anion binding and recognition are two closely related and important concepts that garner much attention as s subfield of host-guest interactions. Anion binding refers to the ability of molecules to bind specifically to an anion through non-covalent interactions such as hydrogen bonding, halogen bonding and van der Waals forces. Anion recognition is the ability of a host to recognize an anion specifically (for example, in presence of a mixture of anions). Anion recognition is achieved through selective binding, undergoing physical and chemical changes in properties in the presence of the anion. Hydrogen and halogen bonding have played a large role in this field.[32, 33] The chalcogens and pnictogens have had an emerging and leading role. For example, Gabbai and coworkers have employed a variety of Lewis acidic main group compounds as anion binding agents.[34, 35] They utilized the highly Lewis acidic nature of antimony(V) complexes to design fluorescent and colorimetric sensors.[36, 37] These anion binding studies form the basis of several applications such as metal free catalysis in organic synthesis, selective sensing of anions, drug design and crystal engineering or molecular templating.[38-43]

4.3.2.1. Chalcogen and pnictogen bonding for anion binding and recognition.

Analogous to chalcogen and halogen bonding, pnictogen bonding has also been utilized for the design of anion receptors. The use of weaker Lewis acidic Pn(III) and Te(II) has been explored because of their ability to form highly directional pnictogen or chalcogen bonds with no appreciable activation barrier; an advantage over the stronger Lewis acids (BX_3, PnX_5). The directionality comes from the localization of the lone pair(s) on the larger Pn(III) and Te(II), which creates an anisotropic charge distribution leading to precise positioning of binding sites. Matile demonstrated the PnB formed with tris(perfluorophenyl)stibane can be used for transmembrane anion transport.[44, 45] It was found that directionality and hydrophobicity exceed all conventional interactions such as hydrogen bond donors and provide precision on molecular level. Cozzolino and coworkers reported the design of an oxo-bridged bis(antimony(III)) compound for anion binding which suffered from self-recognition issues which decreased anion binding efficacy.[46] Computational (DFT) studies suggested that in the gas phase oxygen tends to form intramolecular interactions with adjacent antimony atoms. Although complexes proposed by the Matile and Cozzolino groups display amazing anion reception, they suffer from complicating steric hindrance and intramolecular interaction. These effects create obstacles for selective anion binding and convolutes attempts to study and understand the underlying phenomena. Later, Cozzolino and coworkers found an approach to tackle self-recognition. They proposed the tripodal antimony(III) triskatole complex[47] (**Figure 4.5**), which includes nitrogen in the primary bond and thus ensures the bond polarity and supported pnictogen bonding without the deleterious effects described above.

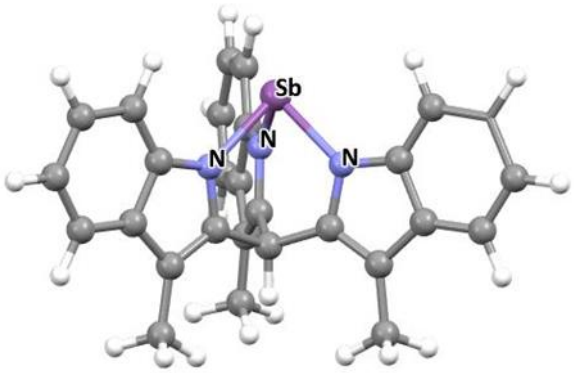

Figure 4.5. Antimony (III) triskatyl complex[47]

The design strategy includes a) using nitrogen (N) to support a polar primary bond in order to reduce the number of available lone pairs, b) incorporating the nitrogen into an indole ring in order to delocalize the remaining N lone pair and c) incorporating the pnictogen into a cage to ensure sufficient space for the formation of up to three PnBs and remove conformational flexibility. This system has been previously used to demonstrate triple pnictogen bonding for complementary molecular recognition.[47, 48] A supramolecular building block that is complementary to a triple PnB donor must include three lone pairs in an arrangement that allows for alignment with the electrophilic regions. Building blocks for a functional PnB-based supramolecular cavitand should contain spacers that create an internal cavity and some level of preorganization favoring simultaneous PnB of three acceptor units. A complementary partner was found with a trispyridyl donor. Crystal structures with pyridine itself, only show two pnictogen bonds with the antimony system and all three with the bismuth system. Negative cooperativity, resulting from the increased stereochemical activity of the pnictogen lone pair with each subsequent PnB, was determined to account for these differences. So far, no studies have been performed to understand the anion binding behavior of PnB donors, i.e., antimony complex (**11**) and bismuth complex (**12**) (**Figure 4.6**) in the absence of complicating effects (steric hindrance, self-recognition and/or conformational flexibility).

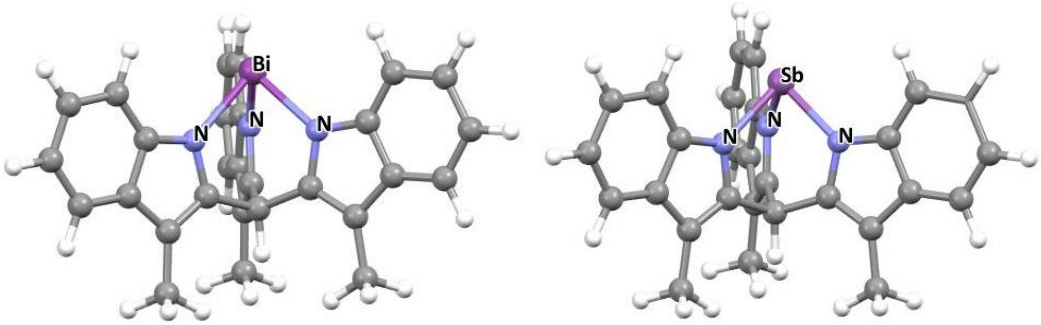

Figure 4.6. Tripodal antimony and bismuth compound[47]

We hypothesized that such Sb and Bi systems will circumvent these complications (vide infra) and provide important quantitative information and theoretical understanding of the anion binding ability (including cooperative effects) of the three PnB sites on the same PnB donor. This cooperativity stands in contrast to typical transition metal coordination chemistry where the metal is always coordinatively saturated in solution in the absence of steric hindrance. Density functional theory (DFT) calculations were used to gain insight into the anion binding ability of these systems and deduce whether it is 1:1 or 1:2 binding between the antimony/bismuth complex and incoming anion. The motivation for the anion binding capabilities came from literature precedents of strong PnBs with neutral molecules.[34, 44] Earlier reports from the Cozzolino group and others have demonstrated that neutral PnB donors are also compatible with anion binding.[46] The Matile group showed that PnB donors could be applied in the transportation of anions through cell membranes.[44]

4.3.3. Methods

The aim of this project is to investigate the interaction of anions with PnB donors such as antimony and bismuth complexes in the solution state and is carried out in collaboration with Dr. Cozzolino's group at Texas Tech University. Preliminary UV-Vis titration studies of antimony complexes with different anions were initiated while I was still at Texas Tech but have subsequently been continued by members of the Cozzolino group and I pivoted to providing supporting DFT calculations to validate experimental results. The calculations were carried out to probe the ability of Sb (**11**) and Bi (**12**) to form PnBs in solution with tetrabutylammonium halides (Cl^-, Br^-, I^-) and pseudo halides (CN^-, OCN^-, SCN^-).
An improved and accurate functional B97-D3[49] was employed along with slightly enhanced basis set def2-TZVPP to analyze main-group thermochemistry and non-covalent interactions.[50] In the literature this method has accurately reproduced the free energy trends associated with the anion binding using chalcogen bonding.[51] Firstly, the antimony complexes were optimized, and the molecular geometry was reproduced, in close approximation to crystal structures; validating the model chemistry to model anion binding for antimony and bismuth complexes (Appendix 4.5.1). With the optimized structures for Sb and Bi in hand, two binding modes were tested, i.e., 1:1 and 1:2 anion binding of Sb/Bi:X. To probe the effect of solvent, the conductor like polarizable continuum model (CPCM)[52] was applied. The solvation correction and basis set superposition error (BSSE) were calculated and added to final Gibb's free energy of complexes and anions and final Gibb's free energy change for binding was calculated using the following equation.

$$\Delta G = \Delta H - T\Delta S + BSSE + \Delta E_{solv}$$

The following discussion will use generic host/guest terminology where the pnictogen bond donor is the Host (H) and the anion is referred to as the Guest (G). The 1:1 and 1:2 H:G binding models were used to obtain the binding constant for the supramolecular structures following the stepwise equilibra depicted in equations 6 and 7.

$$H + G \rightleftharpoons H{\cdot}G \qquad [\textbf{Eq.6}]$$

$$H{\cdot}G + G = H{\cdot}G_2 \qquad [\textbf{Eq.7}]$$

4.4. Results and Discussion

The electrostatic potential energy surface (ESP) of the antimony (**11**) and bismuth (**12**) hosts revealed three maxima in the potential energies (V_{max}) on the 0.001 au surface with values of 147.3 kJ/mol and 185.8 kJ/mol, respectively. High positive Vmax values indicate sites that are attractive towards a nucleophile, in this case an anionic guest. The electrostatic potential values suggest the possibility of anion binding occurring at all three available sites (**Figure 4.7**). The ESP was calculated for the H·G and H·G_2 (for G = Cl^-). For H·G, the remaining sites had Vmax values of –167.2 kJ/mol and –113.7 kJ/mol for antimony and bismuth, respectively. These values are not directly comparable to those of the isolated host due to the presence of the negative charge. An important comparison is the change in values on Sb and Bi for H·G as compared with H. The ΔV_{max} (H_{Bi} – H_{Sb}) is 38.5 kJ/mol whereas the ΔV_{max} (H_{Bi}·G – H_{Sb}·G) is 53.5 kJ/mol. This much larger ΔV_{max} indicates that the second anion binding event will be far less likely for the H_{Sb} than for H_{Bi}. Calculation of the ESP for H·G_2 reveals a further increase in ΔV_{max} to 80.1 kJ/mol. The similar binding trend was suggested by the changes in the calculated Hirshfield charges on different atoms in complex (**Table 4.6 & Table 4.7**) The Hirshfield charge on the pnictogen decrease with each chloride. Concurrent with this, the charge on the nitrogen atom opposite the PnB decreases. This is consistent with a model where the anion donates electron density into the Pn–N σ* orbital. The decrease in partial charge on the pnictogen is in agreement with the anticipated negative cooperativity as was observed with neutral nucleophiles.

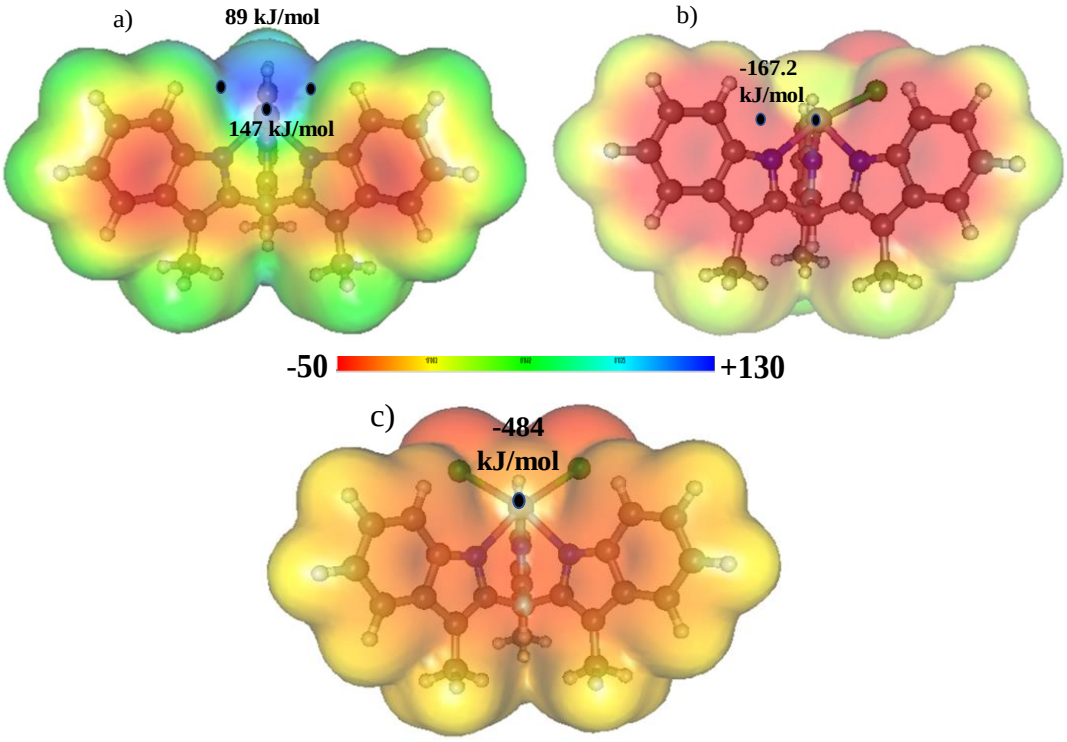

Figure 4.7. ESP mapped onto electron density plotted at 0.001 au for H_{Sb}, H_{Sb}:Cl^- and H_{Sb}:Cl^-. The black dot represents the location of V_{max} at the pnictogen.

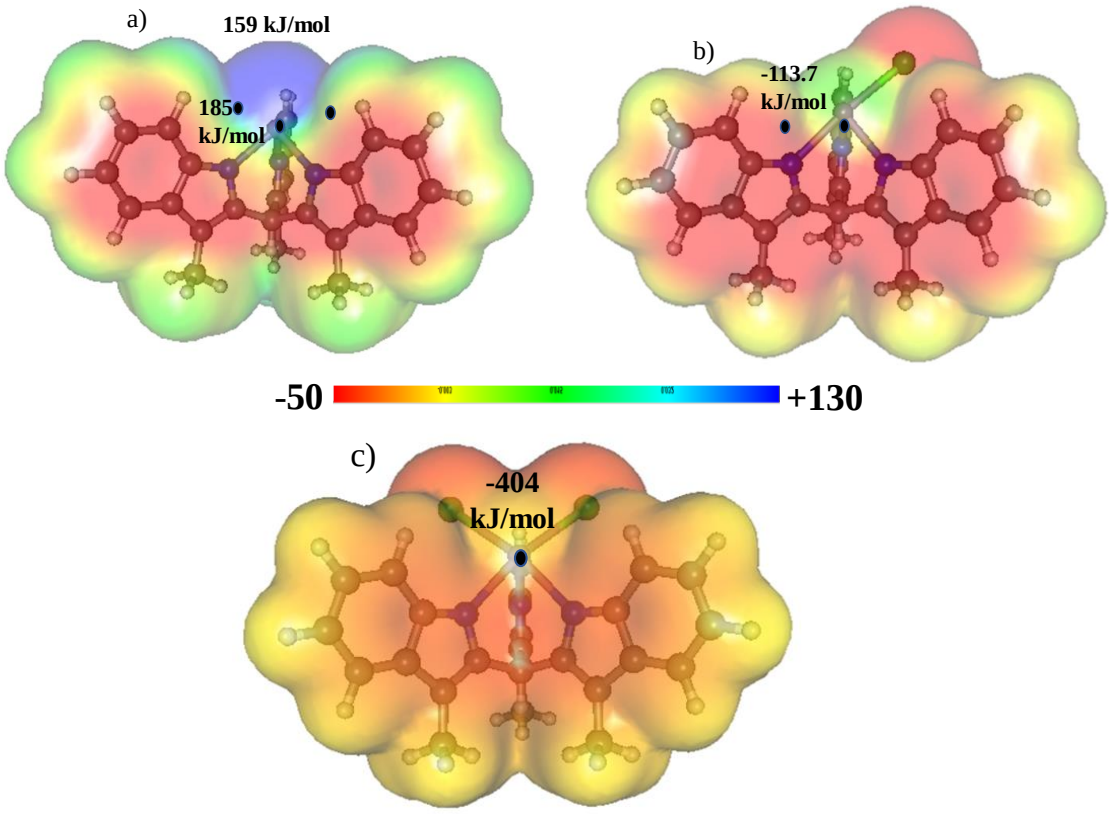

Figure 4.8. ESP mapped onto electron density plotted at 0.001 au for H_{Bi}, H_{Bi} :Cl^- and H_{Bi}:Cl^-. The black dot represents the location of Vmax at the pnictogen.

Both **Eq.6** and **Eq.7** were employed to obtain the Gibbs free energy (and binding constant) associated with binding of various anions to the hosts (**Table 4.4)**. Generally, larger binding constants were calculated for bismuth as compared to antimony. This aligns with the ESP maps as well as the shorter PnB distances (and greater nuclearity) in the crystal structures of H_{Bi} with different anions as compared to the corresponding H_{Sb} structures. Preliminary solution titration data is also consistent with larger binding constants for H_{Bi} with a variety of anions. In most cases it was observed that the binding constants became smaller as anions became softer. The binding constant values depicted that antimony favors formation of 1:1 supramolecular structure whereas bismuth appears able to expand beyond 1:1. Among halides, the binding constant and bond distances support the following trend: Cl >Br >I. The PnB distance between H_{Sb} and the halides were 2.61, 2.80 and 3.01 Å for chloride, bromide, and iodide respectively. Among the pseudohalide ambidentate anions, it was found that binding is more favorable through nitrogen coordination as compared to other atoms (carbon, oxygen, or sulfur) in cyanide, cyanate and isothiocyanates respectively. In most cases, Gibbs free energy was found to be positive when binding was taking place through other atom than nitrogen (**Table 4.5**) All the binding and bond distance

reproduced from DFT aligned well with the crystal structures, validating our DFT results. The only notable difference was in the connectivity for the cyanate anion. Initial refinement of the structure was performed with it κ-O. These calculations resulted in a reassessment of the model to be κ-N. The binding constant values for different halides and pseudo halides were consistent with experimental work carried out in the Cozzolino group.[53]

Table 4.4. The binding constant values calculated using Eq 6 and Eq 7

Anions	Antimony		Bismuth	
	K_{11}	K_{12}	K_{11}	K_{12}
Chloride (Cl^-)	13.33	2.35E-04	1661.72	31.88
Bromide (Br^-)	3.46	2.13E-05	1294.79	0.52
Iodide (I^-)	0.47	1.89E-04	128.59	2.44
Isocyanide (NC^-)	0.12	-	-	-
Cyanide (CN^-)	12.72	1.43E-06	897.16	1.80E-02
Isocyanate (NCO^-)	92.25	4.02E-08	6031.29	1.52E-02
Cyanate (OCN^-)	2.92E-04	-	0.015	-
Isothiocyanate (NCS^-)	0.38	7.64E-07	78.20	3.77E-03
Thiocyanate (SCN^-)	0.29	-	34.73	-

4.4.Conclusions

We have successfully employed computational chemistry to probe the behavior of two distinct systems in pnictogen chemistry. First, we explored an arsenic transformation which we hope to employ in future synthetic work to help assess reasonable pathways to access a key secondary arsine oxide intermediate and learned that such a species will likely undergo tautomerization to the corresponding As(III) species. Secondly, in a collaborative project with researchers at Texas Tech University, we examined pnictogen bonding and, in

particular, the supramolecular properties of bismuth and antimony compounds which exhibit directional bonding with anions.

4.5. Appendix

Table 4.1. Tautomerization energies are calculated using different model chemistries employing dimethyl arsine oxide as model substrate.

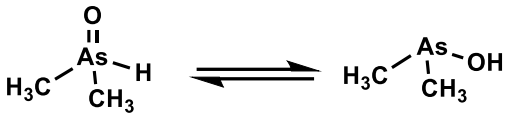

Model Chemistry	B3LYP (kcal/mol)	M062X (kcal/mol)	wB97xD (kcal/mol)
Basis1 (6-311g(dp)	-27.70	-29.32	-26.80
Basis2 (cc-pvDZ)	-28.89	-30.05	-27.83
Basis 3 (cc-pVTZ)	-25.96	-26.44	-24.72
Basis 4 (aug-cc-pVDZ)	-28.19	-28.94	-26.93
Basis5 (def2TZV)	-28.72	-33.49	-29.63
Basis6 (def2TZVPP)	-26.18	-26.85	-25.01
Basis7(aug-cc-pvTZ)	-	-	-24.51

4.5.1. The optimized geometry was well reproduced according to the crystal structures**.**

Bond Parameters Sb:I	Crystal structure	Optimized geometry	Bond Parameters Sb:Br	Crystal structure	Optimized geometry
Sb(1) - N(1)	2.135(2)	2.247	Sb(1) - N(1)	2.150(3)	2.247
Sb(1) - N(2)	2.043(2)	2.102	Sb(1) - N(2)	2.047(2)	2.105
Sb(1) - N(3)	2.059(2)	2.103	Sb(1) - N(3)	2.063(3)	2.106
Sb(1) - I(1)	3.040(7)	3.104	Sb(1) - Br(1)	2.877 (6)	2.809
N(1)-Sb(1)-I(1)	167.44(1)	170.81	N(1)-Sb(1)-Br(1)	168.18(7)	169.73

Bond Parameters Sb:CN	Crystal structure	Optimized geometry
Sb(1) - N(1)	2.197(5)	2.280
Sb(1) - N(2)	2.056(4)	2.100
Sb(1) - N(3)	2.056(4)	2.100
Sb(1) - C(1)	2.445(7)	2.361
N(1)-Sb(1)-C(1)	162.05(2)	163.61
Sb(1)-C(1)-N(4)	172.93(6)	163.38

Bond Parameters Sb:OCN	Crystal structure	Optimized geometry
Sb(1) - N(1)	2.190(2)	2.191
Sb(1) - N(2)	2.052(2)	2.096
Sb(1) - N(3)	2.047(2)	2.092
Sb(1) - O(1)	2.287(2)	2.355
N(1)-Sb(1)-O(1)	161.87(8)	163.90

Table 4.5. Gibb's free energy associated with the 1:1 and 1:2 binding.

Anions	Antimony		Bismuth	
	ΔG (1:1) (kJ/mol)	ΔG (1:2) (kJ/mol)	ΔG (1:1) (kJ/mol)	ΔG (1:2) (kJ/mol)
Chloride (Cl^-)	-6.42	20.72	-18.38	-8.58
Bromide (Br^-)	-3.07	26.66	-17.76	1.63
Iodide (I^-)	1.86	21.25	-12.04	-2.21
Isocyanide (NC^-)	5.21	-	-	-
Cyanide (CN^-)	-6.30	33.37	-16.85	9.95
Isocyanate (NCO^-)	-11.21	42.21	-21.57	10.38
Cyanate (OCN^-)	20.17	-	10.42	-
Isothiocyanate (NCS^-)	2.38	34.91	-10.81	13.83
Thiocyanate (SCN^-)	3.00	-	-8.79	

Table 4.6. Changes observed in the Hirshfield charges of antimony complex after binding with incoming anion.

Atom in antimony complex	**Hirshfield Sb_complex**	**Hirshfield $Sb:Cl_1^-$**	**Hirshfield $SbCl_1^- : Cl_2^-$**
Sb	0.558	0.491	0.472
N	-0.116	-0.145	-0.135
N	-0.116	-0.109	-0.135
N	-0.116	-0.109	-0.101
Cl_1	-	-0.407	-0.465
Cl_2	-	-	-0.465

Table 4.7. Changes observed in the Hirshfield charges of bismuth complex after binding with incoming anion.

Atom in bismuth complex	**Hirshfield Bi_complex**	**Hirshfield $Bi:Cl_1^-$**	**Hirshfield $BiCl_1^- : Cl_2^-$**
Bi	0.641	0.589	0.564
N	-0.124	-0.161	-0.151
N	-0.124	-0.118	-0.151
N	-0.124	-0.118	-0.111
Cl_1	-	-0.428	-0.478
Cl_2	--	-	-0.478

4.6. References

1. Sharma, A. K.; Tjell, J. C.; Sloth, J. J.; Holm, P. E., Review of arsenic contamination, exposure through water and food and low cost mitigation options for rural areas. *Applied Geochemistry* **2014,** *41*, 11-33.
2. Taylor, V.; Goodale, B.; Raab, A.; Schwerdtle, T.; Reimer, K.; Conklin, S.; Karagas, M. R.; Francesconi, K. A., Human exposure to organic arsenic species from seafood. *Science of The Total Environment* **2017,** *580*, 266-282.
3. *Service NMF Service NMF. Fisheries of the United States, 2019. 2022*.
4. Borak, J.; Hosgood, H. D., Seafood arsenic: Implications for human risk assessment. *Regulatory Toxicology and Pharmacology* **2007,** *47* (2), 204-212.
5. Amin, M. H. A.; Xiong, C.; Glabonjat, R. A.; Francesconi, K. A.; Oguri, T.; Yoshinaga, J., Estimation of daily intake of arsenolipids in Japan based on a market basket survey. *Food and Chemical Toxicology* **2018,** *118*, 245-251.
6. Müller, S. M.; Ebert, F.; Galla, H.-J.; Francesconi, K. A.; Schwerdtle, T., Arsenic-containing hydrocarbons disrupt a model *in vitro* blood-cerebrospinal fluid barrier. *J. Trace Elem. Med. Bio.* **2018,** *49*, 171-177.
7. Ravenscroft, P.; Brammer, H.; Richards, K., *Arsenic Pollution: A Global Synthesis*. Wiley: 2011.
8. *Inorganic Arsenic in Rice Cereals for Infants: Action Level Guidance for Industry*; FDA 2020.
9. Meyer, S.; Schulz, J.; Jeibmann, A.; Taleshi, M. S.; Ebert, F.; Francesconi, K. A.; Schwerdtle, T., Arsenic-containing hydrocarbons are toxic in the in vivo model Drosophila melanogaster. *Metallomics* **2014,** *6* (11), 2010-2014.
10. Parajuli, R. P.; Fujiwara, T.; Umezaki, M.; Watanabe, C., Association of cord blood levels of lead, arsenic, and zinc with neurodevelopmental indicators in newborns: A birth cohort study in Chitwan Valley, Nepal. *Environmental Research* **2013,** *121*, 45-51.
11. Rodrigues, E. G.; Bellinger, D. C.; Valeri, L.; Hasan, M. O. S. I.; Quamruzzaman, Q.; Golam, M.; Kile, M. L.; Christiani, D. C.; Wright, R. O.; Mazumdar, M., Neurodevelopmental outcomes among 2- to 3-year-old children in Bangladesh with elevated blood lead and exposure to arsenic and manganese in drinking water. *Environmental Health* **2016,** *15* (1).
12. Sinha, D.; Prasad, P., Health effects inflicted by chronic low-level arsenic contamination in groundwater: A global public health challenge. *Journal of Applied Toxicology* **2020,** *40* (1), 87-131.
13. Bellinger, D., Inorganic Arsenic Exposure and Children's Neurodevelopment: A Review of the Evidence. *Toxics* **2013,** *1* (1), 2-17.
14. Tsuji, J. S.; Garry, M. R.; Perez, V.; Chang, E. T., Low-level arsenic exposure and developmental neurotoxicity in children: A systematic review and risk assessment. *Toxicology* **2015,** *337*, 91-107.
15. Sun, Y.; Liu, G.; Cai, Y., Thiolated arsenicals in arsenic metabolism: Occurrence, formation, and biological implications. *J. Environ. Sci.* **2016,** *49*, 59-73.
16. Escudero-Lourdes, C., Toxicity mechanisms of arsenic that are shared with neurodegenerative diseases and cognitive impairment: Role of oxidative stress and inflammatory responses. *Neurotoxicology* **2016,** *53*, 223-235.
17. Taleshi, M. S.; Seidler-Egdal, R. K.; Jensen, K. B.; Schwerdtle, T.; Francesconi, K. A., Synthesis and Characterization of Arsenolipids: Naturally Occurring Arsenic Compounds in Fish and Algae. *Organometallics* **2014,** *33* (6), 1397-1403.
18. Bange, C. A.; Waterman, R., Zirconium-catalyzed hydroarsination with primary arsines. *Polyhedron* **2018,** *156*, 31-34.

19. Roering, A. J.; Davidson, J. J.; MacMillan, S. N.; Tanski, J. M.; Waterman, R., Mechanistic variety in zirconium-catalyzed bond-forming reaction of arsines. *Dalton Transactions* **2008,** (33), 4488-4498.
20. Tay, W. S.; Lu, Y.; Yang, X. Y.; Li, Y.; Pullarkat, S. A.; Leung, P. H., Catalytic and Mechanistic Developments of the Nickel(II) Pincer Complex-Catalyzed Hydroarsination Reaction. *Chemistry – A European Journal* **2019**.
21. Janesko, B. G.; Fisher, H. C.; Bridle, M. J.; Montchamp, J.-L., P(═O)H to P–OH Tautomerism: A Theoretical and Experimental Study. *The Journal of Organic Chemistry* **2015,** *80* (20), 10025-10032.
22. Janesko, B. G.; Fisher, H. C.; Bridle, M. J.; Montchamp, J. L., P(horizontal lineO)H to P-OH Tautomerism: A Theoretical and Experimental Study. *J Org Chem* **2015,** *80* (20), 10025-32.
23. Han, J.; Kim, J.; Lee, J.; Kim, Y.; Lee, S. Y., Boron Lewis Acid-Catalyzed Hydrophosphinylation of N-Heteroaryl-Substituted Alkenes with Secondary Phosphine Oxides. *J Org Chem* **2020,** *85* (23), 15476-15487.
24. Becke, A. D., Density-functional thermochemistry. III. The role of exact exchange. *The Journal of Chemical Physics* **1993,** *98* (7), 5648-5652.
25. Zhao, Y.; Truhlar, D. G., The M06 suite of density functionals for main group thermochemistry, thermochemical kinetics, noncovalent interactions, excited states, and transition elements: two new functionals and systematic testing of four M06-class functionals and 12 other function. *Theoretical Chemistry Accounts* **2008,** *120* (1-3), 215-241.
26. Lee, C.; Yang, W.; Parr, R. G., Development of the Colle-Salvetti correlation-energy formula into a functional of the electron density. *Physical Review B* **1988,** *37* (2), 785-789.
27. Han, J.; Kim, J.; Lee, J.; Kim, Y.; Lee, S. Y., Boron Lewis Acid-Catalyzed Hydrophosphinylation of N-Heteroaryl-Substituted Alkenes with Secondary Phosphine Oxides. *The Journal of Organic Chemistry* **2020,** *85* (23), 15476-15487.
28. Benz, S.; Poblador-Bahamonde, A. I.; Low-Ders, N.; Matile, S., Catalysis with Pnictogen, Chalcogen, and Halogen Bonds. *Angewandte Chemie International Edition* **2018,** *57* (19), 5408-5412.
29. Moaven, S.; Yu, J.; Yasin, J.; Unruh, D. K.; Cozzolino, A. F., Precise Steric Control over 2D versus 3D Self-Assembly of Antimony(III) Alkoxide Cages through Strong Secondary Bonding Interactions. *Inorganic Chemistry* **2017,** *56* (14), 8372-8380.
30. Brammer, L., Halogen bonding, chalcogen bonding, pnictogen bonding, tetrel bonding: origins, current status and discussion. *Faraday Discuss.* **2017,** *203*, 485-507.
31. Frontera, A.; Bauza, A., On the Importance of Pnictogen and Chalcogen Bonding Interactions in Supramolecular Catalysis. *International Journal of Molecular Sciences* **2021,** *22* (22), 12550.
32. Brown, A.; Beer, P. D., Halogen bonding anion recognition. *Chemical Communications* **2016,** *52* (56), 8645-8658.
33. Sun, S.-S.; Lees, A. J., Anion recognition through hydrogen bonding: a simple, yet highly sensitive, luminescent metal-complex receptor. *Chemical Communications* **2000,** (17), 1687-1688.
34. Christianson, A. M.; Gabbaï, F. P., A Lewis Acidic, π-Conjugated Stibaindole with a Colorimetric Response to Anion Binding at Sb(III). *Organometallics* **2017,** *36* (16), 3013-3015.
35. Christianson, A. M.; Gabbaï, F. P., Anion sensing with a Lewis acidic BODIPY-antimony(v) derivative. *Chemical Communications* **2017,** *53* (16), 2471-2474.
36. Ke, I.-S.; Myahkostupov, M.; Castellano, F. N.; Gabbaï, F. o. P., Stibonium ions for the fluorescence turn-on sensing of F–in drinking water at parts per million concentrations. *Journal of the American Chemical Society* **2012,** *134* (37), 15309-15311.

37. Hirai, M.; Gabbaï, F. P., Squeezing Fluoride out of Water with a Neutral Bidentate Antimony(V) Lewis Acid. *Angewandte Chemie International Edition* **2015,** *54* (4), 1205-1209.
38. Custelcean, R., Anions in crystal engineering. *Chemical Society Reviews* **2010,** *39* (10), 3675-3685.
39. Gale, P. A.; Caltagirone, C., Anion sensing by small molecules and molecular ensembles. *Chemical Society Reviews* **2015,** *44* (13), 4212-4227.
40. Docker, A.; Marques, I.; Kuhn, H.; Zhang, Z.; Félix, V.; Beer, P. D., Selective Potassium Chloride Recognition, Sensing, Extraction, and Transport Using a Chalcogen-Bonding Heteroditopic Receptor. *Journal of the American Chemical Society* **2022,** *144* (32), 14778-14789.
41. Tresca, B. W.; Berryman, O. B.; Zakharov, L. N.; Johnson, D. W.; Haley, M. M., Anion-directed self-assembly of a 2,6-bis(2-anilinoethynyl)pyridine bis(amide) scaffold. *Supramolecular Chemistry* **2016,** *28* (1-2), 37-44.
42. Gale, Philip A.; Howe, Ethan N. W.; Wu, X., Anion Receptor Chemistry. *Chem* **2016,** *1* (3), 351-422.
43. Lim, J. Y. C.; Beer, P. D., Sigma-Hole Interactions in Anion Recognition. *Chem* **2018,** *4* (4), 731-783.
44. Lee, L. M.; Tsemperouli, M.; Poblador-Bahamonde, A. I.; Benz, S.; Sakai, N.; Sugihara, K.; Matile, S., Anion Transport with Pnictogen Bonds in Direct Comparison with Chalcogen and Halogen Bonds. *Journal of the American Chemical Society* **2019,** *141* (2), 810-814.
45. Jentzsch, A. V.; Emery, D.; Mareda, J.; Nayak, S. K.; Metrangolo, P.; Resnati, G.; Sakai, N.; Matile, S., Transmembrane anion transport mediated by halogen-bond donors. *Nature Communications* **2012,** *3* (1), 905.
46. Qiu, J.; Song, B.; Li, X.; Cozzolino, A. F., Solution and gas phase evidence of anion binding through the secondary bonding interactions of a bidentate bis-antimony(iii) anion receptor. *Physical Chemistry Chemical Physics* **2018,** *20* (1), 46-50.
47. Moaven, S.; Andrews, M. C.; Polaske, T. J.; Karl, B. M.; Unruh, D. K.; Bosch, E.; Bowling, N. P.; Cozzolino, A. F., Triple-Pnictogen Bonding as a Tool for Supramolecular Assembly. *Inorganic Chemistry* **2019,** *58* (23), 16227-16235.
48. Moaven, S.; Watson, B. T.; Polaske, T. J.; Karl, B. M.; Unruh, D. K.; Bowling, N. P.; Cozzolino, A. F., Self-Assembly of Complementary Components Using a Tripodal Bismuth Compound: Pnictogen Bonding or Coordination Chemistry? *Inorganic Chemistry* **2021,** *60* (15), 11242-11250.
49. Grimme, S., Semiempirical GGA-type density functional constructed with a long-range dispersion correction. *Journal of Computational Chemistry* **2006,** *27* (15), 1787-1799.
50. Weigend, F., Accurate Coulomb-fitting basis sets for H to Rn. *Physical Chemistry Chemical Physics* **2006,** *8* (9), 1057-1065.
51. Garrett, G. E.; Gibson, G. L.; Straus, R. N.; Seferos, D. S.; Taylor, M. S., Chalcogen Bonding in Solution: Interactions of Benzotelluradiazoles with Anionic and Uncharged Lewis Bases. *Journal of the American Chemical Society* **2015,** *137* (12), 4126-4133.
52. Grimme, S.; Ehrlich, S.; Goerigk, L., Effect of the damping function in dispersion corrected density functional theory. *Journal of Computational Chemistry* **2011,** *32* (7), 1456-1465.
53. Jinchun Qiu, C. N. B., Shuai Lu, Gary George, Xiaopeng Li, John Gorden, Serhii and Anthony F. Cozzolino, Solution studies of a Water-stable, Trivalent Antimony Pnictogen Bonding Anion Receptor with high binding affinities for CN^-, OCN^-, OAc^-. *Submitted* **2023**.

Appendix: Copyrights

A tertiary phosphine oxide ligand-based recyclable system for the Suzuki–Miyaura and Negishi reactions: evidence for pseudo-homogeneous catalysis

A. K. King, A. Brar and M. Findlater, *Catal. Sci. Technol.*, 2023, **13**, 301 **DOI:** 10.1039/D2CY01734B

Experimental and Computational Studies of Phosphine Ligand Displacement in Iridium–Pincer Complexes Employing Pyridine or Acetonitrile

Author: Sara Shafiei-Haghighi, Aneelman Brar, Daniel K. Unruh, et al
Publication: Organometallics
Publisher: American Chemical Society
Date: Oct 1, 2020